SANDIA REPORT

SAND97-1894 • UC-704
Unlimited Release
Printed August 1997

Mo-Al_2O_3 Cermet Research and Development

S. Jill Glass, Edwin K. Beauchamp, Saundra L. Monroe, John J. Stephens, Roger H. Moore, John P. Brainard, Kevin G. Ewsuk, Edward L. Hoffman, Ronald E. Loehman, Gary A. Pressly, John E. Smugeresky

Prepared by
Sandia National Laboratories
Albuquerque, New Mexico 87185 and Livermore, California 94550

Sandia is a multiprogram laboratory operated by Sandia Corporation, a Lockheed Martin Company, for the United States Department of Energy under Contract DE-AC04-94AL85000.

Approved for public release; distribution is unlimited.

Sandia National Laboratories

Issued by Sandia National Laboratories, operated for the United States Department of Energy by Sandia Corporation.

Available to DOE and DOE contractors from
Office of Scientific and Technical Information
P.O. Box 62
Oak Ridge, TN 37831

Prices available from (615) 576-8401, FTS 626-8401

Available to the public from
National Technical Information Service
U.S. Department of Commerce
5285 Port Royal Rd
Springfield, VA 22161

NTIS price codes
Printed copy: A06
Microfiche copy: A01

SAND97-1894
Unlimited Release
Printed August 1997

Distribution
Category UC-704

Mo-Al_2O_3 Cermet Research and Development

S. Jill Glass*, Edwin K. Beauchamp, Saundra L. Monroe, John J. Stephens
Materials Joining Department

Roger H. Moore*
Ceramic and Glass Processing Department

John P. Brainard
Neutron Tube Development Department

Kevin G. Ewsuk
Materials Processing Department

Edward L. Hoffman
Engineering and Manufacturing Mechanics Department

Ronald E. Loehman
Materials Science Programs and Advanced Materials Lab Department

Gary A. Pressly
Mechanical Engineering Department

John E. Smugeresky
Materials Reliability Department

Sandia National Laboratories
P.O. Box 5800
Albuquerque, NM 87185-0367

Abstract

This report describes the results to date of a program that was initiated to predict and measure residual stresses in Mo-Al_2O_3 cermet-containing components and to develop new materials and processes that would lead to the reduction or elimination of the thermal mismatch stresses. The period of performance includes work performed CY95-97. Excessive thermal mismatch stresses had produced cracking in some cermet-containing neutron tube components. This cracking could lead to a loss of hermeticity or decreased tube reliability. Stress predictions were conducted using finite element models of the various components, along with the thermal coefficient of expansion (CTE), Young's modulus, and strength properties. A significant portion of the program focused on the property measurements for the existing cermet materials and the sensitivity of these measurements to small differences in starting materials, processing conditions, and the measurement technique. The effects of differences in the properties on the predicted residual stresses were calculated for existing designs. Several potential approaches were evaluated for reducing the residual stresses and cracking in cermet-containing parts including reducing the Mo content of the cermet, substituting a ternary alloy with a better CTE match with alumina, and substituting Nb for Mo. Processing modifications were also investigated for minimizing warpage that occurs during sintering due to differential sintering. These modifications include changing the pressing of the 94ND2 alumina and changing to a 96% alumina powder from AlSiMag.

* Authors to contact for additional information.

Acknowledgments

We acknowledge the technical assistance of Denise Bencoe, Richard Brow, Steve Burchett, Brian Damkroger, Bill Fahrenholtz, John Gieske, Mary Gonzales, Clay Newton, Mike Readey, Mark Reece, Iva Segalman, and Dave Van Ornum. This study was supported by Product Realization Backbone and Production LDRD programs.

DISCLAIMER

Table of Contents **Pg.**

List of Figures

Mo-Al_2O_3 Cermet Research and Development

1. Introduction

Purpose of Report

The purpose of this report is to document the research, development, characterization, and finite element analysis stress predictions that have been conducted on molybdenum (Mo)-alumina (Al_2O_3) cermets and related materials used in neutron tubes (MC4277). The report is intended to serve as a comprehensive source of information, references, materials data, and FEA models to be used for component design and as a source of ideas and direction for future cermet-related R&D.

Cermet Applications and Performance Requirements

Mo-Al_2O_3 cermets are used in the insulator, feedthru, and insulator feedthru, which are all subassemblies of the MC4277 neutron tube. Figures 1 (a-c) show drawings of these pieceparts. The material adjacent to the cermet in each of these pieceparts is 94% alumina. Cermets are used in each of these applications because neutron tube designers identified the following benefits that arise from the use of Mo-Al_2O_3 cermet features in alumina neutron tube parts.

1. Cermets can be used as integral hermetic feedthrus to replace pin feedthrus.
2. Using cermets as inlays in the alumina insulator may simplify the brazing process used to join the ceramic insulator to Kovar.
3. The use of cermets near the triple junction in a neutron tube reduces the high fields that often lead to breakdown.
4. Cermets can be used as grading rings to shape electric fields to prevent (or minimize) the electron avalanching that occurs during breakdown.

Additional details are provided in the paragraphs below.

In the feedthru application the purpose of the integral cermet vias is to provide an electrically conducting path through the insulating alumina. The conventional approach is to braze metal pins into holes in the alumina. The limitations of the conventional approach are the processing difficulties associated with brazing pins into alumina and the reliability issues relating to the residual stresses produced by the thermal expansion mismatch between metal pins and the ceramic. For feedthrus of this type, reliable components could not be produced because the hole in the alumina was difficult to metallize, and cracks between the Kovar pin and alumina were common. Producing an alumina part with an integral cermet feedthru was intended to mitigate both of these limitations and has been successful for the MC4277 neutron tube. Although there is a thermal expansion mismatch between the cermet (α=7.69x10^{-6}/°C)[i] and alumina (α=8.31x10^{-6}/°C), it is generally small enough in the source feedthru application that it has not led to excessive residual stresses and cracking. The cermet feedthru appears to be 100% reliable.

Cermets are used as inlays in the alumina for the insulator application because they provide a surface that can be brazed to using fewer steps than the number required for the Mo-manganese and Ni plating process typically used for brazing alumina. We could greatly simplify the brazing

[i] Average linear contraction from 1000 to 37°C.

process and improve joint reproducibility if we could braze cermet directly to Kovar using an active braze alloy. The metallization process of screen printing (on flat surfaces) and hand painting (on non-flat surfaces) has problems with thickness uniformity and with unintentional stringers that can occur when the screen or brush is pulled away from the ceramic surface. The elimination of nickel plating baths would reduce our waste stream flow.

Cermets have a potential application in the tube frame as their presence has been demonstrated to reduce the electric field in the triple junction of the neutron tube. The triple junction (the intersection of the cathode, high voltage insulator, and vacuum) is the region where the high voltage insulator (alumina) is brazed to the cathode electrode (Kovar) on the vacuum side internal to the tube. Here, electric fields can be over ten times the average field in the tube due to non-uniformities such as braze fingers at the ceramic edge or due to gaps between the insulator and cathode (from chips, cracks, or other non-uniformities of the insulator). The enhanced electric fields due to the non-uniformities in this region frequently lead to high voltage breakdown. Brazing a ceramic insulator with a cermet inlay on the surface places these non-uniformities in a relatively field free region, i.e., the defects are between the cathode and cermet, which are at the same potential. The triple junction, in effect, moves to the cermet/insulator joint where there are relatively clean edges.

Cermets may also be used as grading rings to shape the electrical fields. Grading rings allow the neutron tube designer to angle the fields to prevent electron avalanching in addition to lowering the triple junction fields. To help shield the triple junction from high fields, the grading ring (a conductive ring at cathode potential) is either embedded into the high voltage insulator or is external to the tube. An embedded cermet ring is preferred because it is more effective with its close proximity to the triple junction. External grading rings cause problems with the tube encapsulation process, e.g., initiating cracks or causing voids.

In some of these applications, such as the insulator feedthru, where the size of the cermet via is much larger than in the feedthru insulator, cracking has been observed near the interface between the alumina and the cermet. Problems associated with cracking include a loss of hermeticity and the overall issue of reliability.

Program Objectives

The objectives of the program were to predict and measure the residual stresses in cermet-containing components and to develop new materials and processes that would lead to the reduction or elimination of the thermal mismatch stresses. Stress predictions were conducted using finite element models of the various components along with the relevant properties of the material, including thermal coefficient of expansion (CTE) and Young's modulus. One objective was to calculate the effects of differences in the properties on the predicted residual stresses for existing designs. These design stresses were then compared to the generally accepted design stress for alumina of 10 ksi or 70 MPa.

A significant portion of the program focused on the measurement of the properties of the existing cermet materials and the sensitivity of these measurements to small differences in starting materials, processing conditions, and measurement technique. Procedures were developed to ensure the reproducibility of the CTE data. Because the Mo-Al_2O_3 cermet has not seen wide use in weapons components and because it has not been characterized nearly as well as alumina, appropriate design stresses have not been identified. Hence, another objective was to use strength measurements to define a target stress range.

Several processing approaches were identified for reducing the residual stresses and cracking in cermet-containing parts. A significant part of this effort was devoted to examining whether lower vol% Mo cermets could be used to reduce the thermal mismatch stresses to an acceptable level without sacrificing other properties such as electrical conductivity or brazeability. The requirements for higher electrical conductivity in some applications and improved brazeability in others push the required Mo composition in the opposite direction to that required for reducing the CTE mismatch and may allow only a small window in which the composition could be altered as shown in Fig. 2. Our final objectives were to identify this window and to evaluate the feasibility of several other approaches for reducing the CTE of the cermet.

Report Outline

This report is a comprehensive collection of the information and data obtained on the modeling, characterization, and processing of cermets and cermet-containing components. This work was performed during CY95-97. Future reports will cover subsequent work. Some of the data and information from Gary Pressly's Master's thesis, "Characterization of Molybdenum-Alumina Cermets,"[1] is included in this report. This thesis provides detailed information about the processing and properties of materials similar to those used in Sandia's cermet-containing components. Copies of the thesis abstract, introduction and conclusions are included in Appendix B because this information in the thesis form may not be readily available.

Section 1 of this report describes the problem being addressed in this program. Section 2 contains background information and begins with a brief review of other work conducted on cermets, including work conducted at Mound Laboratory and Lockheed Martin Specialty Components (formerly General Electric Neutron Devices Department (GENDD) in Pinellas, FL), where the current CND50 (50 wt% Mo, 50 wt% alumina) cermet material was developed. Section 3 contains descriptions of the two methods currently used to fabricate cermet-containing alumina components. Both methods were used to fabricate the samples used in this study to characterize the cermet properties. Section 4 describes the characterization of the cermets. The most important properties are those used as input for the finite element models. Others are important because they provide baseline information for the current materials. The property measurements also help define the relationships between the processing, structure, and properties and provide us with a starting point for empirical (phenomenological) models of the process space. These models will help us to develop cermets for new applications in which the property requirements may be different.

Section 5 contains the finite element analyses done on various cermet components and experimental verification of the stress predictions. Section 6 contains descriptions of the various approaches for reducing the thermal mismatch stresses in cermet-containing components including the evaluation of lower vol% Mo cermets, development and evaluation of new Mo-containing alloys, evaluation of Nb as an alternative to Mo in the cermet, and modifications to the processing of the current Mo cermet. Section 7 presents conclusions, and Section 8 contains recommendations for future research and development work on cermets.

2. Background

Cermet Definition

Generic

The term cermet refers to a composite of a ceramic (cer) and metal (met). The Materials Handbook[2] defines a cermet as "A composite material made up of ceramic particles (or grains) dispersed in a metal matrix. Particle size is greater than 1 μm, and the volume fraction is over 25% and can go as high as 90%." Note that this definition is not inclusive, and cermets can also be metal particles dispersed in a ceramic matrix. Cermet applications often combine the hardness and stiffness of the ceramic phase with the ductility, thermal, or electrical properties of the metal phase.

SNL Definitions (historical):

- alumina cermet: a composite structure composed of monolithic regions of 94% alumina and Mo/94% alumina cermet composite
- solid cermet: a monolithic composite of molybdenum and 94% alumina

Development of Mo-Alumina Cermets for Defense Program Applications

Cermets, as defined in this context, were developed in the late 1970's by personnel at LMSC (then GENDD) as an alternative to conventional ceramic/metal pin feedthrus.[3] This cermet was also used as an insert for high voltage hold-off improvement for ceramic/metal vacuum devices. Those involved in that development include W. Schmidt, W. Dupree, W. F. Ierna, I. Levine, and A. Eylward. Documentation of this development effort is sparse, except for two patents 4,704,557[4] and 4,488,673[5] (both expired). The focus of the GENDD work was to develop robust manufacturing processes to meet development and production needs for hermetic electrical feedthrus in neutron tubes.

The cermet material developed at GENDD is designated CND50 in which the "C" stands for cermet, the "ND" for Neutron Devices, and the "50" for the wt% Mo. The alumina used in the CND50 cermet is designated 94ND2. This is a 94 wt% aluminum oxide. The "2" refers to the glass composition, which consists of MgO, CaO, and SiO_2 and constitutes the remaining 6 wt%. Fifty wt% Mo in the CND50 cermet corresponds to 27 vol% Mo. For purposes of comparison and conversion between wt% and vol%, the densities of Mo and 94ND2 alumina are 10.2 and 3.8 g/cm^3 respectively.

Development of the Mo-alumina cermet also occurred at MRC-Mound Facility in Miamisburg, OH.[6] In one study by Mound, the effects of Al_2O_3 concentration and sintering parameters on the resistivity of the cermet were determined. The resistivity of the cermet decreased significantly as the alumina purity decreased from 99 to 91% alumina and decreased with increased firing temperature. The effect of the increased firing temperature was attributed to the increased density and greater connectivity between the conducting Mo particles.

Another Mound study of Mo and Nb pins as alternatives to CND50 cermets in alumina components provides some insight into a possible mechanism of bonding between the Mo and the alumina. Alumina powder was pressed around the metal pins and then sintered.[7] Microprobe analyses and microhardness measurements of the Mo were conducted to reveal whether a reaction had occurred between the alumina and the Mo pins. No direct evidence of a reaction was found; however, differences in bonding behavior between the pins and 94 and 99% alumina suggested that there might be a reaction between the Si in the glass phase of the alumina and the Mo to form a

Mo-Si compound such as $MoSi_2$, which is an electroconductive intermetallic with a room-temperature resistivity of 21.6×10^{-6} Ω-cm.[8] Other Mo-Si compounds also exist.[9]

During the design and development of the MC4277 neutron tube in the early 1990's, the application of cermet materials and processing was extended beyond the initial concept of hermetic electrical feedthrus. Under the direction of J. Brainard (SNL) and D. McCollister (LMSC), cermet materials were employed as field shaping rings, joining interfaces, and feedthrus (see Fig. 1). Eylward led the effort to apply existing processing techniques to these larger components with larger cermet features. He documented many of those processes with Operating Procedures (OP) and Special Use Specifications (SS) for fabrication of these development cermets for the MC4277. The processing discussion in Section 3 draws heavily on those OPs as well as processing experience at SNL.

Beginning in FY93, the cermet manufacturing technology resident at LMSC was transferred to SNL and AlSiMag[ii]. AlSiMag is currently applying the manufacturing processes at their facility, eventually leading to War Reserve (WR) qualification of their processes and products to meet the present development and future production requirements for the MC4277 neutron tube. The processing descriptions in Section 3 are *representative* of processes at LMSC, SNL, and AlSiMag and should not be considered as exact.

[ii] AlSiMag Technical Ceramics, Inc., Laurens, SC 29630

Survey of Other Work on Mo-Alumina Cermets

Studies were conducted by McHugh et al.[10] on the strengthening of alumina by Mo dispersions up to 16 vol%. The significant increase in the average strength as a function of Mo content, with a doubling in strength at Mo contents greater than 5 vol%, was attributed to the inhibition in grain growth by the Mo dispersion. Sintering studies showed that the Mo-alumina cermet densified at a lower rate in the early stages of sintering but reached an equal relative density by the end of the hold at the sintering temperature. This study also contained some information about earlier work by Pincus on the reactions between alumina and Mo to form $Al_2(MoO_4)_3$.[11]

The effect of the microstructure on the percolation threshold, φ_c, for electrical conductivity in Mo-alumina cermets was studied by Kelso et al.[12] The variables in this study were the initial particle sizes of the alumina and Mo powders, the alumina glass content (14 vs. 28 vol%), and the dewpoint of the firing atmosphere. The percolation threshold varied from ~9 to 18 vol% Mo. The φ_c decreased when the particle size of the alumina relative to the Mo increased, when smaller particles of Mo were used relative to a given alumina particle size, with higher glass contents, and with higher dew point sintering atmospheres, which promoted the growth of less round particles. The resistivity data for the cermet samples in this study were fit with McLachlan's General Effective Media (GEM) Equation[13] using the percolation threshold for the lower resistivity phase, φ_c, the conductivities of the two end members, and t, an exponent related to the product of φ_c and m, a particle shape factor.

$$\frac{f\left(\sigma_l^{1/t} - \sigma_m^{1/t}\right)}{\sigma_l^{1/t} + A\sigma_m^{1/t}} + \frac{(1-f)\left(\sigma_h^{1/t} - \sigma_m^{1/t}\right)}{\sigma_h^{1/t} + A\sigma_m^{1/t}} = 0 \quad = \frac{(1-\phi)\left(\rho_m^{1/t} - \rho_h^{1/t}\right)}{\rho_m^{1/t} + A\rho_h^{1/t}} + \frac{\phi\left(\rho_m^{1/t} - \rho_l^{1/t}\right)}{\rho_m^{1/t} + A\rho_l^{1/t}} \qquad (1a)$$

where

A=constant in the GEM equation ($f_c/(1-f_c)$) or ($(1-\phi_c)/\phi_c$)

f = volume fraction of the poor conductivity phase ($1-\phi$)

ϕ = volume fraction of the high conductivity phase (1-f)

t = exponent in the percolation and GEM equations ($t = m_f f_c - m_\phi \phi_c$)

ρ_m = resistivity of the composite ($1/\sigma_m$)

ρ_h= resistivity of the low-conductivity phase ($1/\sigma_l$)

ρ_l=resistivity of the high conductivity phase ($1/\sigma_h$)

In the limiting cases, where σ_l=0 on the left and ρ_l=0 on the right, the above equations can be written as the classical percolation equations:

$$\sigma_m = \sigma_h(1-f/f_c)^t \qquad (1b)$$

and $$\rho_m = \rho_h(1-\varphi/\varphi_c)^t \qquad (1c)$$

where

f_c and ϕ_c are the percolation thresholds.

The data in this study used t~0.5.

A study was also performed on a material similar to the Mo-Al_2O_3 cermets in the Sandia study. The cermet was a chromia-alumina composition with 30 wt% (20 vol%) metal.[14] Physical properties measured included firing shrinkage, density, CTE between 75 and 2400°F, hardness, modulus, strength, and oxidation resistance. Of greatest interest to the present cermet study, because of the need for a cermet with a coefficient of thermal expansion that matches alumina, was the value of the CTE, which was 8.7×10^{-6}/°C between 25 and 800°C and 9.5×10^{-6}/°C between 22 and 1315°C, which was just slightly greater than that for the 99.5% pure alumina.

3. Processing

Starting Materials

The Mo in the Mo-Al_2O_3 cermet is from General Electric.[iii] The starting powders for the 94ND2 alumina and their weight percentages are shown in Table 1.

Table 1. Starting materials for fabrication of 94ND2 alumina.

Material	Wt%
aluminum oxide	93.4
magnesium hydroxide	1.6
calcium carbonate	0.6
silica	4.4

The glass phase in the 94ND2 plays an important role in both the sinterability and properties of the cermets. An electron microprobe analysis of the glass grain boundary phase in 94ND2 indicated the oxide constituents and mol%'s shown in Table 2.[15]

Table 2. Oxide constituents of the grain boundary phase in 94ND2 alumina.

Oxide	Mol%
SiO_2	43.6
Al_2O_3	34.2
CaO	4.4
MgO	12.4
Na_2O	0.5
K_2O	0.1
B_2O_3	4.1
BaO	0.01
TiO_2	0.1
ZrO_2	0.3
FeO	0.1
Cr_2O_3	0.01
P_2O_5	0.1

Manufacture of Alumina Cermets:

The alumina cermet manufacturing process is shown in Fig. 3. It begins with dry pressed cylindrical compacts of spray dried 94% alumina. For cermet processing at LMSC and SNL, the alumina body (94ND2) was supplied by LMSC per SS305195.[iv] Initial efforts at AlSiMag were with 94ND2, but as it will no longer be available, AlSiMag is applying these techniques to their alumina body, AlSiMag 771. For dimensional control, the compacts are pressed to a green density of 2.00 g/cc + 0.02 - 0.001 g/cc. This is critical to establishing the initial dimensions prior to filling and firing the cermet. Recent work at SNL by Readey/Ewsuk suggests that higher densities may help control firing distortions, and formation of cermets from higher density compacts is certainly feasible. At this density (~52% of the theoretical density) the compact is relatively fragile

[iii] General Electric, Tungsten Products Plant, 21800 Tungsten Rd., Cleveland, OH 44117

[iv] SS305195 - Ceramic Body, 94ND2

and must be handled carefully to accommodate the subsequent machining operations. For MC4277 components compact diameter =0.875" and height = 0.8" are routinely used. The compact orientation during pressing should be noted as the diameter varies from one end to the other by ~0.001 in.

Due to the fragile nature of the compacts, closely machined collets are used to hold them during the first several machining steps (before subsequent isopressing). These collets are made to precisely fit one end of the compacts. Therefore, identifying the up or down end of the compact is recommended to permit holding the compact with only a slight pressure from the collet. Because the low density compact is fragile, only the machining that is required for producing features that require filling with cermet material is done at this time. These features consist of thruholes, blind holes, and channels. Standard green ceramic machining techniques are used including the use of diamond tooling for facing, turning, and parting operations. For drilling thruholes and blind holes in alumina and CND50, sharp carbide tooling is recommended. Tool speeds and feed rates are determined by the operator based on experience. Once complete, the compact is ready for filling with the cermet composite. Prior knowledge of the pressing-to-firing shrinkage factor is necessary to properly size these features prior to filling.

Cermet filling is accomplished using a liquid slurry suspension of the Mo/94% alumina mixture (e.g., CND50). The procedure for blending the powder mixture is described below for Solid Cermets. The slurry preparation process is detailed in SS443970.[v] The vehicle used is diethlyene glycol monobutyl ether (DGME) acetate (SS305003[vi]). Blending is accomplished in a tilted mixer commonly used for metallization slurries. The slurry is constantly stirred to prevent settling and separation of the Mo and alumina portions. An eyedropper or syringe is used to withdraw the slurry from the mixer, and it is immediately squirted into the appropriate feature in the alumina compact. When filling vias or thruholes, a vacuum assist is used to aid the flow of the slurry into the feature. Entrapped air in the slurry stream may result in large voids within the cermet feature or subsequent distortions of the cermet via after isostatic pressing. Significant operator skill is required to produce vias of uniform diameter and fill. Due to the porous nature of the alumina compact and the high volatility of the vehicle, the slurry dries rapidly. For long vias with small diameters, pre-wetting of the via feature with DGME acetate is sometimes used to delay drying so that the slurry may fill the via completely. For blind holes or channels (typically braze interfaces), where a vacuum assist is not possible, pre-wetting is used to aid filling of the slurry into the corners of these features.

Following the filling operation, the component is thoroughly dried (130°C for 17 hr) to remove the solvent from the filled part. After drying, the parts are isostatically pressed to 30 ksi to increase part density and strength so that subsequent machining can be accomplished with high yield. Again, the machined features are introduced with a prior knowledge of the isopressed-to-fired condition shrinkage factor. There is some flexibility in the uniaxial and isostatic pressures used in this process; however, process uniformity and repeatability are crucial to meeting the dimensional requirements. Therefore, small changes in pressing pressure can lead to missed fired dimensions if modifications to the shrinkage factors are not incorporated. It should be noted that linear and diametral shrinkage factors will be different, and depending on the complexity of the component, these factors can change depending on the location of the cermet feature within the alumina body. For example, cermet vias located near the OD of an alumina compact will experience a greater shrinkage after isostatic pressing than vias located near the center point of the compact. Therefore, establishing the shrinkage factors is done empirically and usually requires fabrication and measurement of the actual components. Once established for a particular lot of 94ND2 powder, the shrinkage factors remain constant providing that compact density, isostatic pressure,

---

[v] SS443970 - Cermet Slurry

[vi] SS305003 - Diethylene Glycol Monobutyl Ether Acetate

and firing conditions remain constant. Process control is thus very important to produce cermets with the required dimensions.

If performed incorrectly, bagging of the filled and dried compacts for isostatic pressing can lead to subsequent leakage of pressing fluid into the bags, thus ruining the component. Latex tubing and heat-sealable vacuum storage bags have been successfully used for isopressing these components. Voids in the cermet and sharp edges (pressed or machined alumina surfaces) have been shown to stretch or puncture the tubing and form pinholes in the latex. To reduce the occurrence of bag leakage, cermet surfaces should be inspected and smoothed, and sharp edges should be broken. Recently, we have suspected that 0.005 in. thick polyethylene bags have contributed to subsequent cracking of isopressed parts. Therefore, this type of bag should be avoided.

From experience, the size of the cermet features (typically diameter) will determine the necessary thickness of the alumina wall surrounding the feature prior to sintering. For alumina wall thicknesses less than 50% of the cermet feature diameter, excessive thermal mismatch stresses that may develop during cooling from the sintering temperature can lead to cracking of the alumina wall. It is recommended that components of this type have a minimum alumina wall thickness equal to the diameter of the cermet feature. The extra alumina stock that this requires is removed after firing by diamond grinding operations.

Sintering (co-firing) of cermet materials is accomplished under slightly oxidizing conditions. Wet hydrogen environments have been successfully used to prevent oxidation of the Mo constituent and to allow oxidation and removal of the residual organic binders. Both LMSC and SNL have used periodic furnaces with flow-through wet hydrogen atmospheres. In both cases, the dewpoints of H_2O were ~45°C . AlSiMag currently uses a continuous furnace with a wet hydrogen environment produced by "cracked" ammonia. In all cases, cermets of acceptable sintered density (3.75 g/cc) have been produced when fired at 1625°C for 2.5 hr. Following firing, diamond grinding processes are used to establish the remaining feature dimensions.

Inspection of the components using both dye penetrant (SS305182)[vii] and vicinal lighting techniques (SS707252)[viii] has been shown to be effective for locating cracks and other stress concentrating defects. X radiography is used to verify the continuity and dimensions of internal cermet vias.

Manufacture of Solid Cermets:

Solid cermets are monolithic bodies of CND50 powder and require fewer processing steps than alumina cermets. The details of this process are described in SS443883[ix] and are shown in Fig. 4. For both solid cermets and the cermet features in alumina cermets, a blended mixture of Mo (46A101593)[x] and 94ND2 alumina is prepared using dry ball milling methods (SS321504).[xi] 94ND2 is a spray dried powder containing intentionally large agglomerates of alumina powder. For dry blending with Mo powder (for either alumina cermet slurries or for powders for solid cermets), it is recommended that a finer distribution of 94ND2 be used. Traditionally, this finer distribution is obtained from the fines collector on the spray dryer when the 94ND2 slurry is spray dried. This powder is called "secondary" and is preferred to the "primary" product of the spray

---

[vii] SS305182 - Dye Penetrant Inspection

[viii] SS707252 - Vicinal Inspection of Alumina/Cermet Interfaces

[ix] SS443883 - Cermet

[x] 46A101593 - Molybdenum Powder

[xi] SS321504 - Cermet Powder CND50

dryer. Primary powder may also be used; however, longer milling times are required to produce uniform blends of CND50 powder.

Billets of CND50 powder are prepared by isostatically pressing at 30 ksi. For the MC4277 neutron tube, the solid cermet components are typically rings or flat discs. After applying shrinkage factors to the required dimensions, the components are machined from the isopressed billets. The components are fired identically to the alumina cermets and also require finish grinding to achieve the required features and surface finish. The cautions concerning shrinkage factor and process control for alumina cermets apply here as well.

4. Characterization of CND50 Cermet and Lower Vol% Mo Cermets

Property measurements have been made on the conventional CND50 cermets being used for cermet-containing components and the 94ND2 alumina. 94ND2 is the alumina used adjacent to the cermet material in neutron tube components, and it is the base alumina in the Mo-alumina cermet. Some property measurements have been conducted on the new cermet materials being developed to reduce the thermal contraction mismatch, such as the lower vol% Mo cermets, the Mo-V alloys, and the Nb-alumina cermet. The remainder of these characterizations will be the subject of future investigations and reports.

Properties that feed directly into the finite element models (Section 5) are the coefficient of thermal expansion (CTE) as a function of temperature, the elastic modulus as a function of temperature, and the stress-free temperature (discussed in Section 5). A significant effort has been devoted to the evaluation of the accuracy and reproducibility of the thermal expansion data because of the sensitivity of the residual stresses to the thermal expansion mismatch between the CND50 cermet and 94ND2 alumina. The strength data provides an estimate of the residual stress level that we must stay below and can be used along with subcritical crack growth data (not yet measured) as input for lifetime prediction models. All of the property values required for the FEA models have been obtained on the conventional CND50. We have completed measurements of CTE and the elastic moduli at room temperature for lower vol% Mo cermets, and we have the moduli for 20 vol% Mo cermets as a function of temperature. Strength has not been measured for any of the lower vol% Mo cermets.

We have also measured the hardness and fracture toughness for CND50, lower vol% Mo cermet materials, and for a series of cermet materials fabricated by Gary Pressly. Because of the sensitivity of these properties to the processing conditions and density, they serve as a basis for quick comparisons of the quality and uniformity of the cermet material from lot to lot.

We have measured the electrical resistivity of conventional CND50 cermets, Gary Pressly's CND50-like cermets with modified sintering temperatures and glass contents, lower vol% Mo cermets, and the Nb-alumina cermet. This data is critical for determining whether cermets made with a lower vol% Mo or different compositions satisfy the electrical requirements.

Although the bulk of our observations and models suggest that the thermal expansion mismatch is the source of cracking in cermet-containing components, we have also made some observations that suggest that sintering shrinkage differences may produce cracks in some parts. These differences also contribute to distortion of parts during sintering and should be minimized to reduce the amount of machining required to bring the parts to their final tolerance. Machining operations contribute to the cost and time to build parts and are also likely to introduce flaws that might contribute to failure in regions where high residual stresses exist. Shrinkage measurements have been used to identify processing strategies that will minimize or eliminate these differences. We have measured sintering shrinkage differences between the CND50 cermet, lower vol% Mo cermets, and 94ND2 alumina.

CTE Measurements

Introduction

Small differences in thermal contraction behavior between the baseline cermet composition (27 vol% Mo/73 vol% alumina) and 94ND2 alumina result in tensile stresses sufficient to cause cracking in some MC4277 neutron cermet tube geometries. In order to accurately model those stresses using finite element analysis (FEA) and make recommendations for replacement materials, extensive testing was initiated to collect accurate coefficient of thermal expansion (CTE) and contraction (CTC) data. Initial measurements were made using an alumina dual pushrod dilatometer system to collect data over the entire processing temperature range; however, the system measurement error exceeded the difference between the materials expansion/contraction behavior. A fused silica dual pushrod dilatometer system was selected for more reproducible and accurate testing and was used for the CTE and CTC measurements reported in this document.

Experimental Conditions

Thermal expansion/contraction measurements were made on alumina and cermet compositions using a Netzsch dual pushrod dilatometer operated by Denise Bencoe and Dick Brow, Dept. 1833. The fused silica pushrod and support system limited the maximum measurement temperature to 1000°C. A 99.5% alumina standard reference material was selected for these tests because reference materials with similar thermal properties to the unknown (expansion/contraction and conductivity) help minimize measurement error. All tests were conducted in a 15 cc/min flowing argon atmosphere under the following conditions: 1) heat from room temperature to 1000°C at 5°C/min, 2) hold 20 min, and 3) cool from 1000°C to room temperature at 2°C/min. The 20 min hold at 1000°C and slower cooling rate were also selected to minimize error due to thermal gradients in the sample. Sample size was one inch long by approximately 1/8 inch wide and 1/4 inch thick.

Results

All data are reported and compared as contraction strain (delta L/L) versus temperature in Figures 5-8, and a summary in Table 3 compares the average linear contraction calculated over two temperature ranges, 1000 to 37°C and 800 to 37°C. In addition to Figures 5-8 and Table 3, an abbreviated set of tabular data is included in Appendix C, which summarizes contraction strain at 100 degree intervals for all materials tested. An electronic copy of the complete data set for all samples is archived with Bencoe and Brow. Thermal contraction strain data are compared in this report rather than expansion data because differential contraction from the "stress free" temperature is used as direct input for the FEA calculations. Discussion of "stress free" temperature selection is found in Section 5.

The Netzsch dilatometry system can incorporate an internal baseline correction calculated by measuring a standard reference material, in this case alumina, and comparing it to the published standard reference expansion/contraction data. A baseline correction curve was established, and a baseline system correction error was calculated by measuring the alumina reference material five times during the duration required to test the 94ND2 alumina and cermet samples and comparing those values with the original baseline correction curve. A single baseline correction curve was used for all measurements reported in this document, and error bars reflecting slight changes in the system error are presented with data in Figures 5-8. In Figures 5 and 7 error bars on Mo represent a standard deviation based on five and ten alumina reference runs, respectively, and cover the duration over which data plotted in the figures were measured. Error bars on 94ND2 alumina in Fig. 5 represent standard deviation of the delta L/L measurement on five different lots of the 94ND2 alumina. This value is slightly less than the baseline system error indicating very little

difference in the coefficient of thermal contraction (CTC) between these lots of 94ND2. Error bars in Fig. 6 on 94ND2 and on Mo in Fig. 8 represent baseline system error calculated from reference alumina measurements made over the duration required to collect data plotted in the respective figures. Differences in CTC are least resolvable when comparing behavior of 17 to 27 vol% Mo-cermet. The thermal contraction data were supplied for FEA calculations; discussion of residual stress in specific geometries based on CTC mismatch is found in Section 5.

Table 3. Summary of the average linear contraction over the ranges 1000 to 37°C and 800 to 37°C.

Material	Lot-sample #	File ID	Date Meas.	Contract. 1000 to 37°C		Contract. 800 to 37°C	
				$x10^{-6}$/C	avg.	$x10^{-6}$/C	avg.
94ND2	9408-2	M67	3/14/96	8.24		7.9	
94ND2	9408-3	M11	4/4/96	8.43		8.1	
94ND2	9408-4	M67	3/11/96	8.19	8.29	8.07	8.02
94ND2	9311-2	M80	3/26/96	8.23		7.94	
94ND2	916-2	M6	3/27/96	8.46		8.12	
94ND2	9410-2	M80	4/1/96	8.32		8	
94ND2	9411-2	M9	4/2/96	8.32		8.05	
All 94ND2					8.31		8.03
Cermet	27%Mo-1	M65	3/13/96	7.63		7.4	
Cermet	27%Mo-3	M19	4/16/96	7.75	7.69	7.39	7.395
Cermet	23%Mo-1	M73	3/20/96	7.86		7.56	
Cermet	20%Mo-1	M63	3/12/96	7.69		7.42	
Cermet	20%Mo-2	M71	3/19/96	7.82		7.51	
Cermet	20%Mo-3	M12	4/8/96	7.88	7.80	7.59	7.51
Cermet	17%Mo-1	M76	3/21/96	7.82		7.53	
LCAC Mo		M97	6/18/96	6.3		6.17	
Mo12V		M82		6.67		6.47	
Mo15V		M98	6/6/96	6.86		6.62	
Mo18V		M91	6/4/96	6.89		6.64	
Mo28V	ingot 1	M3	5/30/96	8.17		7.92	
Mo28V	ingot 2	M90	6/3/96	7.9		7.66	
75Mo22V3Fe	as cast-1	M57	5/28/96	7.64		7.37	
75Mo22V3Fe	as cast-2	M58	5/29/96	7.7	7.67	7.4	7.39
75Mo22V3Fe	HT std.sint.	M37	9/11/96	7.68		7.4	
75Mo22V3Co	as cast-1	M8	7/24/96	7.67		7.32	
75Mo22V3Co	as cast-2	M10	7/25/96	7.73	7.70	7.42	7.37
75Mo22V3Co	HT std.sint.	M36	9/10/96	7.64		7.36	

Preliminary measurements were also made of the CTE for AlSiMag's 96% alumina vs. their 94% alumina. These measurements were made using the alumina pushrod system and are probably only accurate relatively speaking. At 1000°C, the 96% alumina had a higher CTE by approximately five percent. Use of 96% alumina in the cermet composition could therefore partially counteract the low expansion of the Mo bringing the CTE for the cermet closer to that for 94% alumina.

Mechanical Properties

Elastic Properties

The room temperature to 1100°C Young's modulus (E), shear modulus (G), bulk modulus (B), and Poisson's ratio (ν), were obtained for a slurry-processed CND50 cermet, 94ND2 alumina (lot 9408), and a 20 vol% Mo sample (dry-processed).[16,17] The elastic properties shown in Table 4 were calculated from the longitudinal and transverse wave velocities measured by John Gieske (Org. 9752) using the pulse echo technique. The measurements were made on cylindrical cermet samples with an approximate thickness of 15.65 mm and a diameter of 15.08 mm. The alumina samples were also cylinders and were similar in size.

Table 4. Elastic modulus data for 94ND2 alumina and 20 and 27 vol% cermets.

Material	Density (g/cm^3)	Young's Modulus (GPa)	Shear Modulus (GPa)	Bulk Modulus (GPa)	Poisson's Ratio
94ND2 Alumina (lot 9408) @23°C	3.74	317.0 GPa 46.0 mpsi	127.1 GPa 18.4 mpsi	209.0 GPa 30.3 mpsi	0.25
94ND2 Alumina (lot 9408) @ 1100°C		249.6 36.2	95.1 13.8	222.4 32.3	0.31
CND50 cermet @ 23°C (lot 9511B from lot 9408 94ND2)	5.46±.02	308.4 44.7	123.7 18.0	202.4 29.7	0.25
CND50 cermet @ 1100°C (lot 9511B from lot 9408 94ND2)		235.9 34.2	13.94	20.8	0.23
20 vol% Mo @23°C (lot 9605 from lot 9408 94ND2)	5.08	317.1 46	126.5 18.4	214.1 31.1	0.25
20 vol% Mo @1100°C (lot 9605 from lot 9408 94ND2)		283.1 41.1	112.8 16.4	192.8 28.0	0.26

The data as a function of temperature between 23 and 1100°C are shown in Fig. 9 along with the polynomial fits to the data.

The room temperature Young's modulus (E), shear modulus (G), bulk modulus (B) and Poisson's ratio (ν), were also obtained for dry-processed lower vol% Mo cermet bars (size B bend bars) using the pulse echo technique.[18] Two measurements were made for each sample in the two transverse directions, but the differences were not significant. The data for the average of the two directions are shown in Table 5.

Table 5. Elastic modulus data for dry-processed, lower vol% Mo cermets.

Material	Density (g/cm^3)	Young's Modulus (GPa)	Shear Modulus (GPa)	Bulk Modulus (GPa)	Poisson's Ratio
14 vol% Mo	4.71	335.0	134.8	217.5	0.24
17	4.91	333.2	133.9	217.3	0.24
20	5.09	329.0	131.9	216.9	0.25
23	5.19	320.0	128.3	211.2	0.25
27	5.44	315.6	126.3	209.7	0.25

The Young's modulus values are shown in Fig. 10 as a function of the vol% Mo in the cermet along with the range of values for the 94ND2 alumina and Mo end members.[xii] The modulus increases with decreased Mo content.

The modulus values for Gary Pressly's dry-processed lower vol% Mo cermets, variable glass content cermets, and cermets with variable sintering times are shown in Table 6. These values were also calculated from wave velocities measured using the pulse echo technique.[19]

Table 6. Elastic modulus data for dry-processed, lower vol% Mo cermets.

Material	Density (g/cm^3)	Young's Modulus (GPa)	Shear Modulus (GPa)	Bulk Modulus (GPa)	Poisson's Ratio
B. CND50	5.44	310.3	124.3	205.4	0.25
E. CND50[xiii]	5.43	310.2	124.4	204.5	0.25
G. 200% sinter	5.50	319.4	127.9	211.8	0.25
H. 50% sinter	5.36	298.9	119.9	196.4	0.25
I. 25% sinter	5.28	288.7	116.0	188.1	0.24
J. 0% sinter	5.13	264.3	106.7	169.0	0.24
K. 14 vol%	4.68	331.0	133.5	212.4	0.24
L. 20 vol%	5.03	320.6	128.8	209.5	0.25
M. 36 vol%	5.90	297.3	118.6	200.5	0.25
N. 47 vol%	6.31	267.1	106.7	179.5	0.25
O. 1/2 x glass	5.06	263.7	106.7	166.2	0.24
P. 2x glass	5.33	296.9	119.2	194.5	0.24

The Young's modulus vs. vol% Mo, including the results for the different glass contents (half and double the glass content in CND50) and sintering times at temperature (0, 25, 100, and 200% soak time), are shown in Fig. 11. The modulus increases as the Mo content decreases. The decrease in the Young's modulus as the % soak time decreases and for the lower glass content specimen are due to the lower density of these samples relative to the theoretical density.

Although there are differences in the modulus values for samples that are nominally the same, the trends are the same. The differences in a given set of samples may be due to density differences and differences in sample geometry.

[xii] Ranges of values are given because the modulus is sensitive to the density and processing of the materials.

[xiii] This CND50 cermet is made with primary powder.

Strength and Weibull Parameters

Size B (4.0 mm wide x 3.00 mm thick x 45 mm long) flexure strength specimens of CND50 cermet were prepared and fractured in 4-pt. bending according to ASTM standard C 1161-90.[20] The strengths of the sixteen specimens were ranked from lowest to highest and a standard two parameter Weibull analysis was conducted. The Weibull plot of the strength data is shown in Fig. 12. The average strength was 407 ± 51 MPa. The range in strength values was 293 to 481 MPa. The Weibull modulus, m, was 9, and the characteristic strength was 428 MPa when all 16 data were included. When the lowest strength value, which appears to be an outlier because it is so much lower than the other strengths, was omitted, the average strength was 415 ± 42 MPa, the Weibull modulus, m, was 12, and the characteristic strength was 433 MPa. Gary Pressly found an average strength of 387 MPa for his CND50 specimens with a range of 377 to 418 MPa. Both of these sets of strength data are higher than the ~310 MPa strength measured for 94% alumina using size B bend bars.

Fracture Surface and Flaw Characterization

Several of the fractured CND50 cermet samples were examined optically and with a scanning electron microscope (SEM). The fracture mode is totally intergranular for the Mo phase and primarily intergranular for the alumina phase. The samples generally appear to have failed from surface flaws. Some edge failures were observed. An example of a tensile surface failure is shown in Fig. 13. This specimen appears to have failed from a flaw that may have originated from a fiber or hair in the original powder.

Hardness

Vickers hardness measurements were made on a polished section of a dry-processed 27 vol% Mo cermet bend bar specimen and a set of dry-processed lower vol% Mo specimens. A Zwick 9212 hardness tester was used with indentation loads of 9.8, 19.6, 49.1, and 98.1 N, although the bulk of the measurements were made at 9.8 and 19.6N. Only the latter results are reported. The hardness in GPa was calculated from the length of the indentation diagonals using the formula:

$$H=1x10^{-9}x(0.47P/d^2) \qquad (2)$$

where P= indentation load in N
d= half length of diagonal in m

The results of the 9.8 N measurements on the Sandia samples and the results of 19.6 N measurements on the Pressly samples are shown in Table 7. The number of measurements is shown in parentheses. There is considerable variability in the measurements that can probably be attributed to differences in the samples themselves, different people making the measurements, and the difficulty of measuring the indentation dimensions. An indentation is shown in Fig. 14. The large contrast between the alumina and Mo phases made it difficult to distinguish the edges of the diagonals using an optical microscope.

Table 7. Vickers hardness for dry-processed cermet specimens.

Material	Lower Vol% Mo SNL Specimens Hardness (GPa)	Specimens Fabricated by Pressly Hardness (GPa)	Other Materials Hardness (GPa)
14 vol% Mo	7.96±0.37 (3)	11.17±1.25 (12)	
17	8.72±0.70 (3)		
20	7.85±0.39 (3)	9.39±0.70 (12)	
23	6.43±0.47 (3)		
27	5.89±0.32 (3)	7.62±0.64 (12)	
27 (0% sinter)		5.91±0.51 (12)	
27 (25% sinter)		7.11±0.38 (12)	
27 (50% sinter)		6.83±0.85 (12)	
27 (200% sinter)		8.00±0.48 (12)	
27 (half glass, 3.4 vol%)		5.38±0.38 (12)	
27 (double glass, 12.9 vol%)		8.26±0.70 (12)	
36		5.96±0.48 (12)	
47		4.14±0.31 (12)	
As received Mo			2.54±0.06 (4)
Annealed Mo			2.12±0.11 (4)
94 ND2 alumina*			11.6-12.8
94% alumina (avg. of Wesgo, Alsimag, Diamonite & Coors)			11.0±0.4

* 11.6 GPa from Coors Ceramics 94% alumina property data and 12.8 GPa for 94ND2 alumina from Ref. 21.

Figure 15 shows that the hardness decreases with increasing Mo content, increases with increased sintering time (related to the higher density of the samples at longer sintering times), and increases with increasing glass content. The last effect is also likely related to the higher density with increased glass content. Figure 15 also shows the rule of mixture predictions for hardness based on the hardness values of the end members, 94ND2 alumina and annealed Mo. Because the predicted values are generally higher than the measured values and the difference becomes larger as the Mo content increases, it appears that the hardness measured for the as-received and annealed Mo may not be representative of the Mo in the cermet. There may be a change in the Mo composition that produces a lower than expected hardness. There may also be interactions between the Mo and alumina that produces a composite with a lower than predicted hardness. Because of the variability in the data, hardness values should only be used to distinguish process or lot differences using measurements made by the same person on the same measurement system.

Fracture Toughness, K_{IC}

Fracture toughness values were obtained for dry-processed CND50 cermets using indentation crack length measurements,[22] using the same indentations used for hardness measurements. The following equation was used to calculate the fracture toughness, K_{IC}, from the indentation load, P (N), hardness, H (GPa), the Young's modulus, E (GPa), and the crack length, 2c (m).

$$K_{IC}=0.016(E/H)^{1/2}\, P/c^{3/2} \qquad (3)$$

A Young's modulus value of 310 GPa was assumed for the calculation. An average K_{IC} value of 6.0±2.9 MPa$\sqrt{m}$ was obtained for 49.1 N measurements. Few data were obtained because the loads used to produce the hardness measurements produced very limited cracking, and those cracks were very hard to observe using optical microscopy as shown previously in Fig. 14. As such the indentation fracture toughness values obtained should be used only as a very rough estimate of the true fracture toughness of the material. Acoustic microscopy appears to be a more effective technique for identifying the crack length as shown in Fig. 16, which is an acoustic micrograph of indentation in a CND50 cermet sample.

Fracture toughness values were also obtained using the indentation strength in bending test,[23] in which an indentation is made on the tensile surface of a bend bar and the sample is then loaded until it fractures. Indentations were made at loads of 9.8, 49.1, 78.5, 98.1, and 245.3 N. Two or three samples were indented at each load. The fracture toughness was calculated using the indentation load, P, the fracture strength, σ_f, the Young's modulus, E (used E=310 GPa), and the hardness, H (used 7.2 GPa), in the following equation; and the values are shown in Table 8.

$$K_{IC} = 0.59\,(E/H)^{1/8}\,(\sigma_f\, P^{1/3})^{3/4} \qquad (4)$$

Table 8. Indentation strength fracture toughness for dry-processed CND50.

Indentation Load (N)	Avg. Fracture Toughness (MPa$\sqrt{m}$)	Std. Deviation (MPa$\sqrt{m}$)	Broke from indent
9.8	4.79	0.20	No
49.1	5.82		2 out of 3
78.5	6.52	0.51	Yes
98.1	6.70	0.1	Yes
245.3	6.58	0.06	Yes

The values obtained for the higher indentation loads, where all of the samples fractured from the indentation load, are probably more representative of the fracture toughness of the material. The average value for these three loads is 6.6 MPa$\sqrt{m}$. For comparison, values obtained for 94ND2 alumina were 3.8±0.1 MPa$\sqrt{m}$ for a 29 N load and 4.5±0.2 MPa$\sqrt{m}$ for a 294 N load.[21] The indented strength of the cermet is plotted as a function of the indentation load in Fig. 17. The slight deviation in the slope (-0.25) from a value of -1/3 suggests R-curve behavior, where the toughness increases as a function of the crack length. This behavior provides the material with a degree of flaw tolerance, i.e., the material is less sensitive to the initial flaw size.

Microstructure

Polished Sections

Cermet specimens were sectioned and polished using conventional metallographic techniques. Figures 18 (a) and (b) show SEM micrographs of un-etched, dry-processed 14 and 27 vol% Mo cermets made for the lower vol% Mo series of specimens. The light phase is the Mo, the gray phase is the alumina and glass, and the dark phase is porosity or pull-out. The Mo phase is fairly uniformly distributed, it is irregular in shape, and often appears to be clusters of Mo particles. The size of the clusters ranges from 1-20 μm. The porosity is also uniformly distributed. At 14 vol% the Mo phase does not appear to be continuous in two dimensions. This is consistent with the fact that this sample was an insulator in resistivity measurements. The connectivity of the Mo phase in the 27 vol% is much higher. Examination of sections made in three directions relative to the original pressing direction did not reveal differences in the microstructure that would indicate that dry-pressing or other processing steps introduce preferred orientation of the Mo phase. Figure 19 is an SEM micrograph of a slurry-processed cermet with 27 vol% Mo. There are no significant differences in the grain sizes of the two phases (compared with Fig. 18(a)), but the distribution of the two phases may be slightly more uniform in this sample relative to the dry-processed cermet.

Gary Pressly's thesis contains a significant amount of information concerning the size and distribution of the Mo, alumina, and porosity in various cermet samples. It also contains SEM micrographs of each of the starting materials.

Fracture Surfaces

Figures 20 (a) and (b) show SEM micrographs of a fracture surface of a dry-processed 27 vol% Mo cermet. In the secondary electron (SE) image, the Mo is slightly lighter in contrast. In the backscattered electron (BSE) image, the Mo is the very bright phase, and the alumina is the dark phase. The Mo phase appears to be clusters of individual Mo particles. The size of the clusters is consistent with observations of the polished cross-section. The size of the individual Mo particles that make up the clusters are generally less than 10 μm. The fracture appears to be totally intergranular (fracture runs between the grains) for the Mo and primarily intergranular for the alumina.

SEM micrographs taken of the same location on a fracture surface at accelerating voltages of 10 and 30 KeV exhibit differences in appearance as shown in Fig. 21 (a) and (b). Because of the deeper penetration of electrons at the higher accelerating voltage, more of the underlying material contributes to the signal, and this produces a fuzzier image. Using a consistent accelerating voltage should be a consideration if microstructural comparisons are being made. A typical EDAX (Energy Dispersive Analysis by X-ray) spectrum for a cermet fracture surface is shown in Fig. 22 (a) and (b) for accelerating voltages of 10 and 30 KeV. At the lower accelerating voltages, the size of the elemental peaks for both the Si and Mo are larger relative to the size of the Al peak compared to the higher accelerating voltage. Due to the lower penetration of electrons at lower voltages, phases such as the grain boundary glass are sampled more than the underlying alumina and Mo. The assumption is that the alumina and Mo grains are covered by a thin layer of glass. Figure 23 is a high magnification SEM micrograph showing the glass phase on alumina grains.

Cermet/Alumina Interface

Examination of fracture surfaces of cermet/alumina samples brazed to Kovar for tensile braze button specimens has shown that there may be glass depletion in both the cermet and alumina materials near the cermet/alumina interface. Figure 24 (a) shows cermet material from a region close to the cermet/alumina interface. Figure 24 (b) shows cermet material from the bulk for comparison. The bulk cermet has a glassier appearance. Presently we do not know whether this is a general observation for the interface region, and a mechanism for glass depletion has not been identified. It may be related to residual stresses at the interface or differential shrinkage during sintering. If this is a general observation, the implication is that material in this region may have different properties than the bulk and may serve as a source of failure if it is weaker. If it is an isolated event, it may have occurred because any region with a low glass content is likely to act as a preferential region for crack initiation and propagation.

Cross sections of the alumina/cermet interface should be examined to determine if glass depletion at the interface is common. Alumina bend bar specimens with a cermet insert have been made as part of the LDRD program on cermets. These are to be used for examining the strength of the cermet/alumina interface. The same specimens will be used for examining the microstructures in both materials as a function of distance from the interface.

Phase Identification

X-ray diffraction measurements were made on cermet samples to determine whether phases other than Mo and α-alumina, such as $MoSi_2$, could be detected. Small differences in composition may influence the shrinkage and CTE measurements. Measurements were also made to determine whether the atmospheres used for CTE measurements (argon) and shrinkage measurements (helium) produced different phases than those observed for samples processed in the normal wet hydrogen environment. As-ground cermet samples are dark gray and shiny. Conventional X-ray diffraction measurements indicated that ground surfaces of the as-processed, variable vol% Mo (14-27%) cermet samples contained only Mo and α-alumina. Surfaces of the samples exposed to helium during the shrinkage measurements were slightly white, and the surfaces of the samples used in CTE measurements were dull gray. These observations suggested that some kind of reaction had occurred.

The silica-based glassy grain boundary and any reaction products from interactions between the Mo, alumina, and the glassy grain boundary are expected to be more apparent on the fracture surface of a specimen because it covers the exposed grains on the fracture surface. As such, grazing angle (2°) X-ray measurements, which sample only the top 1000 Å of the surface of interest, are expected to be more sensitive to detection of phases in this region than conventional normal incidence X-ray measurements. Both kinds of measurements were conducted on the fracture surfaces of a 27 vol% Mo cermet before and after exposure to the argon atmosphere used for CTE measurements. Mo and α-alumina were identified on both samples using both kinds of measurements. The normal incidence XRD measurements of the fracture surface before exposure to argon also showed a trace of what may be aluminum silicate hydroxide ($Al_2Si_2O_5(OH)_4$, PDF#10-446).The surface of a *dry-processed* 27 vol% Mo sample exposed to argon during CTE measurements also showed MoO_2 as a minor phase. This suggests that the sample was exposed to oxygen in the argon atmosphere used for CTE measurements.

The white reaction products that were created during exposure to the helium atmosphere during shrinkage measurements were also expected to be present as very thin layers on the as-sintered surface of the sample. Grazing angle XRD measurements were conducted on *dry-processed* shrinkage samples containing 17-27 vol% Mo. The 17 and 20 vol% Mo samples showed only Mo and α-alumina on the exterior surface and the surface that was ground after the shrinkage measurements. The 23 vol% Mo sample also showed MoO_2 (tugarinovite, PDF#32-0371) on the exterior surface, and the 27 vol% Mo sample showed MoO_2 on both the exterior surface and the surface ground after shrinkage measurements. It may be that all of the samples contain MoO_2, but it is only detected in the higher vol% Mo samples because it is present in sufficient quantities (because of higher vol% Mo) to exceed the XRD detection limits.

Grazing angle and normal incidence X-ray measurements were also conducted on a *slurry-processed* CND50 (27 vol% Mo) cermet shrinkage sample both on the white surface and on a fresh surface that had been exposed by grinding after the shrinkage measurements. The normal incidence measurements of the white surface indicated the presence of a trace of aluminum silicate hydroxide, whereas the grazing angle measurements did not. The fresh surface exposed by grinding showed a trace of MoO_2 using grazing angle measurements, which is consistent with the previous measurements. Differences between the white surface of this sample and the dry-processed 27 vol% sample described previously may be due to processing differences or differences in the helium gas used for the shrinkage measurements.

In summary, there is no evidence from X-ray diffraction measurements that the as-processed cermet samples contain phases other than Mo and α-alumina, although phases that comprise less than 5 vol% are generally below the detection limit for this technique. There is evidence that exposure to helium or argon produces MoO_2 as a reaction product, likely due to the

presence of trace amounts of oxygen. The presence of an aluminum silicate hydroxide phase on the fracture surface of one 27 vol% Mo sample that had not been exposed to either argon or helium and on the white surface of a 27 vol% Mo shrinkage sample exposed to helium may be due to differences in the samples that caused these phases to be present in quantities high enough to be detected.

Sintering Shrinkage Measurements

Differential shrinkage behavior of 94ND2 alumina and Mo-cermet was characterized using a dual pushrod Theta dilatometer system. An alumina pushrod system was used, and these preliminary experiments were limited to thermal cycles of 1500°C because of furnace temperature limitations. All shrinkage experiments were conducted in a flowing helium atmosphere using the following furnace conditions: 1) ramp from room temperature at 1°C /min to 1500°C, 2) hold 5 min, 3) uncontrolled cooling. A standard sintered-processed sample of each composition was used as the reference material for the dilatometry experiments; and we assumed the expansion behaviors were equivalent for the sintered reference and test samples.

Samples of 94ND2 alumina were prepared by uniaxially pressing powder to a density of 2 gm/cm^3 followed by isopressing to 30 ksi and binder burnout at 800°C in wet hydrogen for 60 min. The 14, 17, 20, and 23 vol% Mo-cermet samples were prepared by uniaxially pressing to 5 ksi followed by isopressing to 30 ksi and binder burnout at 500°C in wet hydrogen for 60 min. Samples of CND-50 (27 vol% Mo) cermet were made using the slurry procedure and isopressing to 30 ksi, followed by binder burnout at 500°C in wet hydrogen for 60 min.

Final density and final shrink factor values for data collected in these experiments cannot be compared with normally processed 94ND2 and CND50 because the normal processing temperature of 1625°C was not reached. However, shrinkage behavior at the beginning of sintering process can be compared and is shown in Fig. 25. These data are reported as Delta L/L (%) versus temperature and show very little difference in initial shrinkage behavior of the Mo-cermets (14, 17, 20 and 23 vol% Mo) and 94ND2 alumina. However, shrink factor differences are observed for CND50 and 94ND2 alumina pieceparts, 1.18 and 1.16 respectively, after processing under standard conditions, i.e., 1625°C, hydrogen atmosphere for 2.5 hr. In addition, warpage of co-sintered CND50 and 94ND2 pieceparts supports the occurrence of differential shrinkage. The preliminary shrinkage data is reported; but, because of temperature limitations in the current measurement system, further shrinkage characterization will be deferred until a new measurement system capable of the 1625°C temperature cycle is available.

All samples showed some white surface discoloration following shrinkage experiments. These samples were examined using XRD as discussed in the previous section to determine if oxidation had occurred.

Electrical Resistivity

The electrical resistivity measurements shown in Table 9 were made using a four terminal measurement procedure. Measurements were made on cermet bars that were approximately 0.5 cm x 0.5 cm x 2.6 cm. Two terminals were attached to the ends of the bar and were connected to a constant current source (0.5 and 1.0 A). The potential was measured across the two inner terminals. The voltage and current were measured with a Hewlett Packard Model 3458A multimeter. Other details of the electrical resistivity measurements can be found in the Nov. 14, 1996 memo from O. Solomon to R. Moore on "Cermet Measurements." This memo includes a description of the investigation of various methods for attaching the current supply and voltage sensing leads to the bars and the analysis of the repeatability and uncertainties in the electrical resistivity measurements. Three trials each for currents of 0.5 and 1.0 A were made for five different 27 vol% Mo samples. Each trial consisted of ten measurements. The standard deviation for the five samples ranged from 5.7×10^{-8} to 3.6×10^{-6} ohm-cm. The overall standard deviation for all measurements made on the 27 vol% Mo samples was 2.8×10^{-6} ohm-cm. The resistivity values for Pressly's cermet samples are also shown in Table 9.

Table 9. Measured resistances and calculated resistivities for lower vol% Mo cermets.

Vol% Mo	Resistivity (ohm-cm) of SNL cermets	Resistivity (ohm-cm) of Pressly cermets
14		6.61×10^{8}
20	9.5×10^{-4}	2.6×10^{-3}
27	2.4×10^{-4}	2.7×10^{-4}
27 (0% sinter)		3.7×10^{-4}
27 (25% sinter)		3.1×10^{-4}
27 (50% sinter)		3.0×10^{-4}
27 (200% sinter)		2.7×10^{-4}
27 (half glass, 3.4 vol%)		3.8×10^{-4}
27 (double glass, 12.9 vol%)		2.9×10^{-4}
36		7.84×10^{-5}
47		3.74×10^{-5}

The SNL and Pressly cermet data are shown in Fig. 26 as the logarithm of the resistivity vs. the Mo volume fraction. The percolation threshold for electrical conductivity occurs at ~16 vol% Mo. The values measured for the 27 vol% Mo cermets are below the maximum value specified in the Sandia Specification (SS292680-200)[xiv] that states a maximum resistivity of ρ=0.0005 ohm-cm at 25±2°C. The Pressly resistivity values are slightly higher than the SNL values for similar compositions. This may be due to slight differences in the samples or the measurement technique.

The resistivities predicted with McLachlan's General Effective Media equations,[13] assuming a conductivity of 1.33×10^{5} $(\text{ohm-cm})^{-1}$ for the high conductivity Mo phase and 1×10^{-14} $(\text{ohm-cm})^{-1}$ for the low conductivity alumina phase and a value of t=1.7, are also shown in Fig.

[xiv] SS292680-200 - Issue J, Issued 8/15/81.

26. The experimental values measured at SNL for the 20 and 27 vol% Mo samples agree well with the predictions.

As the resistivities for Pressly samples sintered for various sintering times and the half and double glass samples are tightly clustered on the log scale in Fig. 26, the same data are shown on an expanded scale in Fig. 27. On this scale it can be seen that the half glass sample has the highest resistivity. This may be related to the lower density of this sample and the likelihood that the connectivity between the Mo particles was lower. The double glass sample has a slightly higher resistivity than the regular CND50 cermet. This result may be due to the fact that despite the higher density, there is a greater vol% of the glass phase, which is expected to reduce the overall conductivity. The resistivity decreases steadily as the sintering time increases, which may also be related to the increased specimen density.

Historical electrical resistivity data from Lockheed Martin Specialty Components (LMSC) on CND50 batch qualification test samples from 11/05/81 to 12/19/91 gave an average volume resistivity of 3.18×10^{-4} ohm-cm, which is consistent with the values shown in Table 9. Kramer et al.[6] found values of 1.0×10^{-2} and 1.4×10^{-3} ohm-cm for 27 vol% Mo samples fired at temperatures of 1500 and 1600°C respectively. These values are higher than those measured at SNL and by Pressly, which may be a result of a difference in measurement technique.

5. FEA Modeling of Cermet Components

Finite element calculations have been performed to simulate the residual stresses developed during the manufacturing of four cermet components used in the MC4277 and MC4300 neutron tubes. The components, include the Target Feedthru Insulator (Fig. 1b), Target Insulator (Fig. 1c), Backup Ring, and Source Feedthru (Fig. 1a). Radial cracks have been observed in the alumina portion of the Target Feedthru Insulator. The calculations were performed to assess the residual stress distributions in the various components due to thermal contraction mismatch between 94% alumina and CND50 and to determine the effect of using lower vol% cermets on the residual stresses in these components. All of the finite element calculations were performed using JAC3D,[24] a quasistatic finite element code developed at Sandia National Laboratories.

Model Inputs

Model Geometry

The finite element models of the various cermet components are shown in Fig. 28. The Target Feedthru Insulator (1508 nodes and 1406 elements), Target Insulator (1222 nodes and 1141 elements), and Backup Ring (195 nodes and 168 elements) are axisymmetric geometries, whereas the Source Feedthru (29,889 nodes and 27,180 elements) is a three-dimensional geometry due to the asymmetric placement of the cermet feedthrus. The Source Feedthru model takes advantage of half symmetry by constraining all of the nodes on the symmetry plane to displacement within this plane.

Material Properties

The temperature dependent material properties of CND50 cermet alloy (27 vol% Mo) and 94ND2 alumina are given in Table 10.[25,26] It should be noted that all of the stress predictions presented in this report are based on 1000°C to room temperature thermal contraction (CTC) data, which were extrapolated to the temperature interval of 1200°C to room temperature (based on the 900 and 1000°C data). Typically, the differential in the CTC's of alumina and cermet increases for a greater temperature range. Hence the residual stresses at room temperature are larger than those at any intermediate temperatures during cooling. All results here are for room temperature conditions as this represents the highest stress state experienced during the sintering process.

Table 10. Temperature Dependent Material Properties for 94ND2, CND50, and 20% Mo Cermet.

	94% Alumina (94ND2)			CND50 (27% Mo)			20% Mo		
Temp (°C)	Modulus, ($\times 10^6$ psi)	Poisson's Ratio, v	Thermal Strain	Modulus, ($\times 10^6$ psi)	Poisson's Ratio, v	Thermal Strain	Modulus, ($\times 10^6$ psi)	Poisson's Ratio, v	Thermal Strain
50	46.49	0.240	1.38×10^{-4}	44.88	0.256	2.14×10^{-4}	45.72	0.257	1.94×10^{-4}
100	46.15	0.242	4.92×10^{-4}	43.73	0.264	5.49×10^{-4}	44.76	0.267	5.35×10^{-4}
200	43.53	0.268	1.15×10^{-3}	39.91	0.265	1.17×10^{-3}	42.03	0.290	1.16×10^{-3}
300	41.43	0.287	1.89×10^{-3}	37.63	0.262	1.86×10^{-3}	39.61	0.311	1.86×10^{-3}
400	41.02	0.288	2.69×10^{-3}	37.63	0.267	2.60×10^{-3}	38.56	0.323	2.62×10^{-3}
500	41.69	0.278	3.55×10^{-3}	38.86	0.276	3.37×10^{-3}	39.16	0.320	3.41×10^{-3}
600	42.41	0.267	4.43×10^{-3}	39.97	0.282	4.18×10^{-3}	40.86	0.306	4.23×10^{-3}
700	42.58	0.261	5.32×10^{-3}	40.13	0.278	5.00×10^{-3}	42.46	0.285	5.07×10^{-3}
800	42.21	0.262	6.26×10^{-3}	39.32	0.262	5.86×10^{-3}	42.80	0.271	5.92×10^{-3}
900	41.55	0.266	7.20×10^{-3}	38.03	0.233	6.73×10^{-3}	41.54	0.273	6.80×10^{-3}
1000	40.30	0.276	8.15×10^{-3}	36.61	0.207	7.62×10^{-3}	39.77	0.283	7.70×10^{-3}
1200	32.00	0.33	1.01×10^{-2}	32.00	0.240	9.40×10^{-3}	40.00	0.255	9.51×10^{-3}

Stress-Free Temperature

Prior to sintering, both the alumina and cermet materials are in the powder compact form. When the powder compact is heated to the sintering temperature, the viscosity of the glass phase present in both materials drops to the point that stresses generated in the structure are rapidly dissipated. Upon cooling, the glass viscosity increases. Below a temperature referred to as the "stress-free" temperature, the viscosity is high enough that dissipation of stress cannot occur. Consequently, stresses produced by differential contraction are retained in the structure. To simulate this process, the finite element simulations were initiated at a uniform temperature of 1200°C, the approximate stress-free temperature of alumina (see next section on Model Validation). The finite element model was cooled uniformly to room temperature (25°C), and the resulting residual stresses were computed.

Failure Criterion and Design Stress

Cracking in brittle materials such as ceramics tends to initiate when the largest tensile stress at some point in the material exceeds material's tensile fracture strength. The largest tensile stress at any point in a continuum is one of the *principal stresses*. The directions of the principal stresses, called the *principal directions*, are the orthogonal axes along which the shear stresses are zero. Hence, in three dimensional space there are three principal stresses. The *maximum principal stress* at a given point is the algebraically largest of the three principal stresses and the largest normal stress at that point in any direction. Hence, the potential for crack initiation exists for any point in the material at which the maximum principal stress exceeds the criterion for brittle fracture of the material. The direction of the fractures tends to be perpendicular to the maximum principal stress vector. The tensile strength is determined by both the fracture toughness, K_{IC}, and the flaw size. Because of the wide distribution of flaw sizes in ceramics, the strength typically has a wide distribution. The size of the part also has an effect on the strength, with larger bodies having lower strengths. One way of defining a design stress is the tensile strength (usually measured using a four-point bend test) reduced by a safety factor that accounts for this variability. The strengths used in the present study are the four-point bend strengths of 94% alumina and CND50, which are approximately 45 and 60 ksi (310 and 415 MPa) respectively. The design stresses have been defined as one quarter of the bend strength.[27] This gives ~10 ksi (69 MPa) for 94% alumina and 15 ksi (103 MPa) for the CND50 cermet.

FEA Predictions of Residual Stresses

Because the alumina has a greater CTE than the cermet, the alumina surrounding the feedthrus is placed in tension. The predicted tensile stresses in the cermet feedthrus are consistently well below the 60 ksi bend strength of the cermet. Hence, failure of cermet components typically initiates in the alumina portion of the component. Figure 29 is a plot of the maximum principal stress distribution in the alumina portion of the various cermet components (CND50) at the completion of the sintering process. The location of the largest maximum principal stress is denoted by a "*" on the plot. The largest tensile stress in the Target Feedthru Insulator is 36.1 ksi, below the bend strength of the alumina, but well above its design stress. The maximum stress occurs at the upper edge of the alumina insulator at the cermet/alumina interface, corresponding to the location of the observed radial cracks in the Target Feedthru Insulator. This maximum stress occurs at the surface of the component where crack initiation is more likely to occur. Therefore, cracking in this region is likely. The largest stresses in the other three components are significantly smaller than that in the Target Feedthru Insulator. Furthermore, the largest stresses in these components occur at an internal location where crack initiation is less likely to occur. Hence, cracking in these components is less likely to occur. These results are consistent with experience in manufacturing these components.

The same CTE mismatch calculations were performed using a low vol% cermet (20% Mo) in place of the CND50 (27% Mo) to determine how much the higher CTE of these cermets will reduce the residual stresses. Figure 30 is a plot of the maximum principal stress distribution in the components with the low vol% cermet. The largest tensile stress in the Target Feedthru decreased from 36.1 to 29.2 ksi, nearly a twenty percent reduction in stress but still above the design stress. The location of the maximum principal stress remains the same. Consistent with the Target Feedthru Insulator simulations, the largest tensile stresses predicted in all of the components containing low vol% Mo cermet are approximately twenty percent smaller than the same component using CND50.

Model Validation

Indentation Crack Length Measurements of Stresses

The finite element analysis (FEA) described in the previous section assumed that the residual stress in the cermet/alumina assemblies resulted from cooling from a "set point" of 1200°C at which temperature stress relief from plastic deformation ceased. It also tacitly assumed that "volume constraint", which can limit plastic deformation in certain seal geometries and increase the effective set point, was not active in those analyses. To validate those assumptions, two sets of right circular cylindrical seal assemblies with a cermet core surrounded by an alumina annulus were fabricated. One set contained cermet with 20 vol% Mo, while the other contained 27 vol%. Each set included cylinders with three different alumina annulus thicknesses around a fixed central core with diameter of 0.075 inch. Figure 31 is a schematic of the end face of samples with an OD of 0.2 inch.

We used an "indentation stress" technique to measure local stresses in these seal assemblies and compared those data with FEA results. The indentation stress technique uses a Vickers indenter with a large enough load to produce cracks extending from the diagonals of the indentation. Residual stress present in the material changes the length of the cracks; tensile stress increases the length, while compressive stress decreases it. We limited the measurements to planes perpendicular to the cylindrical axis so that the stresses measured were the hoop and radial stresses in those planes. To ensure that the cracks would be visible in the microscope, these surfaces were polished flat using 0.25 micron diamond paste for the final polish. Indentations were introduced only in the alumina. On each surface four sets of indentations were introduced along radial lines with 90 degree separation between the lines and at least 200 μm between indentations.

The values of residual stress in the seals were determined from the equation

$$\sigma_r = (K_{IC} - \chi_r P / c^{3/2}) / \Phi c^{1/2} \qquad (5)$$

where K_{IC} is the fracture toughness and χ_r is a measure of the force that produces crack growth from the indent (even in the absence of other local stresses). P is the force applied to the indenter, c is the crack length from the center of the indentation, and Φ is a parameter that accounts for the crack geometry. Initially, we used values of 2.60 MPa•$m^{1/2}$ for K_{IC} and 0.0767 for χ_r that had been calculated (using χ_r=0.016$(E/H)^{1/2}$) from the values of E and Hobtained in earlier work on 94ND2 alumina.[21] However, inconsistencies in the stress values indicated that either the value of K_{IC} was too high or that of χ_r was too low. To obtain a value of these parameters for the alumina in the seals, indentations were introduced into stress-free alumina with a range of loads. Those measurements provided a value for the ratio, K_{IC}/χ_r, that implied a value of 2.45 MPa•$m^{1/2}$ for K_{IC}. That value was used to correct the calculations.

Data for one of the samples (20D3L2) are shown in Fig. 32. The sample designation is for a 20 vol% Mo cermet core with an alumina annulus having an OD of 0.2 inch (D3) and a length of 0.05 inch (L2). The indentation data are compared with FEA results that assumed a 1200°C set point. Although the scatter in the indentation data is large, especially at the lower stresses, the agreement is good enough to validate that set point.

To address the question of whether volume constraint might have played a part in determining the stresses in these seals, several of the longer seals (L1 = 0.5 inch) were cut in half on a plane perpendicular to the cylinder axis. Indentations were then introduced onto that exposed plane. The results were essentially identical to those obtained on the end plane of those samples, i.e., the surface that was exposed during fabrication and cooling of the seals. Those results indicate no effect from volume constraint in these geometries and, to the extent that these geometries emulate those in component subassemblies, there should be no effect in those subassemblies.

6. Alternative Processing Routes

During processing, sintering shrinkage differences between the cermet and alumina materials produce shape distortions. These distortions add to the time and expense of post-firing machining that must be completed to shape the parts to their final dimensions. Additionally, stresses generated by CTE mismatches may produce cracking. Cracking raises performance and reliability issues. Possible solutions to the aforementioned problems include changing the compositions of the ceramic and cermet materials to minimize the CTE mismatch and modifying the processing to minimize or eliminate warping. Several alternative processing techniques have been evaluated to various degrees. One alternative is a minor modification to the current process where a 20 vol% Mo-Al_2O_3 has been fabricated instead of a 27 vol% cermet. Cermets with this composition were fabricated, and we have completed almost a full range of tests on this material as described earlier in this report. Additional details are provided in the following section. Another approach uses a Mo alloy with V, Fe, and Co additions to increase the CTE to a value closer to that of 94ND2 alumina. Although the greatest effort has been devoted on the development of this alternative through funding provided by a Laboratory Directed Research and Development,[28] the development of new alloys is still in the early stages, with current work focusing on producing fine Mo alloy powders that can be mixed and co-sintered with 94ND2 alumina to produce cermets. Nb also has a very good CTE match with alumina (Avg. CTE from 18-1000°C=$7.88x10^{-6}$/°K). Experiments were conducted on Nb-Al_2O_3 cermets to examine the feasibility of replacing Mo with Nb in a cermet body. This study included sintering experiments and characterization of some of the properties of Nb/alumina cermets. The final alternative processing routes address the problem of differential shrinkage. Two approaches have been utilized, and they can be used together. The first uses AlSiMag 614 (96% alumina) instead of 94ND2 alumina and the second uses the concept of ensuring that the 94ND2 alumina and slurry-derived cermet have equal starting relative densities prior to sintering. Bi-laminate compacts were made to study and develop this concept.

Lower Vol% Mo Cermets

The approach for reducing the thermal mismatch stresses between cermet and alumina regions of neutron tube components by using lower volume percents of Mo in the cermet was based on the fact that less Mo would produce a cermet with a CTE closer to that of the base alumina. The lower limit for the Mo content was dictated by the amount of Mo that would still produce a conductive cermet with sufficiently low resistivity. The lower limit is dictated by the percolation threshold, which for a three-dimensional equiaxed microstructure, is generally in the range of 15 vol%.[29] For some applications there is no requirement for low resistivity but the cermet must be able to be directly brazed to with an active element braze such as Nioro ABA™.[xv] The ability of the lower vol% Mo cermet to satisfy this requirement was measured using tensile braze button pull tests according to the ASTM standard F19-64.[30] The advantages of a lower vol% Mo cermet over using new Mo alloys or using Nb instead of Mo are that the lower volume percent Mo alloy requires only minor processing modifications, and the properties of this cermet are only incrementally different than those of the CND50 cermet (27 vol% Mo).

The processing of the lower Mo content cermets was the same as described in Section 3. A series of cermets with Mo contents of 14, 17, 20, and 23 vol% was fabricated. Because the 17 vol% sample was too close to the percolation threshold (15-16 vol% as shown in Fig. 26), the 20 vol% sample was chosen as the lower vol% Mo alternative to the 27 vol% Mo in the CND50 cermet. Measurements of some of the properties of the series of lower vol% Mo cermets are described in Section 4. Some of the measurements were made only on the 20 vol% Mo cermet. The reduction of the predicted residual stresses was described in Section 5 for cermets with 20

[xv] Wesgo Technical Ceramics and Brazing Alloy, Belmont, CA 94002.

vol% Mo. The trends in the properties appear to follow a rule of mixtures model for composite properties.

$$A_{(X+Y)} = V_x \bullet A_x + V_y \bullet A_y \quad (6)$$

where A=property
V=volume fraction
X=phase 1
Y=phase 2

As the vol% Mo in the cermet decreases, the property moves closer to the properties of the alumina. For example, as the content of the lower expansion Mo phase decreases, the CTE moves closer to that of the higher expansion 94% alumina.

Recent work has evaluated Nioro ABA™-brazed tensile buttons with 20 vol% Mo cermet inlay in relation to previous work (FY94-5) performed on 27 vol% Mo cermet tensile buttons.[31] Using a dry hydrogen atmosphere, three different braze process profiles were examined, as described in Ref. 31. Hermetic joints have been achieved with both volume fractions Mo cermet tensile buttons. However, the tensile button fracture strength data are consistently lower for the 20 vol% Mo cermet as opposed to the 27 vol% cermet buttons. This trend is illustrated in Fig. 33, which presents tensile button results obtained with Process III (peak temperature = 1015°C, 1 min. hold at peak temperature). These results - and the data from both Process I (1000°C/5 min) and Process II (1015°C/5 min.) - indicate that the 20 vol% Mo cermet buttons have average strengths that are lower than with the 27 vol% Mo cermet buttons. On the other hand, the tensile button strengths obtained with monolithic 94ND2 buttons are comparable to that of the 20 vol% cermet buttons, while the data for the monolithic AL-500 buttons are somewhat lower.

Fractographic examination of the 20 vol% Mo cermet inlay buttons indicate that the tensile failures always initiate at an excess braze ball located on the outer diameter (OD) of the braze joint. Individual braze balls are located on the OD of all of the brazed 20 vol% Mo cermet samples. These braze balls are expected to contribute to the lower observed strengths in these samples by serving as stress riser sites for crack initiation. We are currently examining the 27 vol% Mo cermet tensile button samples to locate and identify their fracture origins.

New Mo Alloys

Introduction

Because of its excellent wet hydrogen compatibility at temperatures in excess of 500°C, the idea that a Mo base alloy could be made with an appropriate binary addition to increase the CTE while maintaining good hydrogen compatibility was pursued. An experimental effort was launched during the spring of 1995 to examine promising candidate binary additions to Mo, investigating CTE, microstructure, and hydrogen compatibility. The results are summarized below. Additional details can be found in Ref. 32.

A survey of binary phase diagrams and thermal expansion behavior of binary Mo-X alloy systems[33] suggested that both binary Mo-V and Mo-Cr alloys were candidates. Previous work[34] on these binary alloys indicated that increases in CTE relative to the properties of unalloyed Mo could be realized. However, due to the relatively high vapor pressure of Cr, it was decided that Mo-Cr alloys would not be compatible with the vacuum bakeout process. For example, the vapor pressure of elemental Cr reaches 10^{-6} and 10^{-4} Torr at the respective temperatures of 838°C and 970°C. Both of these values are incompatible with the use of high vacuum furnace equipment, and thereby eliminated Cr as a candidate alloying element. No such limitation existed with the binary Mo-V alloys, and their use appeared to be feasible, as indicated by the CTE tabulated in Ref. 34. Thus, a number of binary Mo-V alloys were produced in laboratory batches to permit evaluation of CTE, microstructure, and hydrogen compatibility. Subsequent work has concentrated on developing a ternary alloy that will allow us to reduce the amount of vanadium needed to increase the CTE; this later work has concentrated on Fe or Co ternary additions.

Materials Preparation and Experimental Procedures

Experimental alloys were fabricated as small, cylindrical ingots using a small furnace equipped with a non-consumable tungsten electrode and a water-cooled copper hearth. Both powder and wire were used as the starting materials, with a total starting weight of 180-200 gms. In order to achieve homogeneity, the buttons were remelted five times prior to being cast into a cylindrical shape approximately 1.5 cm diameter by 10 cm length. Following fabrication, slices from the ingot top and bottom were examined metallographically. Longitudinal CTE samples were fabricated from sections cut generally from the top of the ingot. Multiple samples blanks were cut using wire EDM from a full cylindrical section of the ingot and were subsequently ground to final specimen dimensions of 4 x 4 x 25.4 mm.

Following thermal expansion tests, the CTE samples were metallographically mounted, ground and polished, and quantitative electron microprobe analysis (EMPA) was performed. Probe linescans with points spaced approximately 80 μm apart were run along the length of the CTE samples, with approximately 300 points acquired for each sample. These linescans were averaged to obtain the "mean" alloy compositions shown in Table 11.

Table 11. Results of quantitative electron microprobe analyses of CTE samples. Data (wt.%) were obtained from the length of each CTE sample and are presented as average composition (± standard deviation) based on 300-320 points. Note: the ternary alloys represent avg. of two data sets obtained from adjacent CTE samples.

Nominal Alloy	Vanadium	Molybdenum	Cobalt	Iron
Mo-12.4V	10.91 (1.20)	89.09 (1.43)		
Mo-15.5V	12.61 (1.34)	87.39 (1.67)		
Mo-18V	15.32 (0.91)	84.68 (1.24)		
Mo-28V, #1	30.82 (2.30)	69.18 (2.57)		
Mo-28V, #2	29.00 (1.77)	71.00 (2.04)		
Mo-15V-9Fe	13.89 (1.51)	77.94 (4.52)*	0.00 (0.00)	8.17 (3.32)*
Mo-15V-10Co	13.72 (2.06)	79.06 (11.39)*	7.21 (9.14)*	0.01 (0.01)
Mo-22V-3Fe	21.50 (1.54)	76.10 (2.55)	0.04 (0.028)	2.37 (0.86)
Mo-22V-3Co	20.99 (1.46)	76.56 (2.73)	2.43 (1.29)	0.02 (0.014)

* Large standard deviations for these two alloys are attributable to their two-phase microstructure.

Characterization of Binary Mo-V Alloys

All of the binary Mo-V alloys studied were found to have a single phase BCC microstructure. These results are consistent with published phase diagrams, which indicate a continuous series of solid solution alloys across the Mo-V diagram.

On-heating dilatation data for the various binary Mo-V alloys studied, the 94% alumina ceramic (94ND2), and unalloyed Low-Carbon Arc-Cast Molybdenum (LCAC Mo) are shown in Fig. 34. Clearly, the addition of V to pure Mo leads to a monotonic increase in the thermal expansion of the binary alloys. A summary CTE trend curve for the Mo-V alloys and the 94ND2 is shown in Fig. 35. The CTE data for the binary Mo-V alloys were well fit by a polynomial equation, as shown in Fig. 35. These data indicate that a precise fit to the center of the CTE range for the 94ND2 is obtained at a binary composition of about Mo-32.5V. Tabulated average CTE results for both on-cooling and on-heating data, along with the apparent density of the various alloys, are shown in Table 12.

Table 12. Average thermal expansion (between 37 and 1000°C) for the various alloys studied. Note that both on-cooling and on-heating data are included. The last column contains density measurements acquired from CTE samples.

Nominal Alloy	Actual Composition	Avg. CTE **On-Cooling** (10^{-6}/°C)	Avg. CTE **On-Heating** (10^{-6}/°C)	Density (gm/cc)
LCAC-Mo	100 Mo	6.302	6.262	
Mo-12.4V	Mo-10.9V	6.674	6.803	9.411
Mo-15.5V	Mo-12.6V	6.867	6.903	9.265
Mo-18V	Mo-15.3V	6.895	7.104	9.114
Mo-28V, #2	Mo-29.0V	7.908	8.090	8.522
Mo-28V, #1	Mo-30.8V	8.172	8.244	8.349
Mo-22V-3Fe	Mo-21.0V-2.4Co	7.705*	7.625*	9.005
Mo-22V-3Co	Mo-21.5V-2.4Fe	7.679*	7.702*	9.015
Mo-15V-9Fe	Mo-13.7V-7.2Co	7.930	7.580	--------
Mo-15V-10Co	Mo-13.9V-8.2Fe	7.770	7.640	--------

* Data represents average of two runs from two separate specimens.

It is also interesting to compare the dilatation results obtained by Prindantseva and Solov'eva[34] with those of the present study. To do this, all of the dilatation data for the binary were fit to a polynomial equation, and the average CTE's between 20 and 800°C were computed. Both on-heating and on-cooling data were included. Figure 36 shows the results of this comparison. Note that there is reasonably good agreement between the results of the present study and Ref.[34] over the range of composition studied.

Wet Hydrogen Compatibility Tests

Extra CTE specimens were used to evaluate the materials' compatibility with the wet hydrogen atmosphere used to sinter the Mo-Al_2O_3 cermet materials. As mentioned in Section 3 (Processing) a wet hydrogen atmosphere is used to ensure oxidation and removal of the organic binder without oxidizing the Mo. Samples were polished with 1 μm diamond paste and then weighed using a Mettler Model M5 microbalance. The samples were then subjected to the standard 3 hr/1625°C wet hydrogen sintering treatment, in most cases using furnace runs that were also being used to sinter development cermet piece parts. The results of these tests were expressed in terms of the normalized weight gain (weight gain divided by surface area of the sample) and are presented in Table 13. The "control" sample of LCAC-Mo exhibited a small weight loss that was presumed to be a result of the reduction of surface oxide during the sintering run. The results for the two binary alloys indicate that there is an increasing tendency for weight gain as the vanadium content is increased. While some of the vanadium oxide formed as an external scale, results discussed in the ternary alloy section indicate that some of the oxidation is internal. These trends in normalized weight gain with respect to increasing V content, led to efforts to develop ternary Mo-V-Co and Mo-V-Fe alloys with slightly reduced V content for the cermet application. Data for Nb are included in Table 13 because of its attractive CTE relative to the 94ND2 alumina. Extensive oxidation and scale spallation was observed in the case of the Nb sample studied. As the weight gain results in Table 13 indicate, the use of Nb as metallic phase in cermets would require sintering atmospheres other than wet hydrogen.

Table 13. Weight gains after exposure to the wet hydrogen atmosphere for 3 hr at 1625°C. Where data from multiple samples are available, the average normalized weight gain is shown, along with the standard deviation.

Nominal Composition	Actual Composition	Number of Samples	Normalized Wt. Gain (gm/cm^2)
LCAC-Mo	100 Mo	1	-1.37E-5
Mo-12.4V	Mo-10.9V	3	2.44E-3 ± 7.25E-5
Mo-28V #1	Mo-30.8V	3	9.46E-3 ± 9.79E-6
Mo-22V-3Co	Mo-21.0V-2.4Co	5	5.73E-3 ± 5.95E-4
Mo-22V-3Fe	Mo-21.5V-2.4Fe	4	6.46E-3 ± 3.71E-4
Unalloyed Nb	100 Nb	1	2.32E-2

We successfully made coarse binary Mo-28V alloy powder using the Plasma Rotating Electrode Process (PREP). The ingot feedstock for the PREP process was a triply melted vacuum arc remelt (VAR) ingot, 12.7 cm in diameter and 17.8 cm long. We are in the process of developing planetary milling parameters that will allow us to process the coarse PREP powder into finer (~10 μm size) powder that can be used for exploratory cermet sintering experiments.

Ternary Mo-V-Co and Mo-V-Fe Alloys

In an effort to minimize the amount of vanadium oxide formed when samples were exposed to the conditions of the wet hydrogen sintering process, ternary additions of Fe and Co were studied. Both were identified as elements that could increase the CTE of Mo-V binary alloys and afford a good possibility of preserving/promoting hydrogen compatibility. The first two ternary alloys investigated had nominal compositions of Mo-15V-10Co and Mo-15V-9Fe. The thermal expansion of both of these alloys (see Table 13 and Fig. 36) indicates that the Fe and Co additions caused an increase in CTE relative to the comparable Mo-V binary alloy. However, microstructural examination of these alloys indicated that these alloys are not single phase. The extensive second phase observed in the Mo-15V-9Fe alloy was identified as Mo_6Fe_7 using EMPA, while Mo_6Co_7 was found in the Mo-15V-10Co alloy. Both line compounds are brittle intermetallics and have relatively low melting points (1550-1600°C). They are not considered suitable for use in cermet materials.

A subsequent examination of the ternary phase stability of the Mo-V-Fe system[35] shows that at 897°C, the maximum amount of Fe that can be added to a 75 wt% Mo alloy and still remain in the single phase BCC region is ~3.5 wt% Fe. Thus, two additional alloy ingots were made with nominal compositions of Mo-22V-3Co and Mo-22V-3Fe. Electron microprobe analysis of CTE samples cut from these ingots indicated actual compositions of Mo-21.0V-2.4Co and Mo-21.5V-2.4Fe (see Table 12). Optical microscopy of both alloys in the as-cast condition indicates that both alloys are single phase BCC. The on-heating dilatation behavior of these alloys is compared to that of the 94% alumina ceramic and LCAC-Mo in Fig. 37. Clearly, the thermal expansion behaviors of these two ternary alloys are consistent with the trend curve for binary Mo-V alloys shown in Fig. 35, with the Fe or Co additions leading to modest increases in CTE relative to the trend curve prediction for a simple binary Mo-21V alloy.

Additional CTE samples of both the Mo-22V-3Co and Mo-22V-3Fe alloys were also subjected to the 1625°C/3 hr. wet hydrogen sintering treatment; the results of those tests are included in Table 13. It would appear, based on comparison with the weight gain results for the two binary Mo-V alloys in Table 13, that the Co and Fe additions have little effect on the weight gain behavior. In other words, one would expect a straight binary Mo-21V alloy to have a normalized weight gain of 5-6 x 10^{-3} gm/cm^2 for the standard sintering treatment, which is consistent with the range of data observed for the two ternary alloys.

Microstructural examination of the Mo-22V-3Fe alloy subjected to the conditions of the sintering process indicated that some of the weight gain attributable to oxidation of vanadium is internal oxidation. Optical micrographs of a treated sample indicated the presence of a second phase located near the grain boundaries. Such a second phase was not observed in the as-cast condition and was analyzed using EMPA. Spot EMPA analysis indicated that the second phase is slightly oxygen rich VO, with an average of five points yielding the following results: V 46.306 ± 0.229 at.%, O 53.508 ± 0.286, Fe 0.024 ± 0.022, and Mo 0.164 ± 0.183. A similar second phase indicative of internal oxidation was observed in the treated Mo-22V-3Co alloy. However, the micrographs for this alloy indicated that the internal oxidation is somewhat more extensive than for Mo-22V-3Fe.

On the basis of the behavior after exposure to the sintering conditions, and the relative cost of Fe to Co, a decision was made to pursue powder production of the Mo-22V-3Fe alloy. Small (100 gm) quantities of this material have been produced at the University of California, Irvine using a mechanical alloying method. We are currently in the process of pressing this powder into CTE samples; and once the CTE data is generated, we will begin evaluation of cermet sintering using this powder. Efforts have also been initiated to make a bulk electrode of the Mo-22V-3Fe, to produce coarse powders via the Plasma Rotating Electrode Process (PREP), followed by planetary milling using WC media to obtain fine powders.

Nb-Alumina Cermets

The near CTE match of Nb with Al_2O_3 makes it an ideal candidate to consider as a substitute for Mo in cermet bodies. Additionally, the commercial experience with manufacturing high pressure sodium vapor lamps suggests that Nb-Al_2O_3 cermets can be fabricated using conventional processing equipment and methods. Sodium vapor lamps, which are used by the millions in street lights, are made of a polycrystalline alumina lamp tube sealed to Nb electrodes. These lamps operate for thousands of hours, cycling daily between room temperature and their 1300°C operating temperature. Nb is used because it is an electrically conducting refractory metal that has a CTE similar to that of alumina. Coupled with the aforementioned properties, the fact that Nb powder is readily available (commercially) makes it an ideal candidate to consider as a replacement for Mo in an improved cermet body.

To demonstrate the feasibility of making Nb-Al_2O_3 cermets, to evaluate materials compatibility, and to prepare prototype samples for property tests, 30 vol% Nb powder (Alfa, -325 mesh, 99.9% pure) was mixed with 70 vol% A16sg alumina powder (Alcoa, -325 mesh, 0.3-0.5 μm crystallite size, 99.7% pure) and hot pressed at 1500°C with 5000 psi for 1 hr. Details of this work can be found in Ref. 36. The favorable results of resistivity, strength, and CTE tests on the Nb cermet are given in Table 14.[37]

Table 14. Properties of Nb-Al_2O_3 cermets.

Composition:	30 vol% Nb - 70 vol% high purity Al_2O_3.
Processing:	hot pressed at 5000 psi, 60 min., 1500°C
Density:	fully dense
Resistivity:	less than 10^{-3} ohm-cm
Strength:	363 MPa avg. (52.7 ksi), 4 pt. bending, surfaces ground to 400 grit
CTE:	30 to 1000°C, 84.6 x 10^{-7}/°C, no hysteresis; 94ND2 alumina is 81.8x10^{-7}/°C

In contrast to hot pressing, conventional, pressureless sintering of Nb-94ND2 alumina at 1630°C for two hr in an atmosphere of 3% H_2 in Ar produced densities <90% of the theoretical density. (NOTE: however, no experiments were conducted with 94ND2 fines, the standard CND50 cermet firing process was not used, and insufficient work was completed to fully optimize the processing of Nb-94ND2 cermets.) Under the same processing conditions, 94ND2 sinters to a density of 3.68 g/cm^3 (95% relative density). Slight improvements in Nb-94ND2 cermet density were achieved by increasing firing times and temperatures, and significantly higher density was achieved after attritor milling the precursors (i.e., reducing the particle size). Even higher Nb cermet densities were routinely achieved with Alcoa A16 alumina as the ceramic precursor. A16 is a high-purity alumina with a fine particle size of 0.3 to 0.5 μm (versus the 5-10 μm average particle size of 94ND2). The data suggest that the densification of the Nb-94ND2 cermet may be limited by the precursor particle size and that the reduction of the 94ND2 particle size may be a key to successful sintering of these materials.

To determine if undesirable interactions between the Nb and the glass phase in 94ND2 could be responsible for the poor sintering of Nb-94ND2 cermets, wetting experiments were conducted at 1630°C in 3% H_2 in Ar. The results indicated that Nb is compatible with and bonds well to both the 94ND2 alumina and the CaO-MgO-Al_2O_3-SiO_2 glass (inorganic binder) phase alone, indicating the glass phase is not a problem for processing. In fact, without the glass phase, the Nb does not bond to alumina.

Nb is a highly reactive metal, with thermogravimetric analysis experiments showing that it oxidizes readily in air at ~400°C. Because 94ND2 alumina contains ~4 wt% organics that burn out (i.e., pyrolyze) during firing, it is possible that the Nb could partially oxidize during firing, which would inhibit sintering. Likewise, if the binder burnout step is carried out in a non-oxidizing atmosphere, it is conceivable that niobium carbide could form, which also would inhibit sintering. Because of Nb's reactivity, it is likely that the wet hydrogen firing process used to make CND50 cermets will not be suitable for processing Nb-94ND2 alumina cermets. As such, if Nb is to be used as a replacement for Mo in cermet bodies, the processing will have to be optimized accordingly.

Alternative Cermet Processing

Warping during sintering has been attributed to differential shrinkage between the cermet and ceramic phases (i.e., processing issues). Warping and the sintering shrinkage differences arise due to the differences in relative densities between the cermet and alumina phases in the subassembly. The cermet, which is formed using a slurry process, has a higher relative density (~58%) than the dry-pressed alumina ceramic (~52%) after uniaxial pressing. Consequently, the ceramic shrinks more than the cermet during sintering, distorting the shape of the subassembly. The warping can be eliminated when the cermet and ceramic phases are formed to the same relative density prior to sintering. This concept was demonstrated initially by Mike Readey using bilaminate samples.

The concept of minimizing relative density differences in the green powder compact was optimized using the measured compaction response (i.e., the density versus forming pressure compaction curve) of the 94ND2 powder. Alumina dry-pressing conditions were modified to produce the same relative density as the slurry processed cermet. For the 94ND2-CND50 system, warping was minimized by prepressing the alumina to 30,000 psi (versus the ~10,000 psi currently used) prior to machining and back filling with the cermet slurry. The improvement was accomplished without the traditional 30,000 psi isopressing step that follows the cermet slurry filling step, reducing the total number of steps in the process.

Warping was also minimized by substituting AlSiMag 614 (96% alumina) for the 94ND2. The 96% alumina presses to ~58% relative density at ~10,000 psi during die pressing, which is approximately the same density as the cermet body after slurry filling. Again, the key to minimizing warping during sintering is to process the alumina and cermet powders in a manner that produces the same relative density prior to sintering.

7. Summary and Conclusions

Excessive thermal expansion mismatch stresses that led to cracking in some cermet-containing neutron tube components can be reduced to acceptable levels using cermets with higher coefficients of thermal expansion than the CND50 cermet. A higher coefficient of thermal expansion can be produced using a lower volume percent Mo in the cermet; the lower the Mo content the closer the match to the 94% alumina used in neutron tubes. As cermets with 20 vol% Mo produced acceptable resistivity values, this composition was chosen for further evaluation as an alternative to the 27 vol% Mo in CND50. Changes in the Mo content do not adversely affect the other properties of the material such as its strength, toughness, hardness, or elastic moduli. These properties generally follow the simple rule of mixtures model for composite properties. Substituting a 20 vol% Mo cermet for the 27 vol% Mo CND50 cermet in the cermet section of the target feedthru insulator produced a twenty percent reduction in the magnitude of the stress in the region of the 94ND2 alumina with the highest tensile stress. This reduction in stress produced a greater margin of safety between the residual stress and the actual strength of the material.

The coefficient of thermal expansion of the cermet can also be increased by using new Mo alloys with additions of V and Fe. These alloys are being prepared as powders and will be evaluated in mixtures with 94% alumina powder for their sinterability. Nb was also evaluated as a substitute for Mo. Hot-pressed cermets made with Nb had good properties in terms of CTE, resistivity, and strength, but its hydrogen compatibility was not as good as that of the Mo or the new Mo alloy. Additionally, we were unable to sinter Nb-Al_2O_3 cermets to densities greater than 90% of their theoretical density using the current processing parameters used for Mo-alumina cermets. Further optimization of the sintering of this cermet is required.

Several issues are still to be resolved regarding the processing and properties of the current cermet composition and those for cermets with the new Mo alloys. One is the identification of the bonding mechanism between the Mo and alumina. A related question is how reactions between the Mo and the alumina affect the electrical properties of the cermet. The issue of what happens at the interface between the cermet and 94ND2 during sintering and whether there is glass depletion at the interface that might have a detrimental effect on one or both of the materials is unresolved. We are currently examining why tensile braze buttons with the 20 vol% Mo cermets have a lower strength than those with 27 vol% Mo. Processing related issues are the production of a Mo alloy powder with the right particle size distribution, the compaction behavior of cermet powder mixtures with the new Mo alloy, sinterability of these powders, and their sintering shrinkage relative to that of 94% alumina. Properties that will need to be measured for cermets produced with the new Mo alloys are the electrical resistivity, brazeability, thermal expansion behavior, and mechanical properties such as elastic modulus, strength, and toughness.

8. Recommendations

Summarized in this section are recommendations relating to the improvement in the processing, characterization, and modeling of the current cermet materials and recommendations for work to be done to complete our understanding of these materials and the processes used to fabricate them. There are also suggestions for new processing routes, such as gel-casting. There are recommendations relating to alternative compositions; however, much of what should be done next depends on the outcome of the LDRD work on new Mo alloys.

Cermet Composition and Processing Changes

During processing of alumina cermets, the alumina should be pressed to a higher density to match the density of the slurry processed cermet. Another strategy suggested by Gary Pressly's work would be to increase the glass content of the cermet, as higher glass content cermets exhibit a greater degree of shrinkage, and this will bring the cermet closer to the alumina. Both of these changes will minimize the shrinkage differences that lead to warping. If a change in alumina composition is already being made because 94ND2 alumina will no longer be available, a change to 96% alumina should be considered as preliminary results show it exhibits a better CTE match to the cermet.

If the stresses due to CTE mismatch are too large for some configurations and continue to produce cracking, even lower Mo content cermets should be considered where resistivity is not a requirement. In applications where electrical conductivity is required, an investigation of processing modifications that lead to a lower percolation threshold should be considered. Changes to a larger alumina particle size, a smaller Mo particle size, or a change in the shape of the Mo to something that is fiber or whisker-like are all likely to lead to a lower percolation threshold.

For improved reliability and reproducibility, one may consider assessing the feasibility of gel casting cermet components. Gel casting is a near net shape process that could provide manufacturing flexibility for future design of neutron tube components. Direct fabrication techniques may also provide the geometry and compositional flexibility that may be required to make the cermets for the Reduced Pieceparts and Processing (RP^3) neutron tube. To minimize stress mismatches, especially in newly proposed large features, 20 vol% Mo cermets are inadequate. Thus new conductive refractory metals with a CTE match to the alumina need to be identified or developed.

Characterization

There are several tests that remain to be done including measuring the strength of 20 vol% Mo cermets, measuring the cermet-alumina interfacial strength, and examining the interface between the alumina and cermet for glass depletion. Another important measurement that provides the necessary information for reliability and lifetime predictions for Mo-alumina cermets is the rate of subcritical crack growth. Most of the properties that were described in Section 4 will need to be measured for the new Mo alloy cermets. The most important are the CTC, the sintering shrinkage, the elastic modulus, the strength, and the electrical resistivity.

Alternative Compositions and Processing

Further optimization of processing and sintering of Nb cermets should be conducted, as well as testing for compatibility with existing processes and materials. Any higher expansion cermet, whether it be made with a new alloy or Nb, will need to evaluated for its processing under existing process conditions and tested for hydrogen compatibility and brazing.

Research and Development

The conduction mechanism of the cermet material and what role the glass plays are still unknown. The glass has a high silica content and is normally assumed to be an insulator.

The development of empirical process models [e.g., fired bulk density = f(T, t, atm, composition, green density), CTE = f(T, t, atm, composition, green density), etc.] will provide an important tool to allow further compositional and processing flexibility. The development of sound physics-based process models for the same properties will allow even greater flexibility.

Directions for Model Improvement

One area for model improvement would be further testing and validation of the FEA predictions. Our present measurements, although consistent with the predictions, have a lot of scatter and require preparation of special samples. The ultimate model validation would be to make a series of parts that have previously shown a significant incidence of cracking using the new alloy or a lower vol% Mo cermet. A comparison of the number of cracked parts would provide a direct measurement of the improvement due to the minimization of the residual stresses. The feedthru insulator for the MC4277 is one candidate for such a test.

Cermet Design Methodology

Incorporate the FEA models developed in this program into the design methodology.

References

[1] G. A. Pressly, "Characterization of Molybdenum-Alumina Cermets," Master's Thesis, U. of Florida, 1996.
[2] G. S. Brady and H. R. Clauser, Materials Handbook, 12th Edition, McGraw-Hill Book Company, New York, pp. 172-173 (1986).
[3] W. H. Kohl, Handbook of Materials and Techniques for Vacuum Devices, Reinhold Publishing Corporation, New York, 1967.
[4] Patent 4,704,557, "Cermet Insert High Voltage Holdoff Improvement for Ceramic/Metal Vacuum Devices," W. F. Ierna, Seminole, FL, 3/11/86.
[5] Patent 4,488,673, "Direct Metal Brazing to Cermet Feedthroughs," A. C. Hopper, Jr., St. Petersburg, FL, 12/18/84
[6] D. P. Kramer, K. White, and M. D. Kelly, "Effect of Sintering Parameters and Composition on the Resistivity of a Cermet Used as an Electrical Feedthrough," pp. 512-518 in Ceramic Engineering and Science Proceedings, The American Ceramic Society, Vol. 3, No. 9-10, (1982).
[7] M. D. Kelly, "Direct Bonding of Mo and Nb Feedthroughs in Electronic-Grade Al_2O_3," pp. 504-511 in Ceramic Engineering and Science Proceedings, The American Ceramic Society, Vol. 3, No. 9-10, (1982).
[8] M-Y. Kao, "Properties of Silicon Nitride-Molybdenum Disilicide Particulate Ceramic Composites," *J. Am. Ceram. Soc.*, 76 [11] 2879-83 (1993).
[9] J. J. Petrovic, "$MoSi_2$-Based High-Temperature Structural Silicides," pp. 35-40, *MRS Bulletin*, July 1993.
[10] C. O. McHugh, T. J. Whalen, and M. Humenik, Jr., "Dispersion-Strengthened Alumina," *J. Am. Ceram. Soc.*, 49 [9] 486-491 (1966).
[11] A. G. Pincus, "Mechanism of Ceramic-to-Metal Adherence-Adherence of Molybdenum to Alumina Ceramics," *Ceram. Age*, 63 [3] 16-20, 30-32 (1954); p. 17.
[12] J. F. Kelso, R. R. Higgins, and F. J. Krivda, "Effect of Mo Microstructure on the Critical Volume Fraction for Conduction in Mo-Alumina Cermets," *J. Mater. Res.*, Vol. 12 [3] 738-744 (1997).
[13] D. S. McLachlan, M. Blaszkiewicz, and R. E. Newnham, "Electrical Resistivity of Composites," *J. Am. Ceram. Soc.*, 73 [8] 2187-2203 (1990).
[14] A. R. Blackburn and T. S. Shevlin, "Fundamental Study and Equipment for Sintering and Testing of Cermet Bodies; V, Fabrication, Testing, and Properties of 30 Chromium-70 Alumina Cermets," *J. Am. Ceram. Soc.*, 34 [11] 327-331 (1951).
[15] J. R. Hellmann, J. Matsko, S. W. Freiman, and T. L. Baker, "Microstructural-Mechanical Property Relationships in 94% Alumina Ceramics," pp. 367-379 in Tailoring Multiphase and Composite Ceramics. Edited by R. E. Tressler, G. L. Messing, C. G. Pantano, and R. E. Newnham, Plenum Press, NY (1986).
[16] Memo to Roger Moore from John Gieske, Aug. 15, 1995, Elastic Moduli vs. Temperature (RT to 1100°C) for 94ND2 Alumina and CND50 Cermet.
[17] Memo to Roger Moore from John Gieske, May 23, 1996, Elastic Moduli vs. Temperature (RT to 1100°C) for 20% Mo.
[18] Data sheet from John Gieske, 11/3/95
[19] Reference: Data from John Gieske, 1/2/96.
[20] ASTM Standard: C1161-90, Standard Test Method for Flexural Strength of Advanced Ceramics.
[21] A. S. Raynes, "Mechanical Properties and Fatigue Behavior of Metallized Glass-Bonded Alumina," M. S. Thesis, The Pennsylvania State University, May 1989.
[22] P. Chantikul, G. R. Anstis, B. R. Lawn and D. B. Marshall, "A Critical Evaluation of Indentation Techniques for Measuring Fracture Toughness: II, Strength Method, " *J. Am. Ceram. Soc.*, 64 [9] 539-43 (1981).
[23] G. R. Anstis, P. Chantikul, B. R. Lawn, and D. B. Marshall, "A Critical Evaluation of Indentation Techniques for Measuring Fracture Toughness: I, Direct Crack Measurements, *J. Am. Ceram. Soc.*, 64 [9] 533-38 (1981).
[24] J. H. Biffle, "JAC3D - A Three-Dimensional Finite Element Computer Program for the Nonlinear Quasistatic Response of Solids with the Conjugate Gradient Method," SAND87-1305, Sandia National Laboratories, Albuquerque, New Mexico, February 1993.
[25] J. H. Gieske, "Elastic Moduli vs. Temperature (RT to 1100°C) for 94ND2 Alumina and CND50 Cermet," internal memorandum to R. H. Moore, Sandia National Laboratories, Albuquerque, New Mexico, August 15, 1995.
[26] S. L. Monroe, Contraction Data for 94ND2, 27% Mo Cermet, and 20% Mo Cermet, measured 3/96 thru 5/96.
[27] Personal communication from S. Burchett, Org. 9118, Sandia National Labs.

[28] LDRD 3510.530, Effect of Composition and Processing Conditions on the Reliability of Cermet/Alumina Components, Principal Investigators: John J. Stephens and Kevin G. Ewsuk (1995-1997).
[29] J. P. Fitzpatrick, R. B. Malt, and F. Spaepen, "Percolation Theory and the Conductivity of Random Close Packed Mixtures of Hard Spheres," *Physics Letters*, Vol. 47A, No. 3, pp. 207-208, (1974).
[30] ASTM F19-64, Standard Test Method for Tension and Vacuum Testing Metallized Ceramic Seals, 1964.
[31] Memo to G. W. Smith, 2564, and L. A. Malizia, 14482, from J. J. Stephens, 1832, dated October 19, 1995, "Update on FY95 Work - Active Metal Braze Wetting and Tensile Buttons for the MC4277 Tube."
[32] J. J. Stephens, B. K. Damkroger, and S. L. Monroe, "Development of Mo Base Alloys for Conductive Metal-Alumina Cermet Applications," SAND96-1932C, Jan., 1997.(to be published in Proceedings of the 14th International Plansee Seminar, Reutte, Austria, May 12-16, 1997).
[33] J. J. Stephens, Sandia National Laboratories internal memo, dated March 2, 1995.
[34] K. S. Pridantseva and N. A. Solov'eva: Metal Science and Heat Treatment 5-6 (May-June, 1966) pp. 478-480.
[35] V. Rughavan (ed.), Phase Diagrams of Ternary Iron Alloys, Part 6, pp. 997-1003, India Institute of Metals, Calcutta, (1993).
[36] W. F. Fahrenholtz memo to Kevin Ewsuk, Summary of Nb-Alumina Cermet Work, Nov. 12, 1996.
[37] R. E. Loehman memo to Distribution, Nb-Al_2O_3 Cermet Properties, Dec. 21, 1995.

APPENDIX A - Acronyms

BCC = Body Centered Cubic
CND50 = 50 wt% Mo, 50 wt% alumina cermet
CTC = Coefficient of Thermal Contraction
CTE = Coefficient of Thermal Expansion (also known as TCE)
DGME = Diethlyene Glycol Monobutyl Ether
EDAX = Energy Dispersive Analysis by X-ray
EDM = Electron Discharge Machining
EMPA = Electron Microprobe Analysis
FEA = Finite Element Analysis
GENDD = General Electric Neutron Devices Department
LCAC = Low Carbon Arc Cast
LDRD = Laboratory Directed Research and Development
LMSC = Lockheed Martin Specialty Components
MC = Major Component
MC4277 = neutron tube component
OP = Operating Procedures
PP = Pinellas Plant, Largo, FL (operated by GENDD and LMSC)
PDF = Powder Diffraction File
PREP = Plasma Rotating Electrode Process PREP
RP^2 = Reduced Pieceparts and Processing
SEM = Scanning Electron Microscope
SS = drawing prefix that indicates a Special use Specification
TCE = Thermal Coefficient of Expansion (also known as CTE)
VAR = Vacuum Arc Remelt
WR = War Reserve
XRD = X-ray Diffraction
94ND2 = 94% alumina from GENDD/LMSC

APPENDIX B - Selected Information from Gary Pressly's M.S. Thesis

CHARACTERIZATION OF MOLYBDENUM-ALUMINA CERMETS

By

GARY A. PRESSLY

A THESIS PRESENTED TO THE GRADUATE SCHOOL
OF THE UNIVERSITY OF FLORIDA IN PARTIAL FULFILLMENT
OF THE REQUIREMENTS FOR THE DEGREE OF
MASTER OF SCIENCE

UNIVERSITY OF FLORIDA

1996

Abstract of Thesis Presented to the Graduate School
of the University of Florida in Partial Fulfillment
of the Requirements for the Degree of Master of Science

CHARACTERIZATION
OF
MOLYBDENUM-ALUMINA CERMETS

By

Gary A. Pressly

May 1996

Chairman: Dr. J.J. Mecholsky, Jr.
Major Department: Materials Science and Engineering

Molybdenum-Alumina (Mo-Al_2O_3) cermets are metal-ceramic composites that are fabricated by powder processing. Mo-Al_2O_3 cermets have thermal expansion characteristics similar to solid alumina ceramics; this allows the two materials to be hermetically joined by co-firing. A unique characteristic of Mo-Al_2O_3 cermets is that they have the ability to behave as electrical conductors or as insulators simply by varying the molybdenum percentage. An electrically conductive cermet with 50% alumina and 50% molybdenum by weight has been developed for electrical feedthrough in ceramics. The feedthroughs are created by placing cermet powders into vias of ceramic powder compacts and then sintering. The cermet material is exposed on each end of the feedthrough which allows the electrical leads to be brazed directly to the material resulting in significant cost savings over other techniques. These cost savings, along with other factors, have prompted new applications for Mo-Al_2O_3 cermets. Many of these applications require large complex geometries which have resulted in cracking problems during fabrication. Because of these problems the need to fully characterize Mo-Al_2O_3 has surfaced. This endeavor records electrical, mechanical, thermal and microstructural characteristics of Mo-Al_2O_3 cermet material over a compositional range

of 30% to 70% molybdenum by weight. The investigation focuses on the 50% molybdenum by weight composition and documents how its properties evolve during the fabrication process and how the glass composition affects properties.

It is shown that as the soak time at sintering temperature increases, the shrinkage and density increases. As the percentage of molybdenum increases, the density and thermal expansion behave as expected by the simple rule of mixtures. The conductivity is shown to decrease with decreasing molybdenum percentage until a percolation threshold of 16% by volume is reached at which time high resitivities are encountered. Secondary and primary spray dried powders yield similar properties as long as the ball milling process breaks up and disassociates the granules. The material exhibits R-curve behavior controlled by the bridging of molybdenum particles. Shrinkage and densification are controlled by the percentage of glass in the alumina constituent. The thermal expansion and contraction are controlled by the molybdenum percentage.

In order to create stress free components, thermal properties must be equivalent for the Mo-Al_2O_3 cermet features and the surrounding ceramic material. Adjusting the molybdenum percentage closer to percolation threshold will result in thermal expansions that are closer to the bulk ceramic without sacrificing conductivity. Compensating for the decrease in glass composition will increase the shrinkage factor to match that of the bulk ceramic. The small increase in glass percentage required will not adversely affect the thermal expansion significantly. Therefore, by increasing the glass percentage of the cermet to a least 8% the shrinkage difference can be minimized. Also, by decreasing the molybdenum percentage to 18% the stress due to thermal expansion can be decreased by 15%.

CHAPTER 1
INTRODUCTION

Molybdenum-Alumina (Mo-Al_2O_3) cermets are a group of metal-ceramic composites that have the distinction of containing molybdenum particles dispersed in alumina matrices. These cermets are fabricated from molybdenum and alumina powders that are blended, pressed and sintered to form composite materials that have thermal expansion characteristics similar to solid alumina ceramics. Since the thermal properties and the powder processing techniques of Mo-Al_2O_3 cermets are similar to that of alumina ceramics, these two materials can be joined by co-firing to produce components that have hermetic interfaces between the cermet and ceramic materials. A unique characteristic of Mo-Al_2O_3 cermets is that they have the ability to behave as electrical conductors or as insulators simply by varying the molybdenum percentage.

An electrically conductive Mo-Al_2O_3 cermet was developed in the 1970s by General Electric Neutron Devices Department in Largo, Florida (currently operated by Lockheed Marietta Specialty Components, Incorporated). The scope of this investigation focuses on this particular Mo-Al_2O_3 cermet material, therefore, further background is required. The material was given the designation of CND50 in which the "C" stands for cermet, the "ND" for Neutron Devices, and the "50" for the weight percent molybdenum. The alumina constituent in CND50 has the designation of 94ND2 which consists of polycrystalline aluminum oxide (Al_2O_3) grains joined by a glassy phase. The "94" stands for the actual weight percent of aluminum oxide (Al_2O_3) and the "2" signifies the particular glass composition.

CND50 has historically been used in applications where hermetic electrical feedthroughs in ceramic components is required. The flow chart shown in Figure 1 - 1 outlines the sequences

CND50 Cermet Slurry Processing

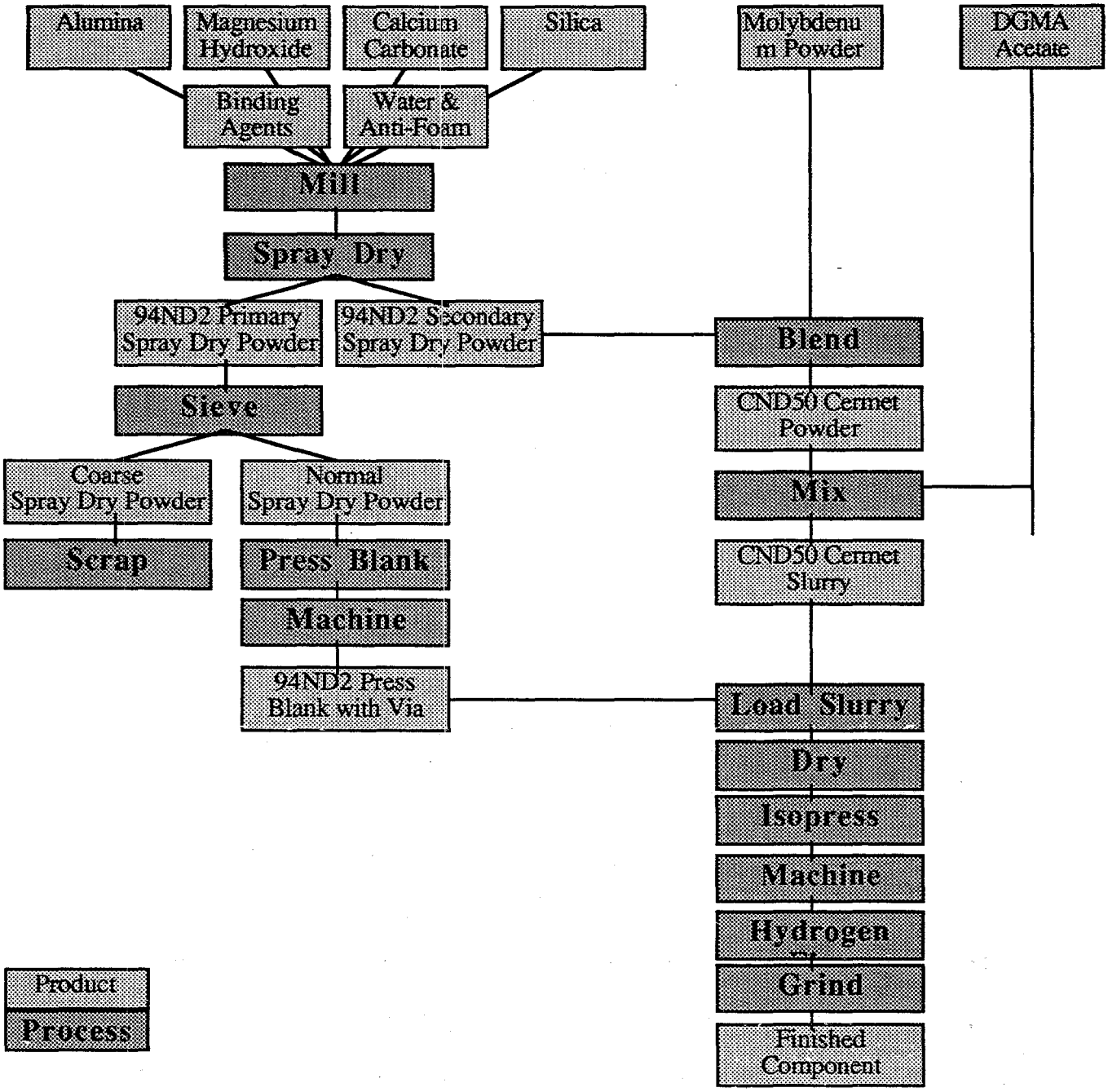

Figure 1-1: Flowchart outlining typical slurry processing used in the fabrication of CND50 cermet feedthroughs.

typically used to fabricate CND50 cermet feedthroughs. The 94ND2 and molybdenum powders are first dry blended and then a vehicle is added to form a slurry. With a vacuum assist, the slurry is loaded into a through hole, or via, of an unfired alumina compact. This compact is also made from 94ND2 powder in order to maintain compatibility and to lower the complexity of the system. After the loaded compact is dried, isopressed and sintered, the CND50 material forms a conductive path through the insulative alumina. The component with its cermet feature is then ground to final dimensions. The exposed surfaces of the CND50 are often conventionally metallized and brazed to leads in order to form electrical connections. Electrical feedthroughs with this cermet design are generally considered to be less labor intensive and more reliable than the alternative method of metalizing and brazing metal pins into through holes. For a detailed description of this cermet slurry process see Appendix A.

The 94ND2 powder that is used to blend with the molybdenum is a spray dried powder consisting of aluminum oxide (Al_2O_3), magnesium hydroxide ($Mg(OH)_2$), calcium carbonate ($CaCO_3$), silica (SiO_2), and a host of other organic binders. Upon sintering, the binders are volatilized while the hydroxide and carbonate are calcined. The calcined components then react with the silica to form a glassy phase. This glassy phase plays an important role in aiding sintering by wetting and bonding to the molybdenum and Al_2O_3 grains. Table 1 - 1 lists the weight and volume compositions of 94ND2 and CND50 at both the blended powder and sintered stages of processing. These values are theoretically calculated from initial powder quantities and assume a 4.24% weight loss during sintering as a result of volatilization and calcination. Table 1 - 2 and Table 1 - 3 tabulate the qualification data collected for each lot of 94ND2 and CND50, respectively. The historical data listed in Table 1 - 3 is the only characterization recorded for CND50 during its fabrication.

In addition to being electrically conductive and thermally compatible with alumina ceramics, Mo-Al_2O_3 cermets have other unique characteristics. Cermet materials have metallic constituents that lend themselves to be more easily and directly joined to metals and as conductors can also be used to shape electrical fields. New applications are currently being explored to take advantage of these characteristics. In some applications, cermet materials are being inlayed (or onlayed) in ceramics to produce intricate and uniform surfaces that are subsequently hermetically joined to metal components. Cermet to metal joints can be produced by either nickel plating and then brazing or directly brazing to inlays, thus, eliminating the need

Table 1 - 1: Weight and volume percentages for 94ND2 alumina and CND50 cermet in powder and sintered forms.

Designation	Compound Name	Compound Formula	Density[1] (g/cm^3)	Weight (kg)	Weight Percent	Volume (cm^3)	Volume Percent
94ND2	Spray Dry Powder						
	Alumina	Al_2O_3	3.99	33.499	90.02%	8403	80.35%
	Magnesium Hydroxide	$Mg(OH)_2$	2.37	0.581	1.56%	245	2.35%
	Calcium Carbonate	$CaCO_3$	2.71	0.238	0.64%	88	0.84%
	Silica	SiO_2	2.20	1.603	4.31%	728	6.96%
	Dispersing Agent	binder	1.3	0.215	0.58%	165	1.58%
	Hydroxpropyl Cellulose	binder	1.3	0.539	1.45%	415	3.96%
	Methycellulose	binder	1.3	0.539	1.45%	415	3.96%
		Total:	3.56	37.214	100.00%	10458	100.00%
94ND2	Sintered Ceramic						
	Alumina	Al_2O_3	3.99	33.499	94.00%	8403	90.53%
	Glass Phase	$MgO+CaO+SiO_2$	2.43	2.138	6.00%	879	9.47%
		Total:	3.84	35.637	100.00%	9282	100.00%
94ND2	Glass Phase						
	Magnesia	MgO	3.58	0.402	18.78%	112	12.74%
	Calcium Oxide	CaO	3.35	0.133	6.24%	40	4.53%
	Silica	SiO_2	2.20	1.603	74.98%	728	82.73%
		Total:	2.43	2.138	100.00%	879	100.00%
CND50	Ball Mill Powder						
	binder	binder	1.3	0.02	1.74%	13.36	7.05%
	94ND2 Spray Dry Powder	$Al_2O_3+Mg(OH_2)+CaCO_3+SiO_2$	3.80	0.483	48.26%	127.15	67.12%
	Molybdenum	Mo	10.22	0.500	50.00%	48.92	25.83%
		Total:	5.28	1.000	100.00%	189.434	100.00%
CND50	Sintered CND50						
	94ND2 Alumina	$Al_2O_3+MgO+CaO+SiO_2$	3.84	0.479	48.92%	124.71	71.82%
	Molybdenum	Mo	10.22	0.500	51.08%	48.92	28.18%
		Total:	5.64	0.979	100.00%	173.64	100.00%

Note: Densities for compounds are from CRC Handbook.[1] Binder densities are nominal values for organic materials.

Table 1 - 2: Historical data for 94ND2 alumina lot qualification at Lockheed Martin Specialty Components, Largo, FL.

Date	Batch	Specific Gravity		Flexural Strength		Dielectric Strength		Volume Resistivity	Dielectric Constant	Dissipation Factor
		Air Fire	H_2 Fire							
mm/dd/yy	#	g/cm³	g/cm³	MPa	kpsi	kV/mm	volts/mil	ohm-cm		
09/15/94	201	3.67	3.79	417.4	60.5	9.74	247.2	2.85E+15	9.29	0.00036
12/19/91	106	3.75	3.79	383.8	55.7	9.18	233.1	5.85E+14	9.63	0.00026
12/17/90	952	3.70	3.76	389.0	56.4	10.46	256.7	3.10E+15	9.40	0.00020
05/06/90	905	3.69	3.77	375.5	54.5	9.19	233.4	6.20E+15	9.50	0.00032
05/06/90	904	3.69	3.76	391.7	56.8	9.55	242.6	6.70E+15	9.71	0.00037
05/06/90	903	3.70	3.76	430.3	62.5	9.36	237.8	2.10E+15	9.75	0.00043
05/06/90	902	3.69	3.77	370.9	53.8	8.97	227.8	3.10E+15	9.50	0.00042
05/06/90	901	3.70	3.75	395.6	57.0	8.98	228.1	3.70E+15	9.52	0.00025
12/29/89	8902	3.69	3.81	320.0	46.5	9.83	249.5	2.13E+15	9.14	0.00028
10/31/89	707	3.69	3.79	309.0	44.8	10.00	254.0	2.70E+15	9.44	0.00022
10/31/89	706	3.69	3.79	357.1	51.8	9.80	248.9	3.10E+15	9.75	0.00045
10/31/89	705	3.69	3.79	334.7	48.5	10.00	254.0	2.10E+15	9.75	0.00033
10/31/89	704	3.69	3.80	314.9	45.7	9.53	242.1	2.50E+15	9.71	0.00044
10/31/89	703	3.69	3.89	381.5	55.3	9.57	243.1	7.10E+14	9.32	0.00030
11/28/88	804	3.70	3.81	363.0	52.6	9.85	250.0	4.90E+15	9.30	0.00036
01/21/88	533	3.69	3.81	363.0	52.8	9.81	249.0		9.40	0.00023
?/1987	?	3.70	3.79	406.0	58.9	10.12	257.0		9.70	0.00013
12/31/86	533	3.68	3.79	427.0	62.0	10.50	267.0		9.50	0.00016
?/1985	417	3.69	3.80	358.0	52.0	10.20	259.0		9.40	0.00020
?/1985	415	3.69	3.80	365.0	53.0	10.60	269.0		9.20	0.00030
?/1985	414	3.69	3.76	393.0	57.0	10.00	255.0		9.30	0.00030
05/26/85	410	3.69	3.80	382.0	55.4	10.40	265.0		9.20	0.00030
?/1984	336	3.70	3.80	386.0	56.0	10.10	257.0		9.30	0.00030
01/16/84	325	3.70	3.81	387.0	56.1	9.60	244.0		10.30	0.00001
01/16/84	324	3.69	3.80	407.0	59.1	9.80	249.0		9.50	0.00001
01/16/84	323	3.71	3.80	390.0	56.7	10.30	261.0		9.70	0.00002
05/08/83	236		3.81	398.0	57.8	10.80	274.0		9.20	0.00037
09/24/82	109	3.70	3.76	394.0	57.1	9.40	240.0		9.60	0.00020
12/14/81	018		3.79	399.0	57.9	9.20	234.0		9.40	0.00040
12/14/81	016		3.78	383.0	55.6	9.60	245.0		9.20	0.00040
12/14/81	015		3.78	399.0	57.9	10.40	263.0		9.20	0.00040
?	QC29016	3.70	3.76	426.0	63.3	9.72	247.0		9.80	0.00010
?	QC29019	3.70	3.77	432.0	62.6	10.00	254.0		9.80	0.00020
?	QC26752	3.71	3.80	399.0	57.9	10.31	262.0		9.60	0.00010
Average:		3.69	3.79	379.7	55.1	9.83	249.6	3.10E+15	9.48	0.00031
Std. Dev.:		0.01	0.03	29.71	4.30	0.49	11.96	1.73E+15	0.25	0.00009

Table 1 - 3: Historical data for CND50 cermet lot qualification at Lockheed Martin Specialty Components, Largo, FL.

Date	Batch	Specific Gravity H_2 Fire	Volume Resistivity
mm/dd/yy	#	g/cm^3	ohm-cm
12/19/91	106	5.540	3.30E-04
12/17/90	952	5.590	3.00E-04
12/29/89	901	5.520	3.30E-04
11/30/88	801	5.540	3.50E-04
01/21/88	701	5.600	3.20E-04
12/30/86	603	5.560	3.10E-04
09/13/84	401	5.580	3.30E-04
11/05/81	101	5.530	2.72E-04
Average:		5.558	3.18E-04
Std. Dev.:		0.030	2.38E-05

for conventional metalizing processes. The volumes and geometries of these inlays are quite different from the typical feedthrough and require a greater understanding of the material properties and their effects on processing parameters. Other applications are employing monolithic cermets to aid in electrical field suppression within high voltage vacuum tubes. Because it is impractical to produce monolithic components from the slurry process used for electrical feedthroughs, dry powder process techniques are being developed. In monolithic components, the cermet material is serving as a structural member, however, little is known about the material's mechanical properties. The lack of characterization has created many design challenges, which have resulted in trial and error design tactics.

Applying CND50 to these new applications has resulted in significant processing difficulties. In some cases gaping cracks are discovered after sintering near the interface between the CND50 and 94ND2. It is theorized that these cracks are produced from the difference in sinter shrinkage of CND50 and 94ND2 materials, either not at the same rate or not to the same extent. In addition to these gaping cracks: fine hairline fractures are being disclosed during

subsequent grinding processes. Typically, these fractures radiate from the interface into the alumina. Two possible theories exist for these finer cracks; 1) internal cracks are created by stresses during the cool down from the sinter temperature or 2) cracks are formed when residual stresses are released during material removal by grinding. In both cases, stresses due to the thermal expansion (or contraction) mismatch between CND50 and 94ND2 is thought to be the driving mechanism. Even though the thermal expansion of cermet and alumina are similar, they are not exactly the same. For cermet features with certain geometries, sizes or locations, this difference may produce stresses large enough to cause cracking in the alumina adjacent to the interface upon cooling from the sinter temperature. This thermal expansion mismatch also makes the junction with alumina susceptible to thermal cyclic failures. Both of these cracking mechanisms are exaggerated when the cermet features become large and more complex such as the features found in the new applications.

The objectives of this endeavor are to 1) mechanically, thermally, electrically, and microstructurally characterize CND50 cermet material, 2) document processing techniques and study the evolution of material properties during sintering, 3) evaluate the effect of compositional variations of Mo-Al_2O_3 cermets on material properties, and 4) relate material properties and processing techniques to the cracking phenomena.

CHAPTER 6
CONCLUSIONS

From the experimental results and discussion the following conclusions about the properties of Mo-Al_2O_3 cermets can be derived;

1) Secondary and primary spray dried powders yield similar properties as long as the ball milling process is sufficient to disassociate the spray dried spherical granules.
2) The materials strength dependence on flaw size exhibits R-curve behavior which is a result of the crack bridging effects by the molybdenum particles.
3) Shrinkage and densification are controlled by the soak time and percentage of glass.
4) The thermal expansion and contraction properties are controlled mainly by the percentage of molybdenum.
5) The electrical resistivity behaves as the percolation theory predicts and the critical volume fraction is approximately 16% molybdenum.
6) The hairline cracks associated with cermet features are caused by residual stresses due to a mismatch in the coefficient of thermal contractions between the CND50 cermet material and the surrounding bulk alumina material.
7) The gapping cracks in cermet features are caused by a difference in shrinkage between the CND50 cermet material and the surrounding bulk alumina material during the sinter fire process.

In order to create stress free components with cermet features, thermal properties must be equivalent for the Mo-Al_2O_3 cermet features and the surrounding alumina material. Adjusting the molybdenum percentage closer to the percolation threshold will result in a thermal expansion

the molybdenum percentage closer to the percolation threshold will result in a thermal expansion closer to the bulk alumina without sacrificing conductivity. At 18% molybdenum the resulting change in thermal expansion is approximately 0.2x10-6 in/in/°C which equates to approximately a 15% decrease in the thermal mismatch between alumina and cermet. This decrease should correspond directly to a decrease in residual stress created during cooling from the sinter temperature. Further work is needed to determine how close the composition can be to the threshold by analyzing the effects of molybdenum particle morphology and process variations. The magnitude of this decrease in stress induced by lowering the molybdenum percentage may be large enough to eliminate the brittle cracks encountered during fabrication.

Compensating for the decrease in glass composition will increase the shrinkage factor for Mo-Al_2O_3 cermets. Increasing the shrinkage factor will better match the alumina. The small increase in glass percentage required will not adversely affect the thermal expansion significantly, i.e., less than 5% of the total mismatch. Matching the shrinkage will help in predicting final sinter dimension that will result in reduced development efforts required for new component designs. Having more glass present may also increase the material's ability to relax or relieve stresses at elevated temperatures due to changes in the glass transition temperature. It may also reduce the amount of backing material required during fabrication which results in a reduction in the amount of grinding required after sintering.

All of these benefits described above relate to cost savings in the fabrication of components containing cermet features. Therefore, it is recommended that the percentage of molybdenum be decreased to 18% by volume and the percent glass be increased to at least 8% by volume. These compositional changes should completely eliminate the shrinkage differences that promote the gapping crack phenomenon and reduce residual stresses due to thermal expansion mismatches which promotes the hairline cracking phenomenon.

APPENDIX C - Contraction Strain at 100 Degree Intervals for All Materials Tested

APPENDIX C

file ww/dprd/cermet/96-6b2.doc

	94ND2 alumina, sample 9408-2,M67		94ND2 alumina, sample 9408-4, M62		94ND2 alumina, sample 9408-3, M11			AVERAGES for lot 9408 ND2	
	3/14/96	temp-37 C	3/11/96	temp-37 C	4/4/96	temp-37 C	9408	9408	9408
Temp.	Delta L/L	CTCx10^-7	Delta L/L	CTCx10^-7	Delta L/L	CTCx10^-7	Delta L/L (Ct)	Delta L/L	CTCx10^-7
C	9408-2	9408-2	9408-4	9408-4	9408-3	9408-3	Avg 9408	Std.Dev	Avg
37	0.00027947		0.0001848		0.00011206		0.00019211	8.39E-05	
100	0.00063455	55.39	0.00053963	57.16	0.00045903	57.85	0.000544403	8.79E-05	56.80
200	0.0012656	60.91	0.0012045	62.87	0.0011355	63.13	0.001201867	6.51E-05	62.30
300	0.0020056	65.34	0.0019478	67.26	0.0018818	67.51	0.001945067	6.19E-05	66.70
400	0.0027836	69.2	0.0027648	71.23	0.0026975	71.36	0.002748633	4.53E-05	70.60
500	0.003635	72.3	0.0036305	74.56	0.0035588	74.6	0.0036081	4.28E-05	73.82
600	0.004506	74.95	0.0045139	77.03	0.0044526	77.23	0.004490833	3.33E-05	76.40
700	0.0053931	77.02	0.0054081	78.86	0.0053578	79.19	0.005386333	2.58E-05	78.36
800	0.0062986	79	0.0063405	80.76	0.0062909	81.04	0.00631	2.67E-05	80.27
900	0.0072624	80.82	0.0072346	81.77	0.0072501	82.77	0.007249033	1.39E-05	81.79
1000	0.0082317	82.47	0.0080682	81.94	0.0082304	84.36	0.008176767	9.40E-05	82.92
	94ND2, 9311-2, M80, 3/26/96		94ND2, 916-2, M6,3/27 /96		94ND2, 9410-2, M8, 4/1/96		94ND2, 9411-2, M9,4/2/96		
		temp-37 C		temp-37 C		temp-37 C		temp-37 C	
Temp.	Delta L/L(ct)	CTCx10^-7	Delta L/L(ct)	CTCx10^-7	Delta L/L (ct)	CTCx10^-7	Delta L/L (ct)	CTCx10^-7	
C	9311-2	9311-2	916-2	916-2	9410-2	9410-2	9411-2	9411-2	
37	0.0001863		0.00007553		0.00011822		0.00011878		
100	0.00054965	56.88	0.00043525	57.87	0.00046011	56.7	0.0004702	56.61	
200	0.001205	62.11	0.0010993	63.16	0.0011136	62.03	0.0011279	62.26	
300	0.001943	66.54	0.0018444	67.47	0.0018483	66.44	0.0018654	66.67	
400	0.0027418	70.21	0.0026582	71.28	0.0026531	70.28	0.0026717	70.5	
500	0.0035861	73.3	0.0035229	74.61	0.0035042	73.54	0.003523	73.97	
600	0.0044563	75.69	0.0044182	77.21	0.0043841	76.13	0.0043995	76.19	
700	0.0053369	77.56	0.0053213	79.19	0.005275	78.06	0.0052894	78.09	
800	0.0062576	79.47	0.0062677	81.22	0.0062223	80	0.0062183	80.05	
900	0.0071848	81.01	0.007239	83.07	0.0071588	81.8	0.0071694	81.8	
1000	0.0081217	82.34	0.0082207	84.62	0.0081172	83.28	0.0081293	83.28	

APPENDIX C

	27 Vol% Mo cermet, 27Mo-1, M65		27 Vol% Mo cermet, 27Mo-3, M19					
	3/13/96	temp-37 C	4/16/96	temp-37 C			Contraction	Contraction
Temp.	Delta L/L	CTCx10^-7	Delta L/L	CTC x10^-7			Delta L/L (ct)	CTCx10^-7
C	27Mo-1	27Mo-1	27Mo-3	27Mo-3			Avg. 27Mo	Avg. 27Mo
37	0.00018543		0.00024214				0.000213785	
100	0.00052108	54.25	0.00057702	53.95			0.00054905	54.1
200	0.0011393	58.90	0.0012015	59.19			0.0011704	59.045
300	0.0018269	62.67	0.0018921	62.95			0.0018595	62.81
400	0.0025674	65.78	0.0026303	65.93			0.00259885	65.855
500	0.0033477	68.47	0.0033981	68.11			0.0033729	68.29
600	0.0041669	70.86	0.0041994	70.43			0.00418315	70.645
700	0.0049918	72.56	0.0050163	72.91			0.00500405	72.735
800	0.005829	74.04	0.0058812	73.99			0.0058551	74.015
900	0.0066776	75.30	0.0067865	75.91			0.00673205	75.605
1000	0.0075368	76.39	0.007704	77.54			0.0076204	76.965
	20 Vol% Cermet, 20 Mo-1, M63		20 Vol% Cermet, 20 Mo-2, M71		20 Vol% Cermet, 20 Mo-3, M12		Contraction	
							20% Mo Cermet	
	3/12/96	temp-37 C	3/19/96	temp-37 C	4/8/96	temp-37 C	AVG Delta L/L	AVG CTE
Temp.	Delta L/L(ct)	CTCx10^-7	Delta L/L(ct)	CTCx10^-7	Delta L/L(ct)	CTCx10^-7		
C	20Mo-1	20Mo-1	20Mo-2	20Mo-2	20Mo-3	20Mo-3	Avg 20%	Avg 20%
37	0.000236		0.00019555		0.00014932		0.000193623	
100	0.00057317	54.24	0.00053681	54.97	0.00049457	55.44	0.00053485	54.88
200	0.0011954	59.17	0.0011643	59.72	0.0011308	60.57	0.0011635	59.82
300	0.0018875	63.02	0.001868	63.68	0.0018367	64.40	0.001864067	63.70
400	0.0026376	66.27	0.0026248	67.00	0.0026022	67.75	0.002621533	67.01
500	0.0034138	68.76	0.0034095	69.50	0.0034033	70.43	0.003408867	69.56
600	0.0042273	71.01	0.0042279	71.70	0.0042337	72.69	0.004229633	71.80
700	0.0050585	72.79	0.0050675	73.51	0.0050727	74.35	0.005066233	73.55
800	0.005896	74.24	0.0059287	75.17	0.0059361	75.93	0.005920267	75.11
900	0.0067549	75.59	0.0068122	76.70	0.0068275	77.47	0.0067982	76.59
1000	0.0076469	76.99	0.0077251	78.23	0.0077389	78.87	0.007703633	78.03

APPENDIX C

23 Vol% Cermet, 23 Mo-1, M73,3/20/96				17 Vol% Cermet, 17 Mo-1, M76,3/21/96			
		temp-37 C				temp-37 C	
Temp.	Delta L/L	CTCx10^-7		Temp.	Delta L/L	CTCx10^-7	
C	23Mo-1	23Mo-1		C	17Mo-1	17Mo-1	
37	0.00008943			37	0.00014019		
100	0.00043187	55.13		100	0.00047981	54.71	
200	0.0010579	59.7		200	0.0011117	59.93	
300	0.0017639	63.85		300	0.001816	63.91	
400	0.0025196	67.08		400	0.0025864	67.51	
500	0.003322	69.95		500	0.0033833	70.17	
600	0.0041538	72.25		600	0.0042016	72.25	
700	0.0049893	73.97		700	0.0050305	73.82	
800	0.0058597	75.69		800	0.0058836	75.33	
900	0.006754	77.28		900	0.0067668	76.84	
1000	0.0076598	78.68		1000	0.0076692	78.24	

	75Mo-22V-3Fe#1, run 2, M57		75Mo-22V-3Fe#1, run 2, M57		75Mo-22V-3Fe#2, M58		75Mo-22V-3Fe#2, M58	
	as cast 5/28/1996	CTCx10^-7	as cast 5/28/1996	CTEx10^-7	as cast 5/28/1996	CTCx10^-7	as cast 5/28/1996	CTEx10^-7
	Delta L/L (Ct)	temp-37 C	Delta L/L (Ex)	37 C- temp	Delta L/L (Ct)	temp-37 C	Delta L/L (Ex)	37 C- temp
Temp. C	75M22V3Fe/#1	75M22V3Fe/#1	75M22V3Fe/#1	75M22V3Fe/#1	75M22V3Fe/#2	75M22V3Fe/#2	75M22V3Fe/#2	75M22V3Fe/#2
37	0.00004423		0.0000986		0.00011358		0.00010148	
100	0.00040973	60.86	0.000516	65.11	0.0004765	60.48	0.00050451	64.53
200	0.0010631	63.65	0.001163	64.91	0.0011554	64.3	0.0011723	66.1
300	0.0017686	66.24	0.001866	66.89	0.0018468	66.69	0.0018907	68.21
400	0.0025119	68.46	0.002587	68.69	0.0025836	68.59	0.0026376	70.02
500	0.0032543	69.77	0.003334	69.98	0.0033642	70.37	0.0034244	71.92
600	0.0040399	71.29	0.004126	71.38	0.0041422	71.93	0.0042457	73.71
700	0.0048396	72.63	0.004901	72.52	0.0049286	72.96	0.0050714	75.08
800	0.0056545	73.76	0.005742	73.87	0.0057537	74.03	0.0058995	76.06
900	0.0065003	75.03	0.006571	75.09	0.0065934	75.35	0.0067126	76.67
1000	0.0073887	76.49	0.007436	76.28	0.0075306	77.09	0.0075837	77.76

APPENDIX C

	75Mo-22V-3Co#1, run 1, M8		75Mo-22V-3Co#1, run 1, M8		75Mo-22V-3Co#2, M10		75Mo-22V-3Co#2, M10	
	as cast 7/24/1996	CTCx10^-7	as cast 7/24/1996	CTEx10^-7	as cast 7/25/1996	CTCx10^-7	as cast 7/25/1996	CTEx10^-7
	Delta L/L (Ct)	temp-37 C	Delta L/L (Ex)	37 C- temp	Delta L/L (Ct)	temp-37 C	Delta L/L (Ex)	37 C- temp
Temp. C	75M22V3Co#1/run1	75M22V3Co#1/run1	75M22V3Co#1/run1	75M22V3Co#1/run 1	75M22V3Co#2	75M22V3Co#2	75M22V3Co#2	75M22V3Co#2
37	-0.000023029		0.00011146		0.00005837		0.00011973	
100	0.00033487	61.68	0.0005041	63.49	0.00030674	60.96	0.00051122	64.61
200	0.0010058	64.3	0.0011468	64.76	0.00095845	64.37	0.0011671	65.19
300	0.0016941	66.03	0.0018481	66.28	0.0016645	66.27	0.0018489	66.83
400	0.0023991	67.66	0.0025786	68.13	0.0023995	68.21	0.0025909	68.52
500	0.0031755	69.54	0.0033292	69.96	0.0031496	69.99	0.0033305	69.99
600	0.0039559	71.3	0.0041437	71.73	0.0039451	71.75	0.0041324	71.56
700	0.0047556	72.39	0.0049509	73.32	0.0047505	73.1	0.004932	73.07
800	0.0055336	73.27	0.0057967	74.6	0.0055736	74.28	0.0057827	74.41
900	0.0063998	74.64	0.006614	75.59	0.0064443	75.58	0.0065981	75.44
1000	0.0073532	76.78	0.0074549	76.33	0.0073677	77.31	0.0074243	76.16

	75Mo-22V-3Fe#4, run 1, M37		75Mo-22V-3Fe#4, run 1, M37		75Mo-22V-3Co#3, M36		75Mo-22V-3Co#3, M36	
	9/11/96	1625 C/3hrs/wetH	9/11/96	1625 C/3hrs/wetH	9/10/96	1625 C/3hrs/wetH	9/10/96	1625 C/3hrs/wetH
		CTCx10^-7		CTEx10^-7		CTCx10^-7		CTEx10^-7
	Delta L/L (Ct)	temp-37 C	Delta L/L (Ex)	37 C- temp	Delta L/L (Ct)	temp-37 C	Delta L/L (Ex)	37 C- temp
Temp. C	75M22V3Fe#4(HT)	75M22V3Fe#4	75M22V3Fe#4(HT)	75M22V3Fe#4	75M22V3Co#3(HT)	75M22V3Co#3	75M22V3Co#3(HT)	75M22V3Co#3
37	0.000126		0.0001217		0.0001109		0.00012789	
100	0.000503	62.71	0.0005614	71.02	0.00052955	69.57	0.00055854	72.09
200	0.001158	64.43	0.0012385	68.96	0.0011591	65.32	0.0012177	68.19
300	0.001858	66.07	0.0019462	69.65	0.0018556	66.54	0.0019163	68.84
400	0.002596	68.2	0.002683	70.78	0.0025855	68.3	0.0026528	70.19
500	0.003352	70.12	0.0034472	71.99	0.0033372	70.1	0.0034111	71.39
600	0.004146	71.75	0.0042338	73.17	0.0041193	71.55	0.0041952	72.39
700	0.00496	73.01	0.0050395	74.29	0.0049253	72.72	0.0049845	73.4
800	0.005753	74.02	0.0058684	75.4	0.0057113	73.67	0.0057918	74.54
900	0.006597	75.23	0.0066974	76.47	0.0065456	74.8	0.0066537	75.9
1000	0.007526	76.89	0.0075844	77.57	0.007472	76.46	0.0075459	77.13

APPENDIX C

	Mo-28V ingot 1, run 2, M3		Mo-28V ingot 1, run 2, M3		Mo-28V ingot 2, run 2, M90		Mo-28V ingot 2 run 2, M90	
	5/30/96	CTCx10^-7	5/30/96	CTEx10^-7	6/3/96	CTCx10^-7	6/3/96	CTEx10^-7
	Delta L/L (ct)	temp-37 C	Delta L/L (ex)	37 C- temp	Delta L/L (ct)	temp-37 C	Delta L/L (ex)	37 C- temp
Temp. C	Mo-28V ingot 1	Mo-28V ingot 1	Mo-28V ingot 1	Mo-28V ingot 1	Mo-28V ingot 2	Mo-28V ingot 2	Mo-28V ingot 2	Mo-28V ingot 2
37	0.00012942		0.00010991		0.00026117		0.0001256	
100	0.00052445	65.81	0.0054295	70.29	0.00065315	65.32	0.0005335	69.98
200	0.0012233	67.47	0.0012902	72.96	0.0013617	67.98	0.0012476	70.89
300	0.0019742	70.91	0.0020667	74.77	0.0020752	69.75	0.0020097	72.33
400	0.0027704	73.32	0.0028735	76.35	0.0028528	71.6	0.0027741	73.85
500	0.0036167	75.46	0.0037034	77.83	0.0036301	73.27	0.0035952	75.33
600	0.0044508	77.13	0.0045535	79.09	0.0044351	74.58	0.0044275	76.72
700	0.0053145	78.31	0.0054091	80.06	0.0052532	75.64	0.0052839	78.08
800	0.0061665	79.22	0.0062635	80.79	0.0061008	76.64	0.0061478	79.17
900	0.0070328	80.26	0.0071289	81.45	0.0069473	77.74	0.0068828	79.86
1000	0.0079934	81.72	0.0080396	82.44	0.0078693	79.08	0.0078801	80.9
	Mo-18V , run 2. M91	6/4/96	Mo-18V , run 2, M91	6/4/96	Mo-15V, run 2, M98	6/6/96	Mo-15V, run 2, M98	6/6/96
		CTCx10^-7		CTEx10^-7		CTCx10^-7		CTEx10^-7
	Delta L/L (ct)	temp-37 C	Delta L/L (ex)	37 C- temp	Delta L/L (ct)	temp-37 C	Delta L/L (ex)	37 C- temp
Temp. C	Mo-18V	Mo-18V	Mo-18V	Mo-18V	Mo-15V	Mo-15V	Mo-15V	Mo-15V
37	0.00027027		0.00010201		0.000068383		0.00010163	
100	0.00060602	55.88	0.00045962	57.58	0.00040793	54.87	0.00046556	58.89
200	0.0012122	58.24	0.0010654	59.28	0.00099487	57.23	0.0010593	59.13
300	0.0018281	59.86	0.0017109	61.44	0.0016205	59.2	0.001688	60.55
400	0.0024863	61.25	0.0023875	63.13	0.0022807	61.14	0.0023517	62.18
500	0.0031847	63.1	0.0030958	64.83	0.0029741	62.89	0.0030442	63.69
600	0.0038953	64.72	0.0038401	66.52	0.0036839	64.34	0.0037614	65.09
700	0.0045978	65.57	0.0046005	67.99	0.0043966	65.36	0.0044916	66.32
800	0.0053335	66.45	0.0053729	69.19	0.0051158	66.23	0.00524	67.42
900	0.0060807	67.57	0.006152	70.21	0.0058738	67.35	0.0059941	68.36
1000	0.0069027	68.95	0.006935	71.04	0.0066745	68.67	0.0067454	69.03

APPENDIX C

	LCAC Mo, run 2, M97		LCAC Mo, run 2, M97		Mo-12V, run 2, M82		Mo-12V, run 2, M82	
	6/18/96	temp-37 C	6/18/96	CTEx10^-7	6/10/96	CTCx10^-7	6/10/96	CTEx10^-7
	Delta L/L (ct)	CTCx10^-7	Delta L/L (ex)	temp-37 C	Delta L/L (ct)	temp-37 C	Delta L/L (ex)	37 C- temp
Temp. (C)	LCAC Mo	LCAC Mo	LCAC Mo	LCAC Mo	Mo-12V	Mo-12V	Mo-12V	Mo-12V
37	1.89298E-05		0.00010573		0.00016711		0.000095575	
100	0.00028575	50.63	0.00046034	56.97	0.0004933	54.34	0.00045995	57.3
200	0.00083129	53	0.0010155	56.04	0.0010862	56.78	0.0010441	58
300	0.001405	54.75	0.0015999	56.96	0.0016849	58.34	0.0016552	59.56
400	0.002028	56.54	0.0022126	58.19	0.0023404	60.06	0.0023126	60.99
500	0.0026644	58.28	0.0029462	59.3	0.0030028	61.65	0.0029895	62.41
600	0.0033314	59.82	0.0034908	60.24	0.0036906	62.97	0.0036895	64.01
700	0.0040258	61.25	0.0041452	61.02	0.0043876	63.94	0.0044224	65.22
800	0.004686	61.7	0.0048108	61.73	0.0050986	64.73	0.0051388	66.24
900	0.0053335	62.2	0.0054781	62.31	0.0058188	65.56	0.005897	67.2
1000	0.0060467	63.02	0.0061316	62.62	0.0065897	66.74	0.0066357	68.03

APPENDIX D - List of Memos

Date	Sent to	Sent from	Subject
01/28/95	Distribution	S. Glass, 1845; R. Moore, 2476	Cracking of Cermet Components
02/22/95	Distribution	S. Glass, 1845; R. Moore, 2476	Characterization of Cermet Materials for Residual Stress Modeling and Developing Processing Guidelines
03/02/95	R. H. Moore, 2476 and J. P. Brainard, 2569	J. J. Stephens, 1832	Thermal Expansion of Candidate Mo-Cr and Mo-V Alloys for Use in 94ND2 Cermet Fabrication
04/07/95	Distribution	R. Moore, 2476; S. Glass, 1845	Meeting Minutes of the MC4277 Sub-PRT for Cermet Cracking and Fabrication Issues
04/27/95	Distribution	R. Moore, 2476; S. Glass, 1845	April 13, 1995 Meeting Minutes of the MC4277 Sub-PRT for Cermet Cracking and Fabrication Issues
05/17/95	Distribution	R. Moore, 2476	May 10, 1995, Meeting Minutes of the MC4277 Sub-PRT for Cermet Cracking and Fabrication Issues
06/06/95	Distribution	R. Moore, 2476	May 24, 1995, Meeting Minutes of the MC4277 Sub-PRT for Cermet Cracking and Fabrication Issues
06/12/95	Distribution	R. Moore, 2476	June 9, 1995, Meeting Minutes of the MC4277 Sub-PRT for Cermet Cracking and Fabrication Issues
06/30/95	Distribution	R. Moore, 2476	June 23, 1995, Meeting Minutes of the MC4277 Sub-PRT for Cermet Cracking and Fabrication Issues
07/14/95	Distribution	R. Moore, 2476	July 11, 1995, Meeting Minutes of the MC4277 Sub-PRT for Cermet Cracking and Fabrication Issues
08/11/95	Distribution	R. Moore, 2476	July 20 and 27, 1995, Meeting Minutes of the MC4277 Sub-PRT for Cermet Cracking and Fabrication Issues
08/22/95	Distribution	R. Moore, 2476	August 21, 1995, Meeting Minutes of the MC4277 Sub-PRT for Cermet Cracking and Fabrication Issues
08/28/95	K. Mahin, 1807	R. Moore, 2476; S. Glass, 1845; K. Ewsuk, 1841	Info and Project Plan for FY96 Smart Cermet Program
09/11/95	R. Moore, 2476	E. Beauchamp, 1845	Analysis of Cermet Ring Failure
09/15/95	K. Mahin, 1807	R. Moore, 2476	Revised Project Plan for Smart Cermet Program
10/3/95	Distribution	R. Moore, 2476	H_2 Compatibility of Mo-V, V, and Nb Metals
10/15/95	Roger Moore, 1492	S. L. Monroe, 1845	CTE Measurements on Cermet and Alumina for Neutron Tube Applications
10/20/95	Distribution	R. Moore, 2476	August 28, 1995, Meeting Minutes of the MC4277 Sub-PRT for Cermet Cracking and Fabrication Issues
10/28/95	R. Moore, 1492	S. L. Monroe, 1845	Thermal Expansion Measurements on Niobium for Cermet Applications

APPENDIX D

12/4/95	Distribution	R. Moore	November 29, 1995, Meeting Minutes of the MC4277 Sub-PRT for Cermet Cracking and Fabrication Issues
12/8/95	R. Moore, 1492	S. Glass, 1845	Estimation and Mitigation of Residual Stresses in Cermet-Containing Piece Parts
12/15/95	Distribution	R. Moore, 1492	December 13, 1995, Meeting Minutes of the MC4277 Sub-PRT for Cermet Cracking and Fabrication Issues
12/21/96	Distribution	R. Loehman, 1808	Nb-Al_2O_3 Cermet Properties
01/11/96	Distribution	R. Pike, 1561	Cermet Tube Components Design Review
02/14/96	G. Smith, 1564	R. Pike, 1561; R. Moore, 1492	Results of MC4277 Cermet Design Review Meeting of January 30, 1996
04/05/96	Distribution	R. Moore, 1492	April 2, 1996, Meeting Minutes of the MC4277 Sub-PRT for Cermet Cracking and Fabrication Issues
08/30/96	J. J. Stephens, 1833	E. Hoffman, 9117	Prediction of Residual Stresses in a Feedthru Insulator Manufactured with New Cermet Composites
09/11/96	Distribution	The MC4277 Sub-Team for Cermet Cracking and Fabrication Issues	Project Status
11/14/96	Roger Moore, 1492	Otis Solomon, 1542	Cermet Measurements
02/06/97	J. Brainard, 1564	E. Hoffman, 9117	Calculation of Residual Stresses in RP^2 Feedthru Insulator
03/26/97	Cermet LDRD Team	J. Stephens, 1833	Action Items Resulting from March 25th Cermet LDRD Meeting
06/23/97	Distribution	David Goy, 1492	Molybdenum Distribution in Slurry-Loaded Cermets - AlSiMag Parts made with 94ND2

APPENDIX E - Publications and Presentations

J. J. Stephens, S. L. Monroe, and B. K. Damkroger, "Thermal Expansion and Solidification Behavior of Mo-V Alloys," 1996 Annual Meeting of TMS (The Minerals, Metals, and Materials Society), Anaheim, CA, Feb. 4-8, 1996.**(SAND 95-2211A)**

S. J. Glass, S. L. Monroe, R. Moore, and G. Pressly, "Percolation Effects on the Structure and Properties of Al_2O_3-Mo Cermets," American Ceramic Society Basic Science Meeting, New Orleans, Nov. 5-8, 1995.**(SAND 95-2375A)**

S. J. Glass, B. N. Turman, J. Halbleib, T. Voth, "High Energy Electron Beam Joining of Ceramics, Cermets, and Glasses," The American Ceramic Society's 99th Annual Meeting, Cincinnati, OH; May 4-7, 1997.**(SAND 96-2913A)**

J. J. Stephens, B. K. Damkroger, and S. L. Monroe, "Development of Mo Base Alloys for Conductive Metal-Alumina Cermet Applications," pp. 87-100 in the Proceedings of the 14th International Plansee Seminar, Reutte, Austria, May 12-16, 1997 Eds. G. Kneringer, P. Rodhammer and P. Wilhartitz, Plansee AG, Reutte (1997). Vol. 1.**(SAND 96-1932C)**

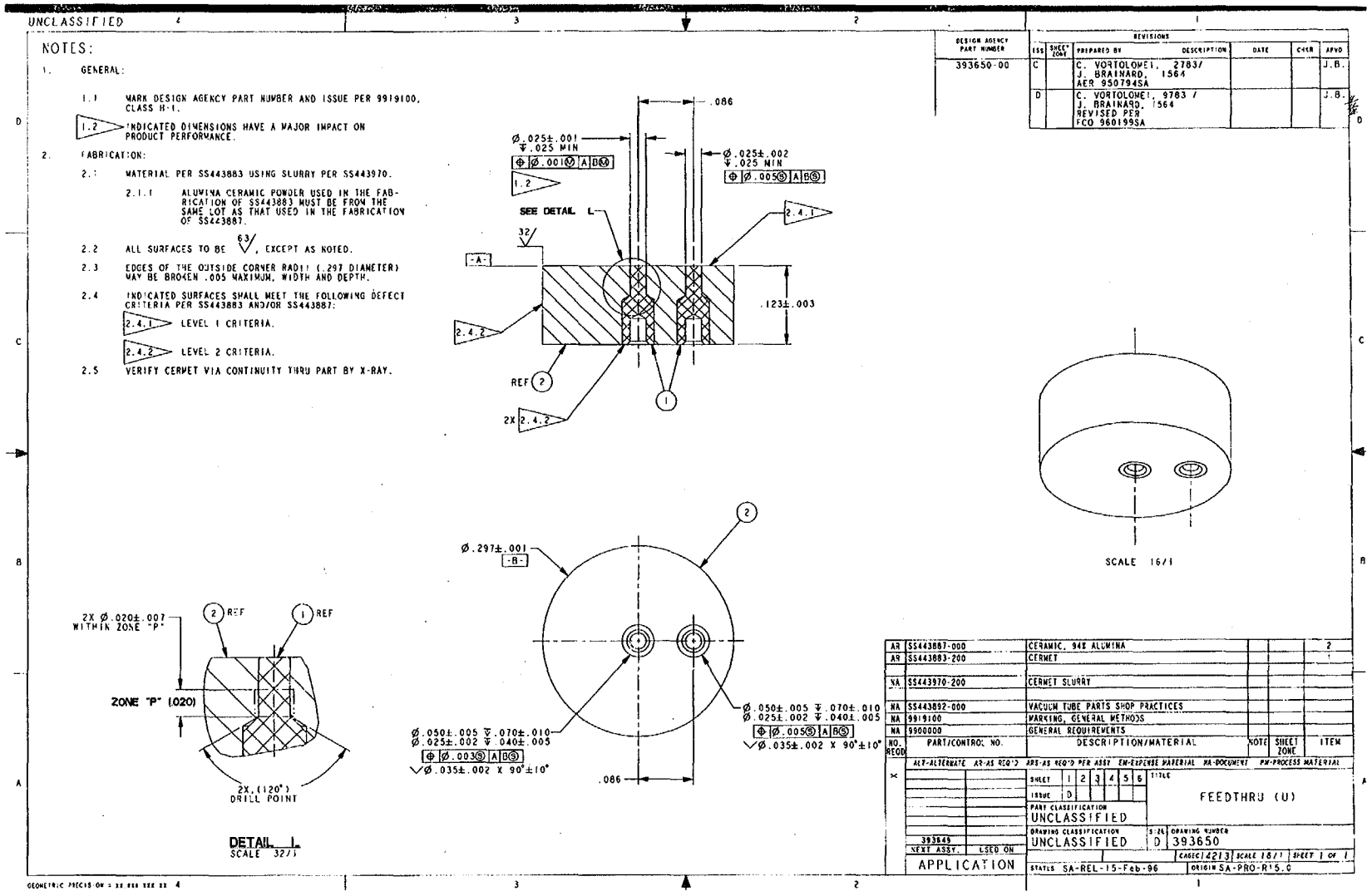

(a) Feedthru

Fig. 1. Drawing of parts of the MC4277 neutron tube that contain Mo-alumina cermet features.

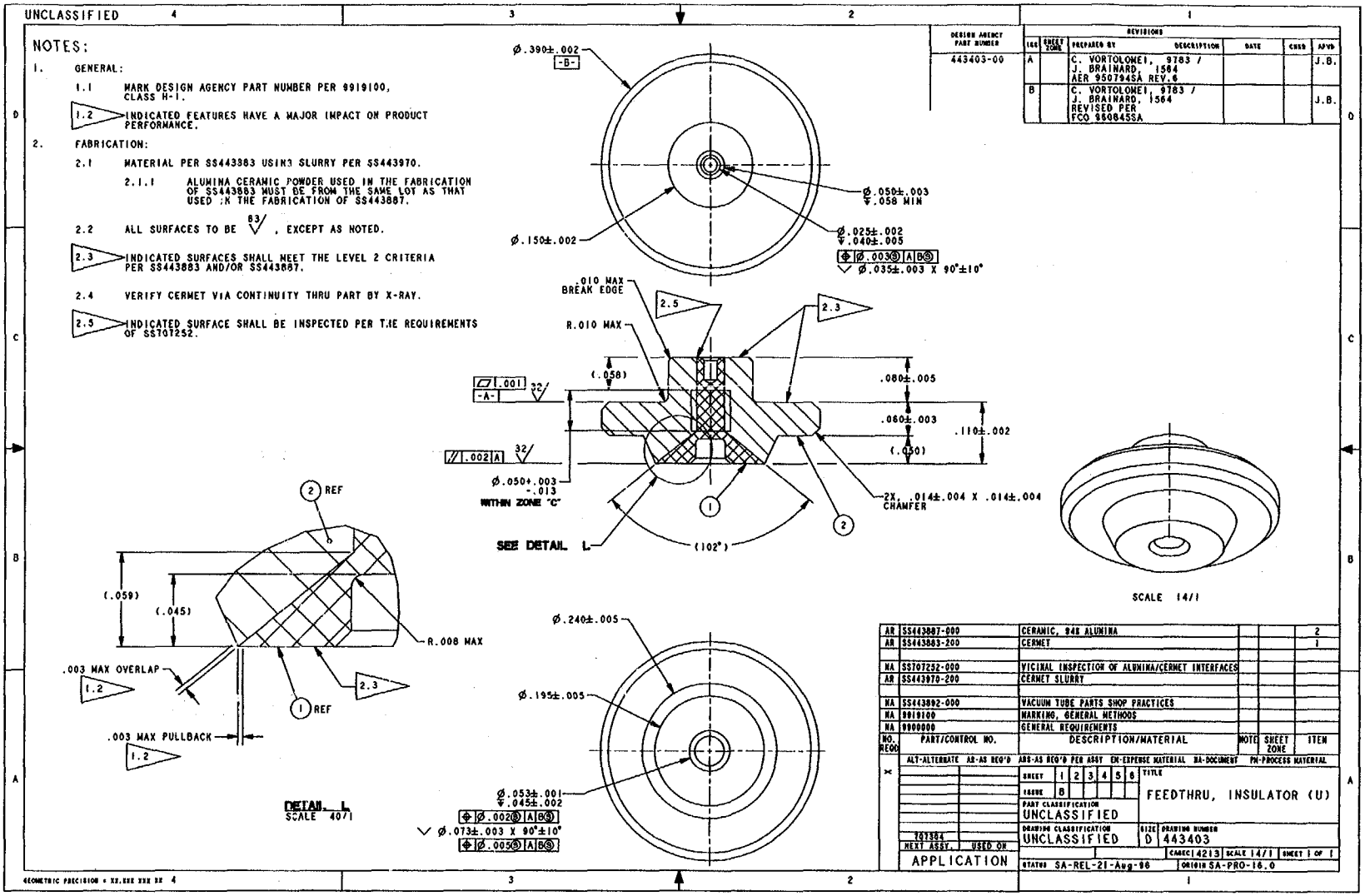

(b) Feedthru insulator

Fig. 1. Drawing of parts of the MC4277 neutron tube that contain Mo-alumina cermet features.

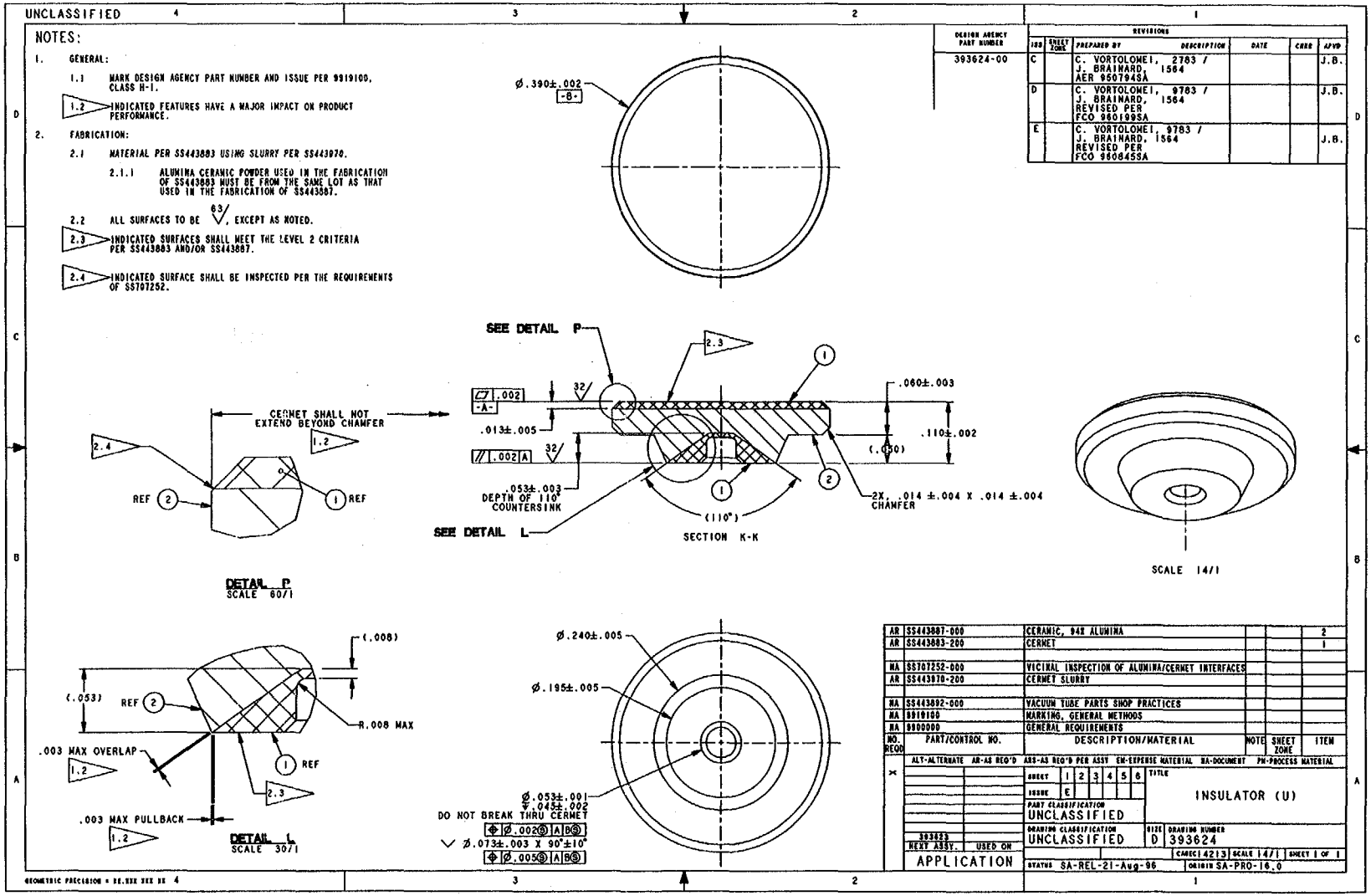

(c) Insulator

Fig. 1. Drawing of parts of the MC4277 neutron tube that contain Mo-alumina cermet features

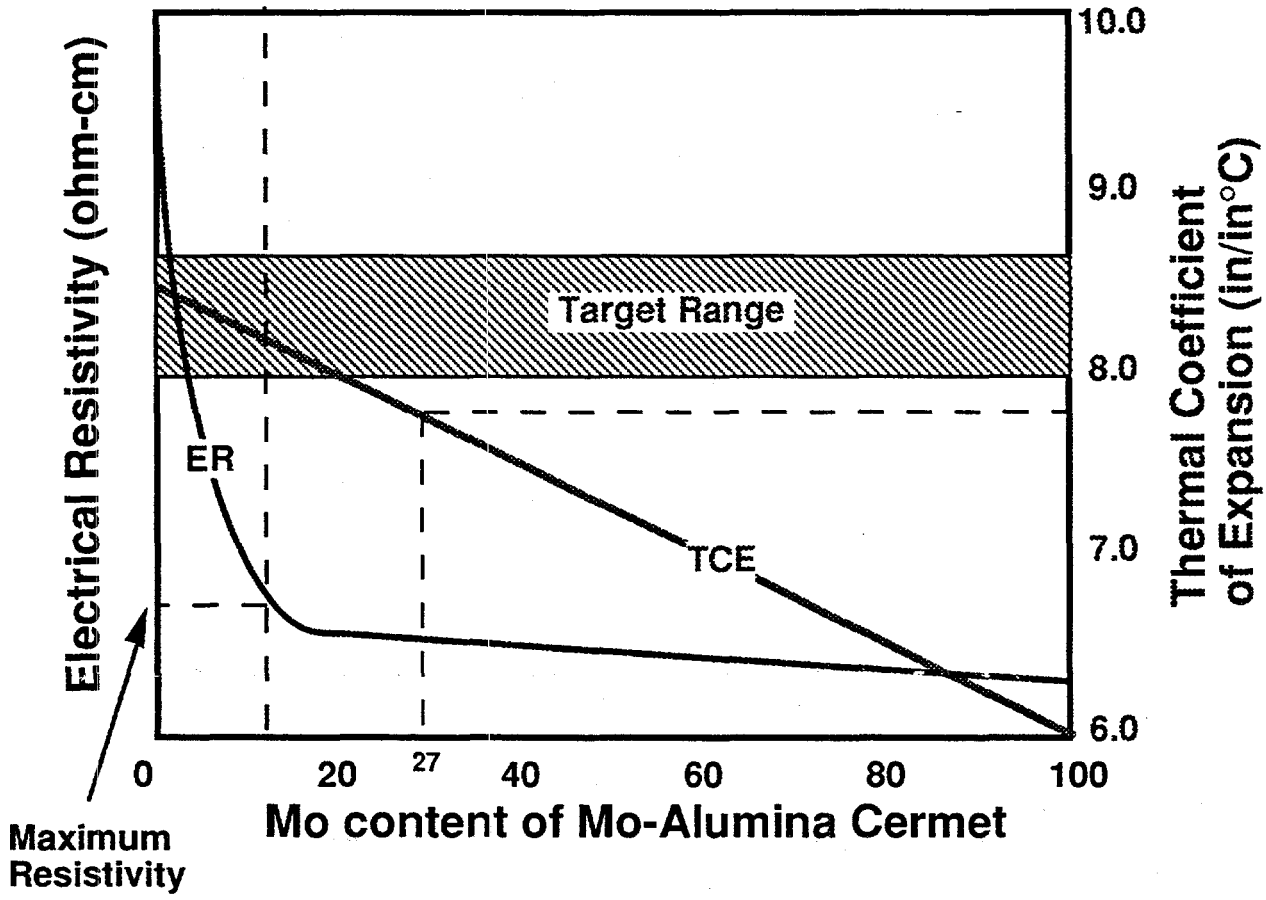

Fig. 2. A schematic of the competing requirements of thermal expansion mismatch and electrical resistivity as a function of the cermet's Mo content.

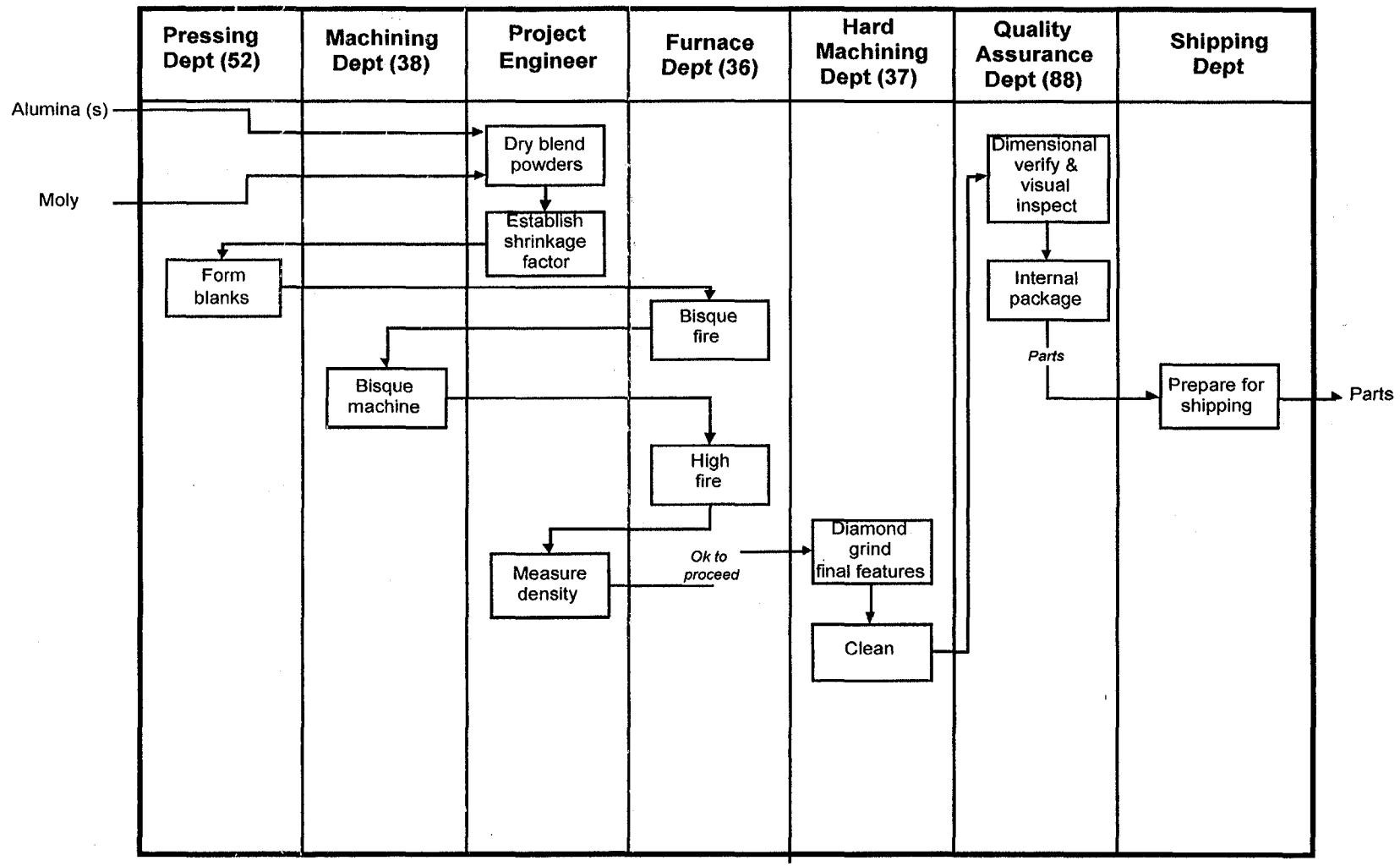

Fig. 3. Processing flow-chart for slurry-processed cermets.

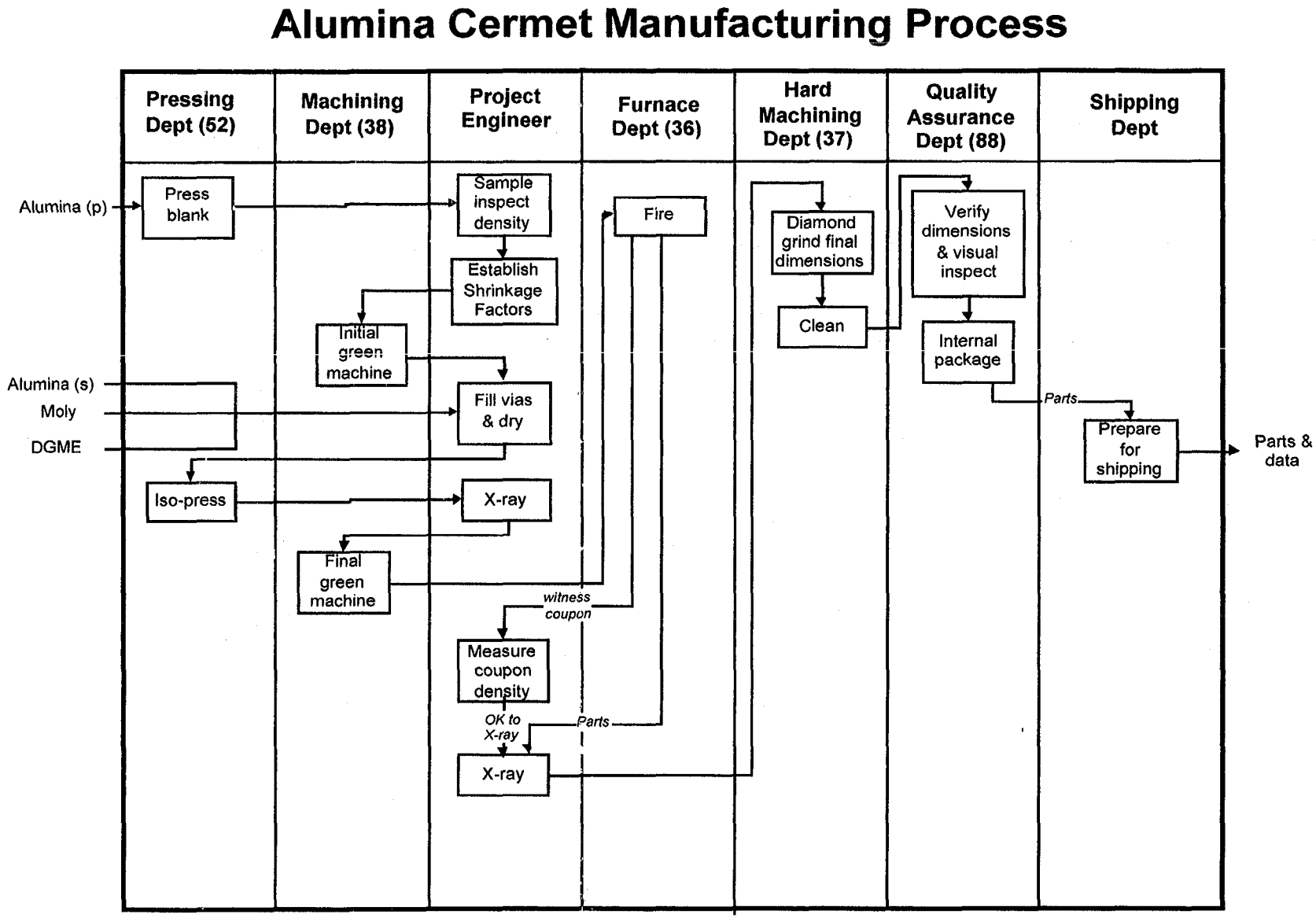

Fig. 4. Processing flow-chart for dry-processed cermets.

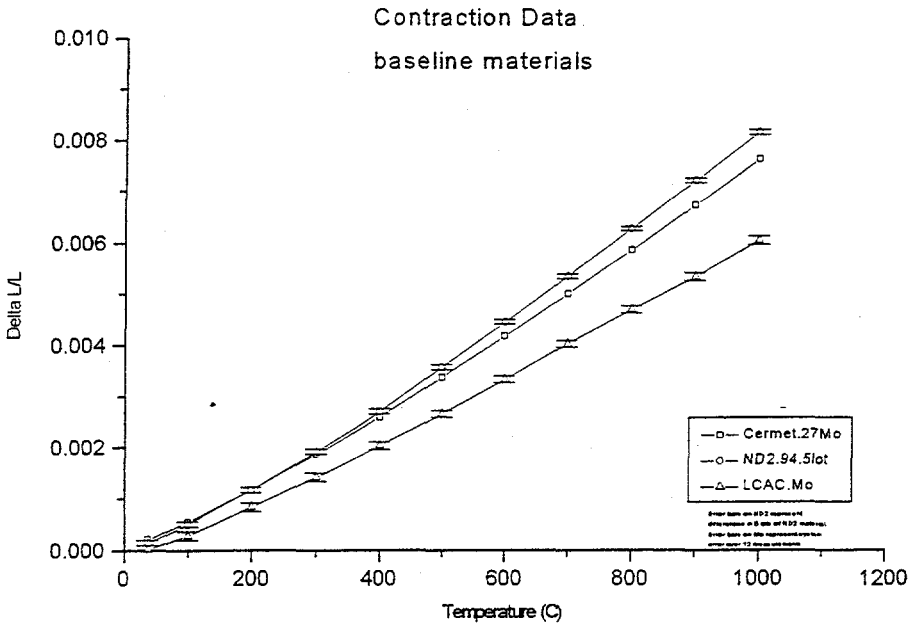

Fig. 5. Contraction strain (delta L/L) versus temperature for baseline materials (27 vol% Mo cermet 94ND2 alumina, and LCAC Mo).

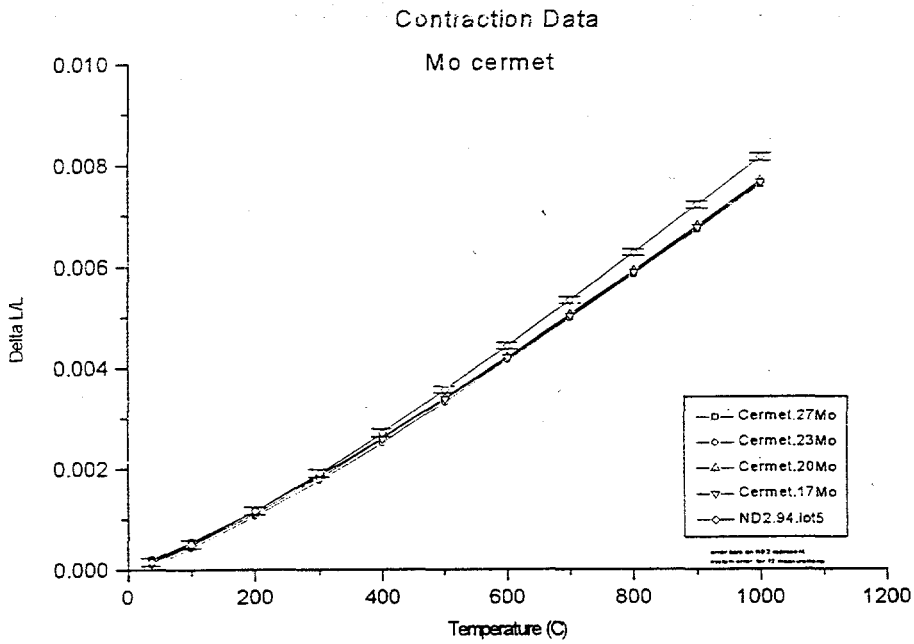

Fig. 6. Contraction strain (delta L/L) versus temperature for lower vol% Mo cermets.

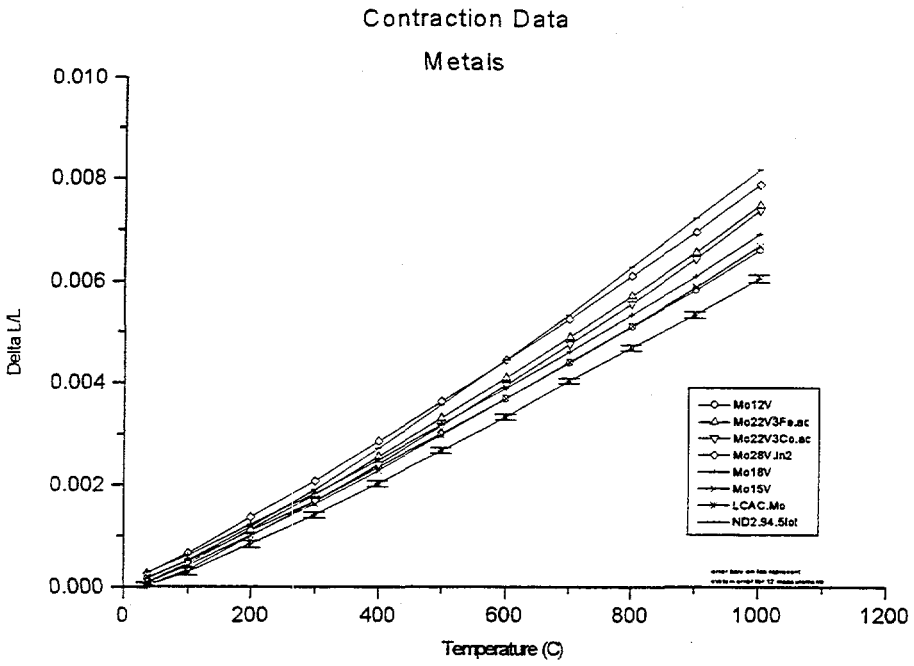

Fig. 7. Contraction strain (delta L/L) versus temperature for Mo and Mo-V alloys.

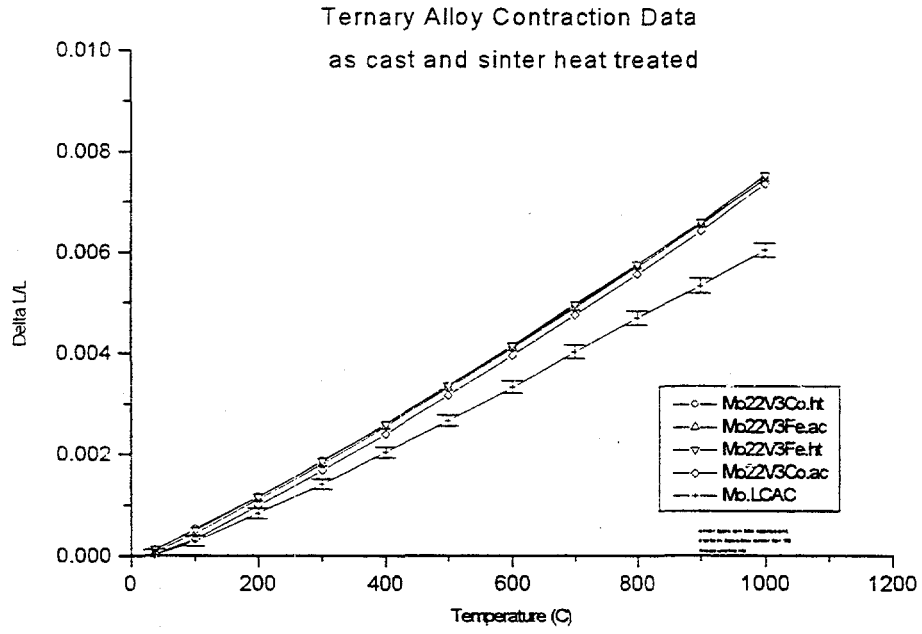

Fig. 8. Contraction strain (delta L/L) versus temperature for as-cast and heat-treated ternary alloys.

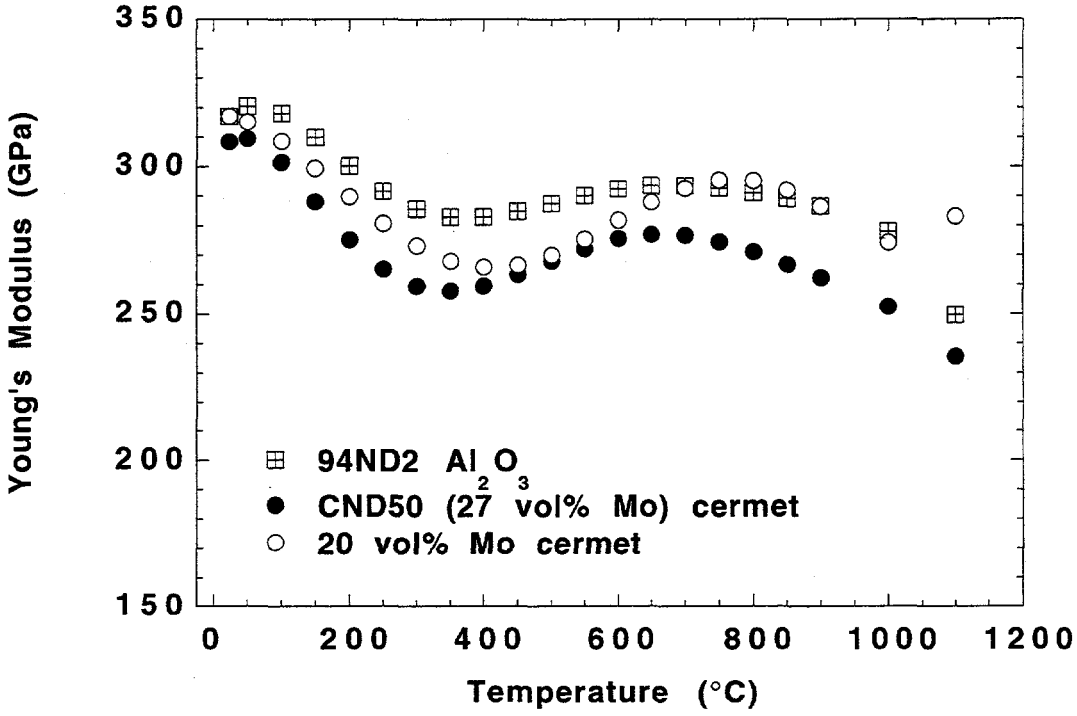

Polynomial fit for CND50 cermet.

$$E(GPa)=-5.17D-15T^{6}+1.89E-11T^{5}-2.62E-8T^{4}+1.67E-5T^{3}-4.48E-3T^{2}+2.57E-1T+2.06E2$$

Polynomial fit for 20 vol% Mo cermet.

$$E(GPa)=1.85E-15T^{6}-3.27E-12T^{5}-2.86E10T^{4}+3.05E-6T^{3}-1.41E-3T^{2}+3.30E-2T+3.17E2$$

Polynomial fit for 94ND2 alumina.

$$E(GPa)=-5.14E-15T^{6}+1.83E-11T^{5}-2.50E-8T^{4}+1.62E-5T^{3}-4.48E-3T^{2}+4.29E-1T+3.09E2$$

Fig. 9. Young's modulus as a function of temperature between 23 and 1100°C for CND50 cermet (slurry-processed), 20 vol% Mo cermet, and 94ND2 alumina (lot 9408).

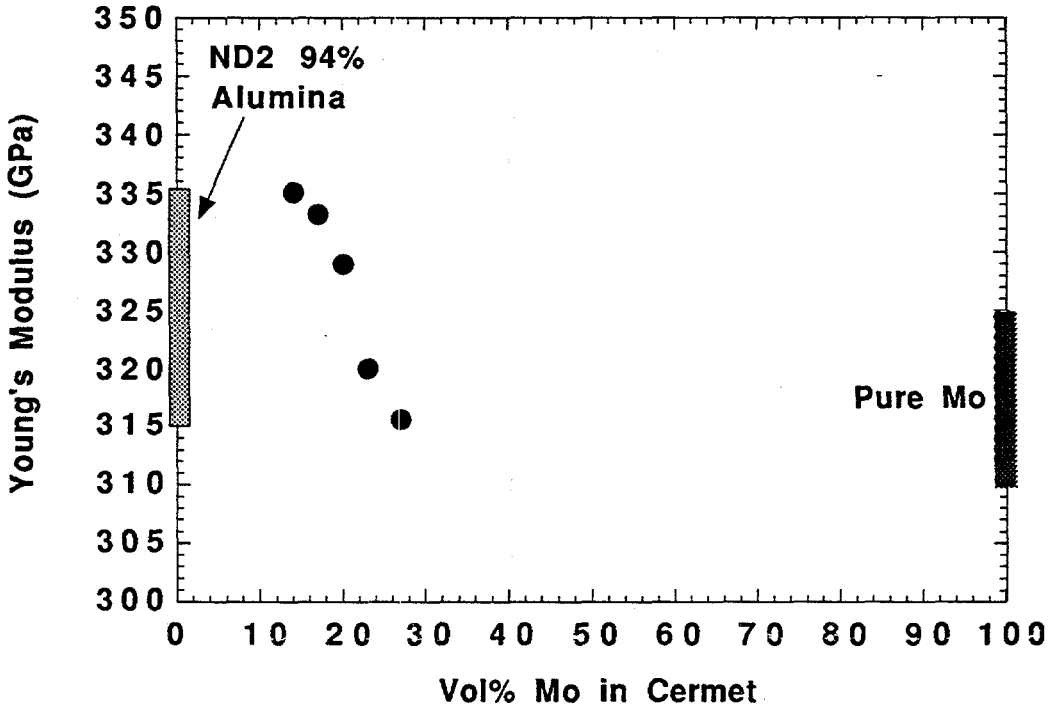

Fig. 10. The Young's modulus as a function of the vol% Mo in the cermet. The range of typical Young's modulus values for the Mo and 94ND2 alumina end members are also shown.

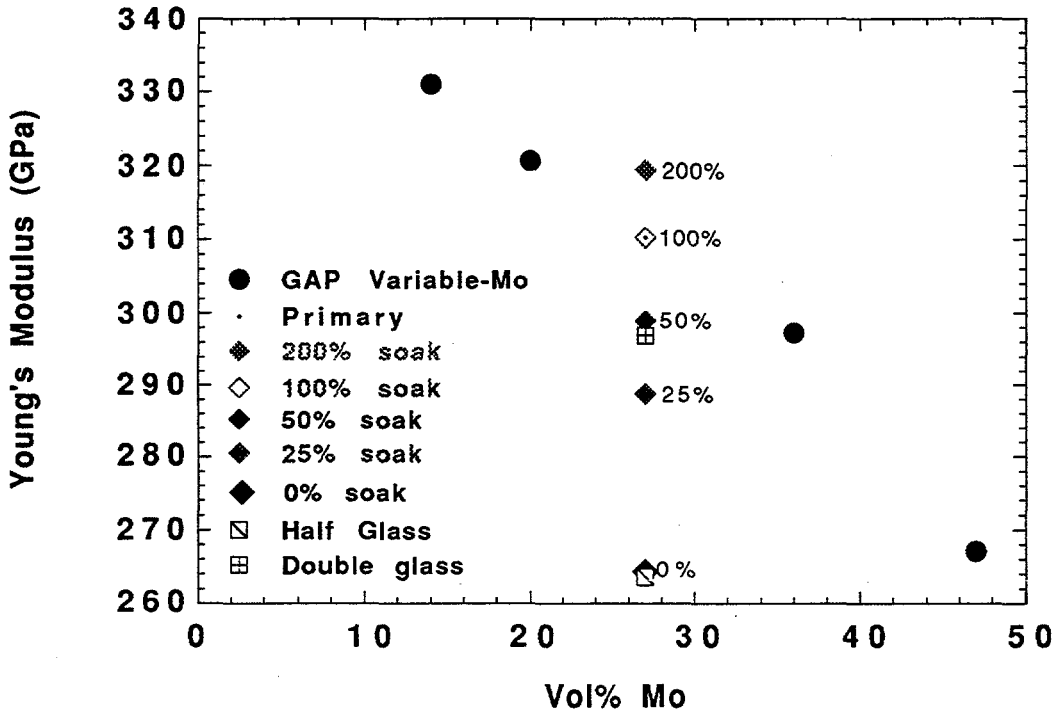

Fig. 11. The Young's modulus vs. vol% Mo, including the results for the different glass contents (half and double the glass content in CND50) and different sintering times at temperature (0, 25, 100, and 200% soak time).

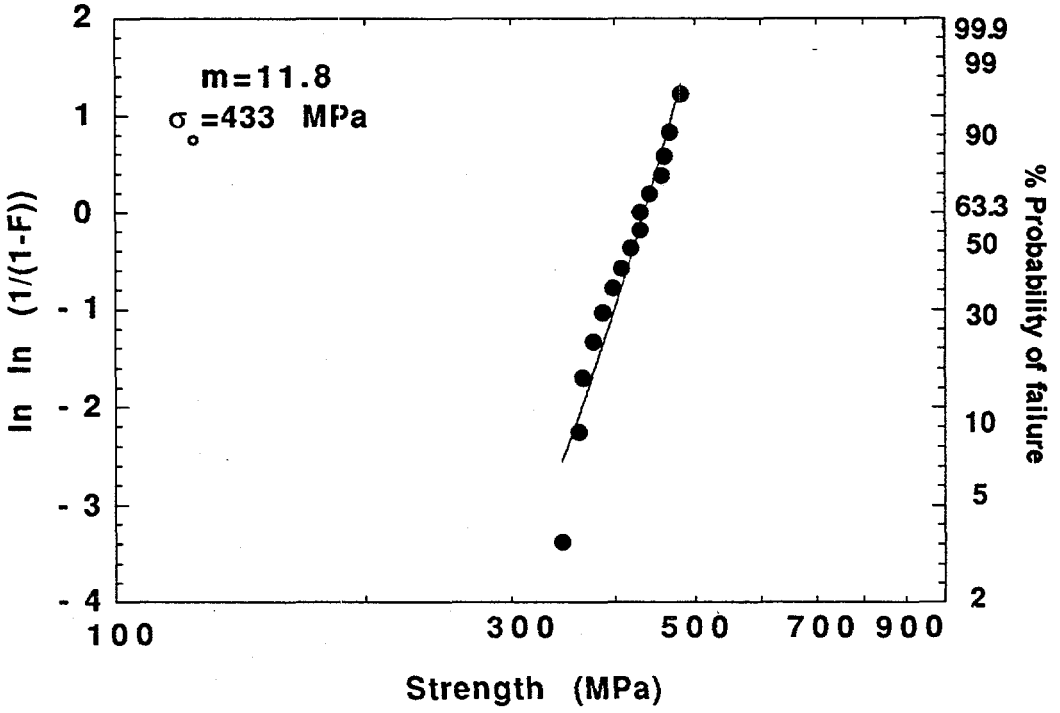

Fig. 12. The Weibull plot of the dry-processed 27 vol% Mo cermet strength data (lowest strength sample omitted).

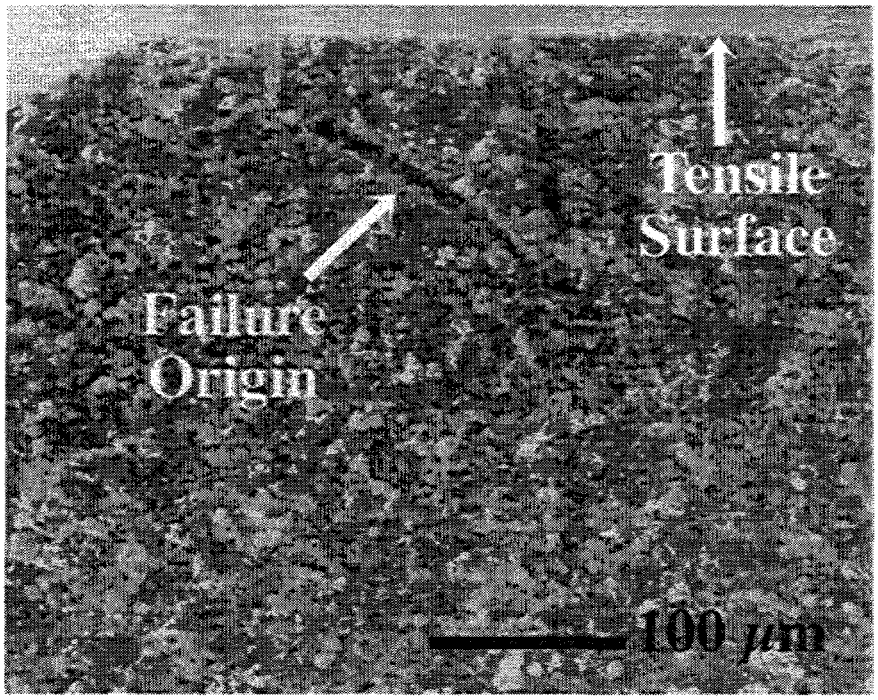

Fig. 13. An example of a tensile surface failure for a CND50 cermet bend specimen.

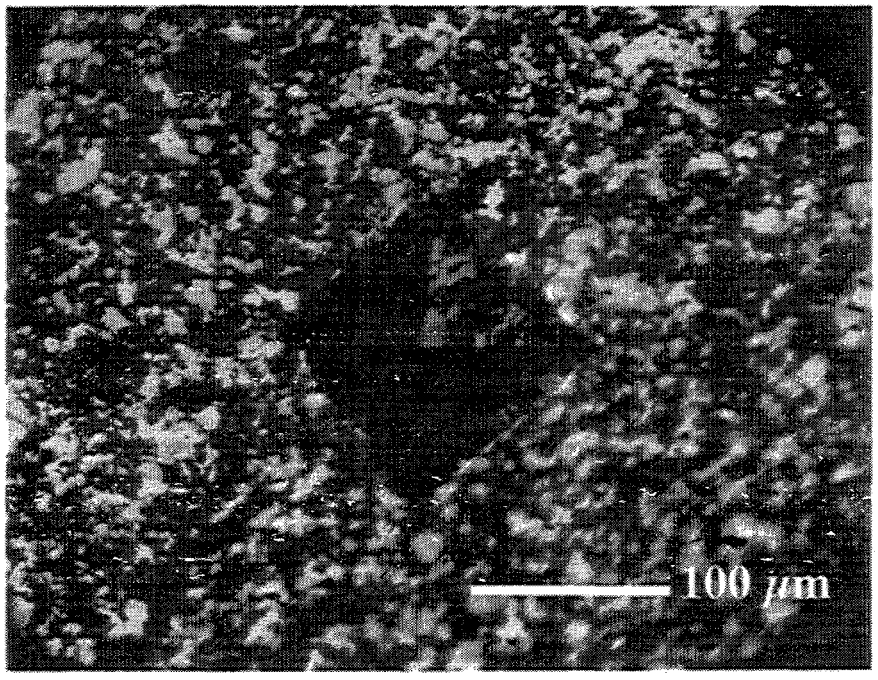

Fig. 14. An optical micrograph of a Vickers indentation in a polished cermet sample.

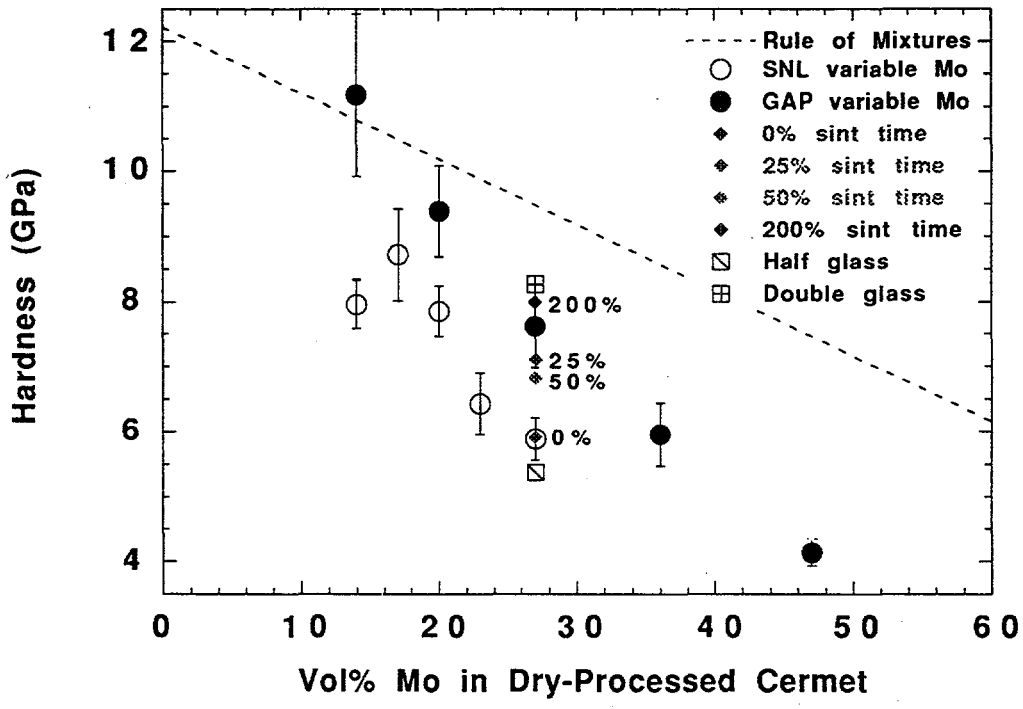

Fig. 15. Vickers hardness as a function of Mo content, sintering time, and glass content for Mo-alumina cermets.

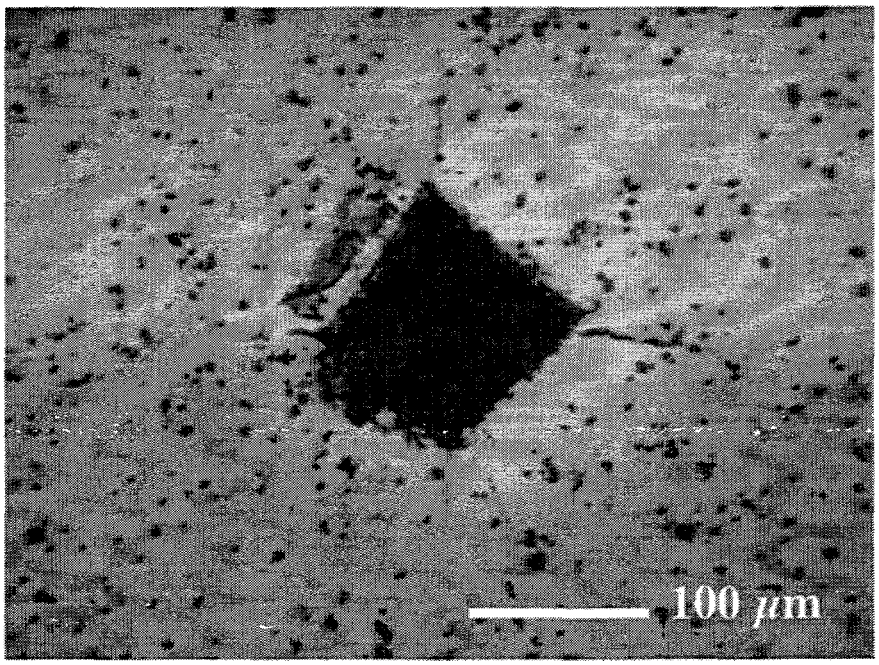

Fig. 16. Acoustic microscopy micrograph of a Vickers hardness indentation in CND50 cermet. The visibility of the cracks in this micrograph compared to Fig. 14 shows that this technique is a much more effective method for identifying the crack length.

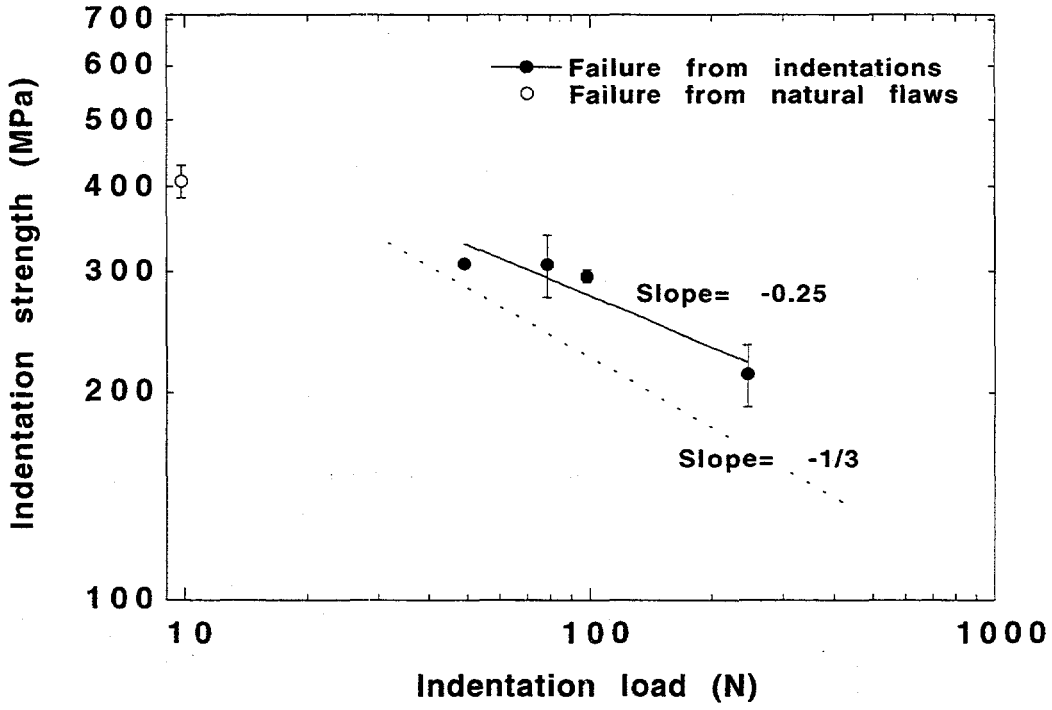

Fig. 17. The indented strength as a function of the indentation load for dry-processed 27 vol% Mo cermet.

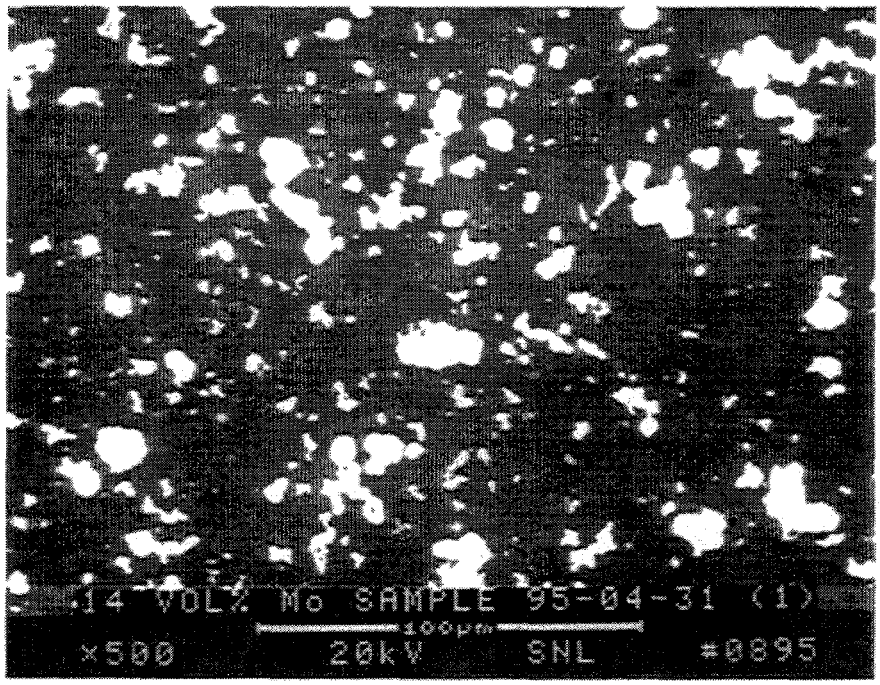

(a)

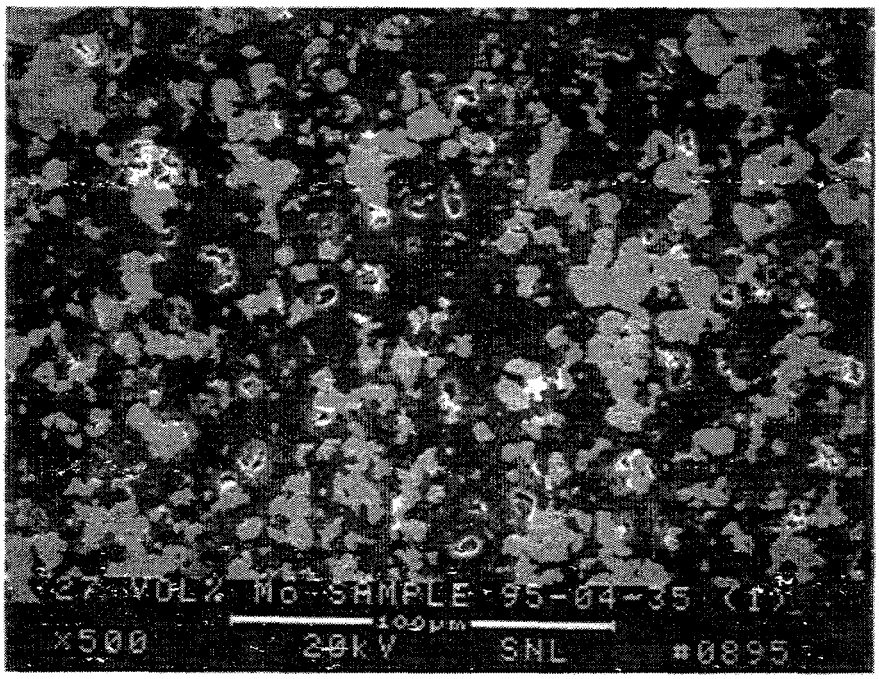

(b)

Fig. 18. SEM micrographs of un-etched, dry-processed cermets (a) 14 vol% and (b) 27 vol% Mo.

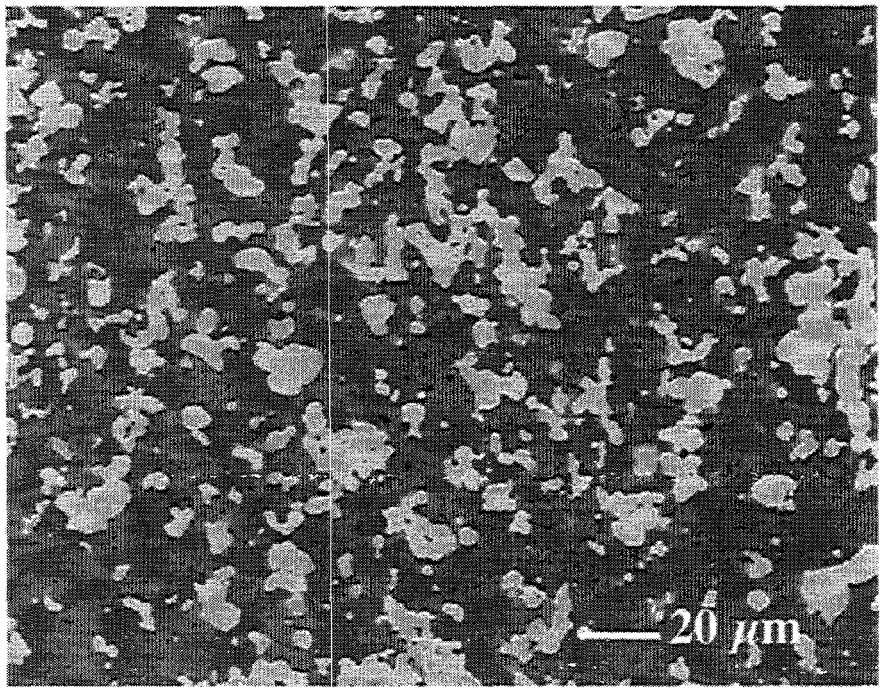

Fig. 19. SEM micrograph of un-etched, slurry-processed 27 vol% Mo cermet.

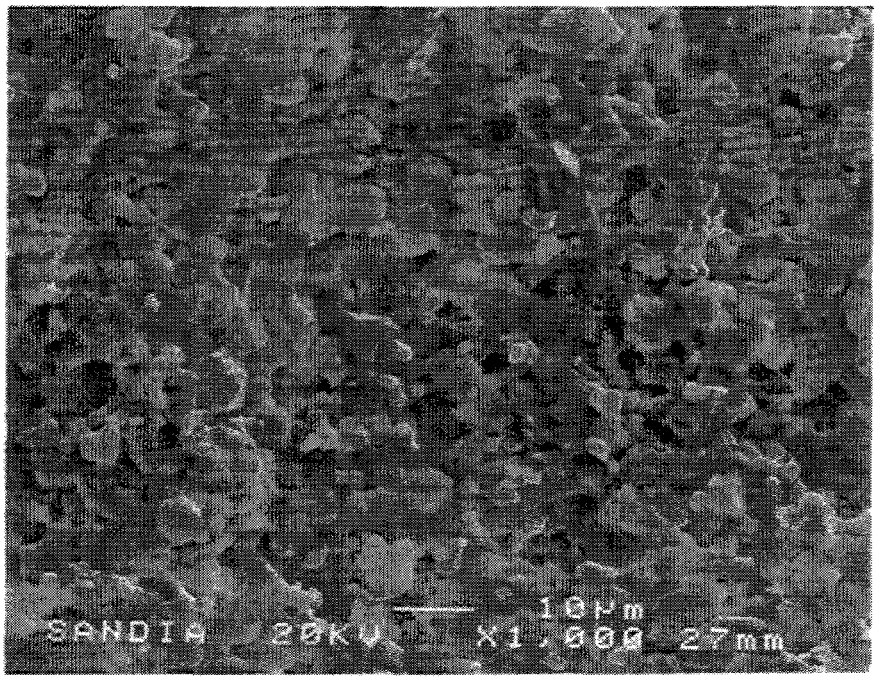

(a)

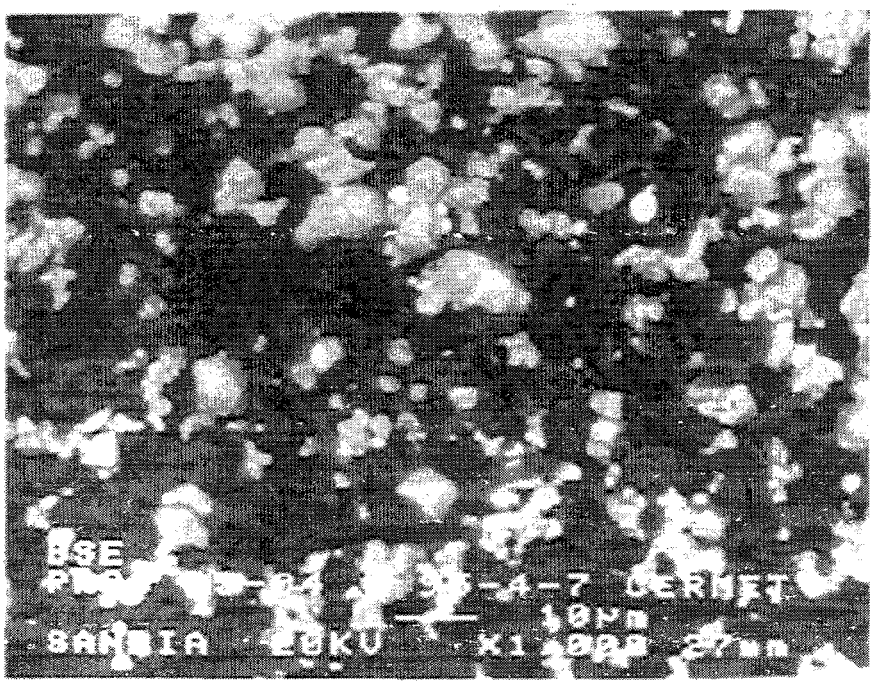

(b)

Fig. 20. SEM micrographs of a fracture surface of a dry-processed 27 vol% Mo cermet a) Secondary electron image b) Backscattered electron image.

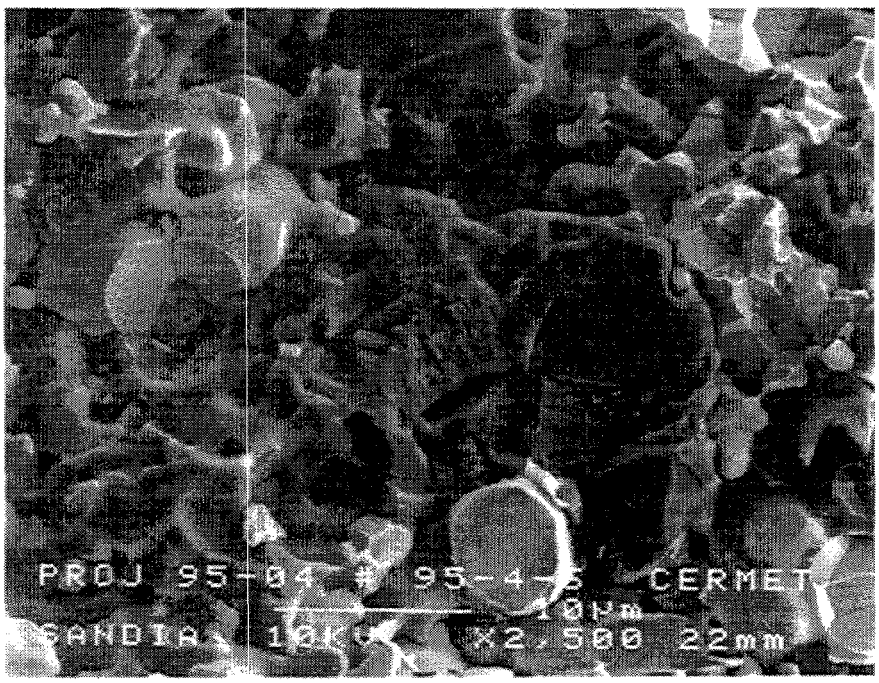

(a)

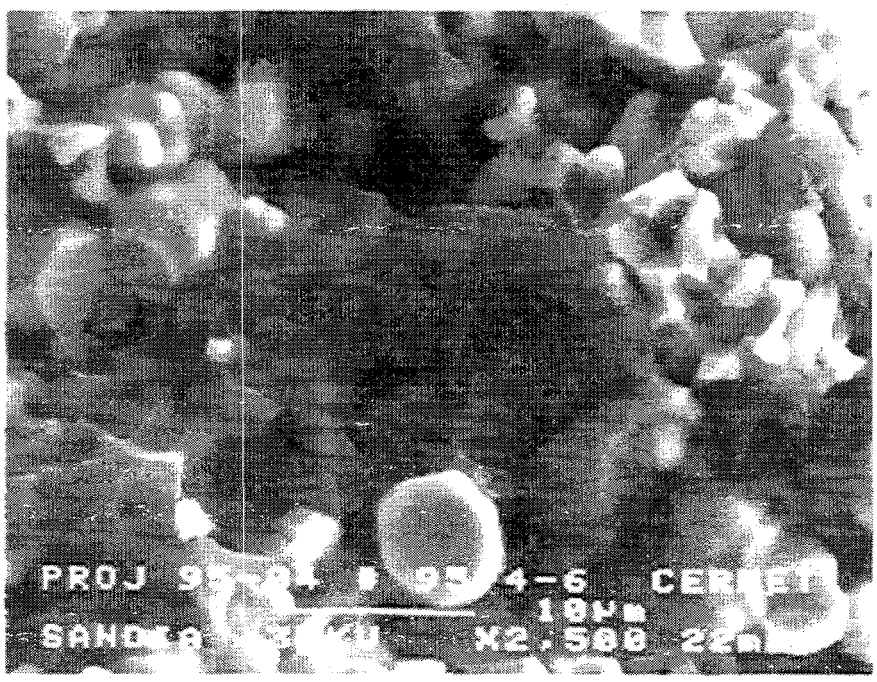

(b)

Fig. 21. SEM micrographs taken of the same location on a fracture surface at accelerating voltages of a) 10 and b) 30 KeV.

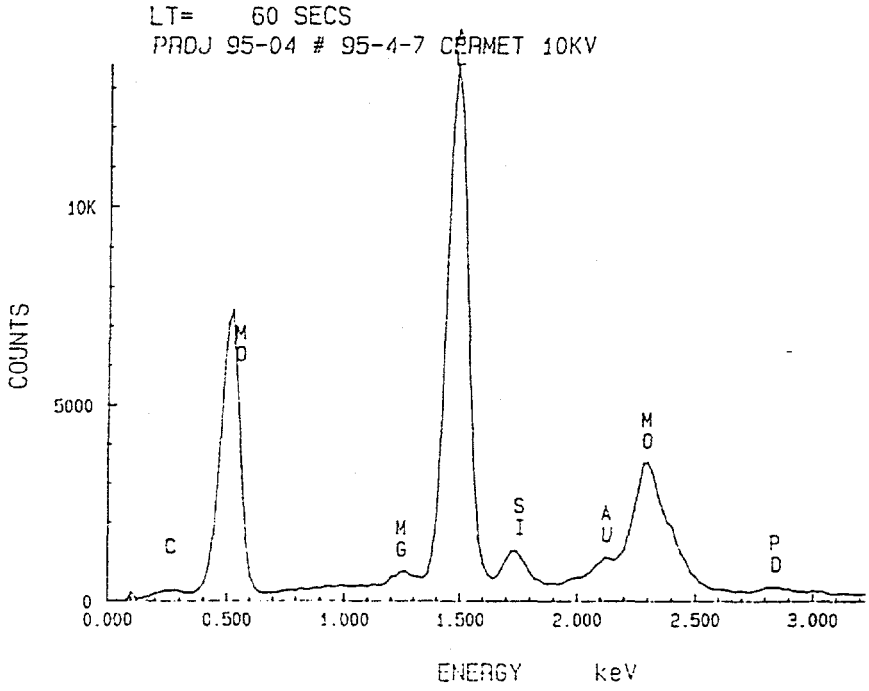

(a)

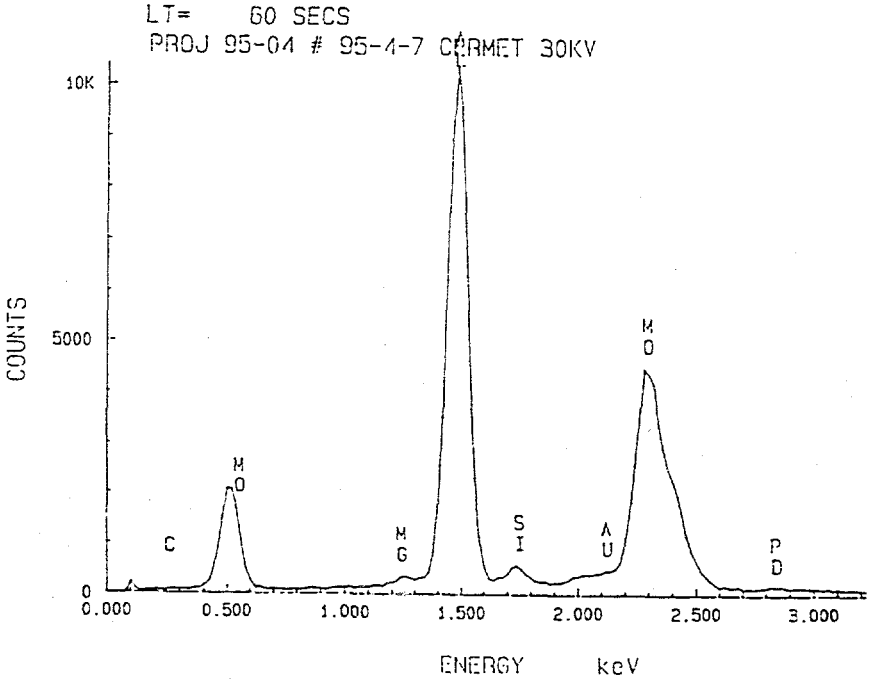

(b)

Fig. 22. Typical EDAX (Energy dispersive analysis by X-ray) spectra for a cermet fracture surface for electron beam accelerating voltages of a) 10 and b) 30 keV.

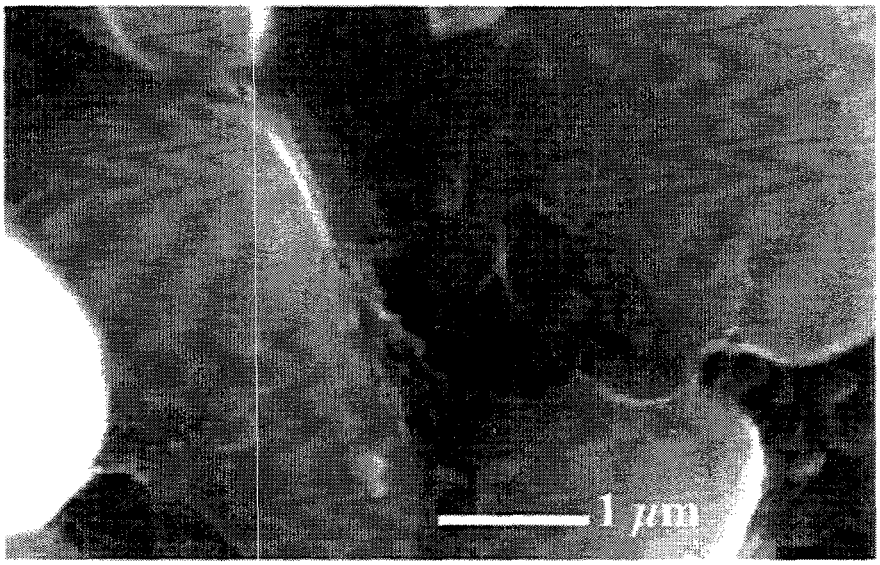

Fig. 23. A high magnification SEM micrograph showing the glass phase on alumina grains.

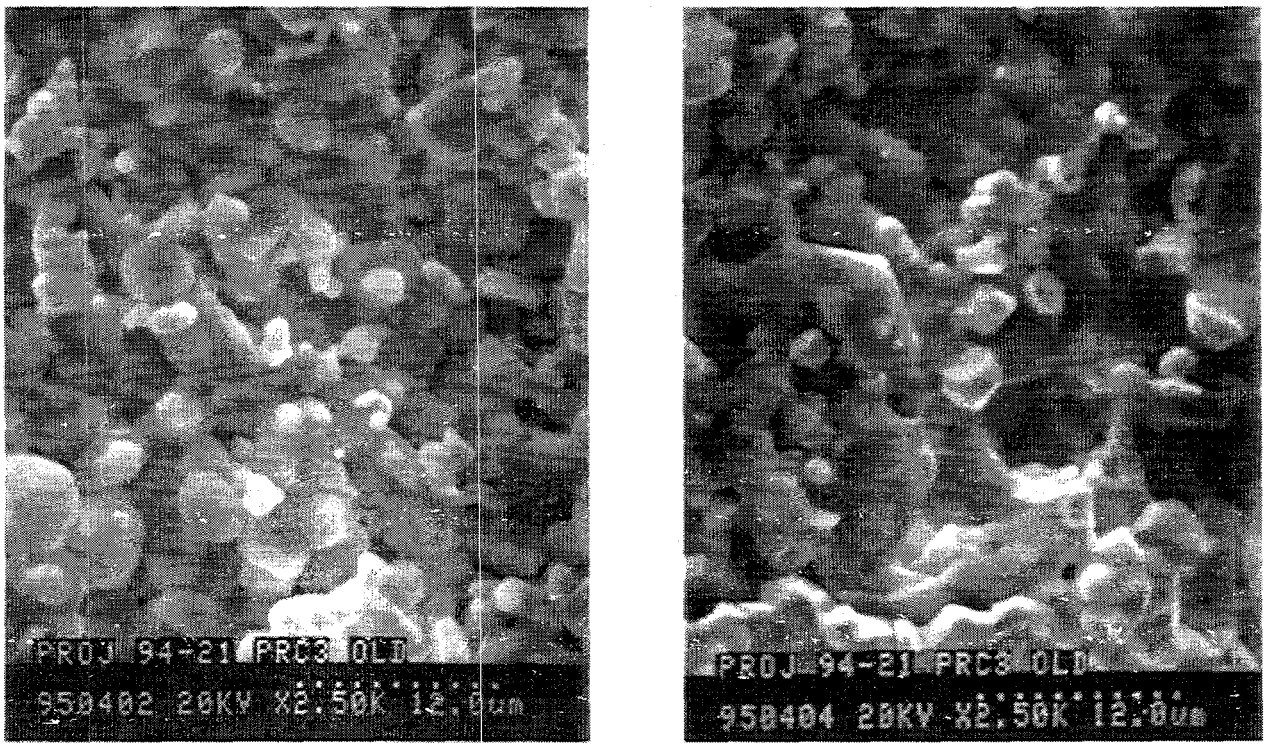

(a) **(b)**

Fig. 24. Cermet material from a) region close to the cermet/alumina interface b) bulk.

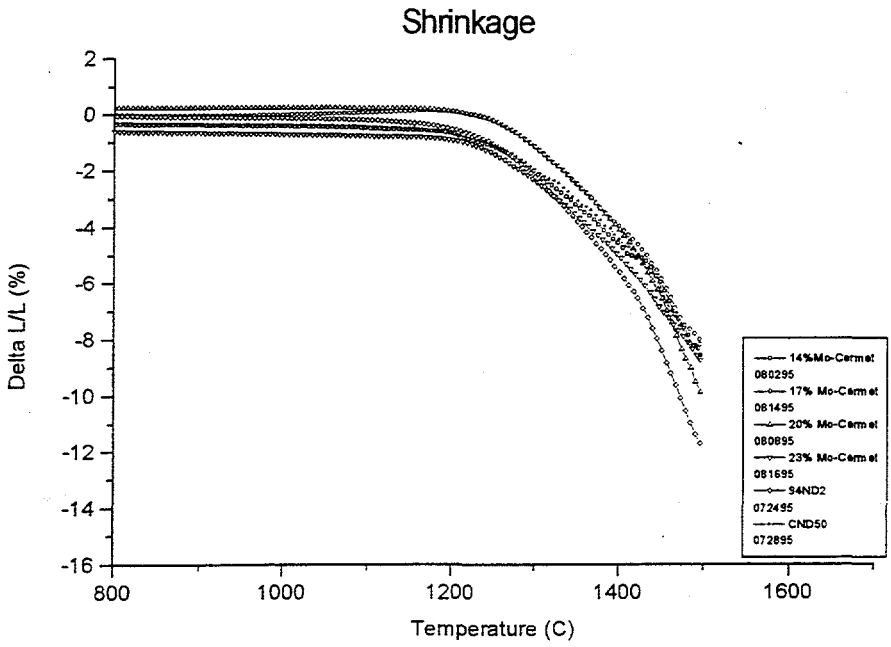

Fig. 25. Shrinkage behavior at the beginning of sintering process.

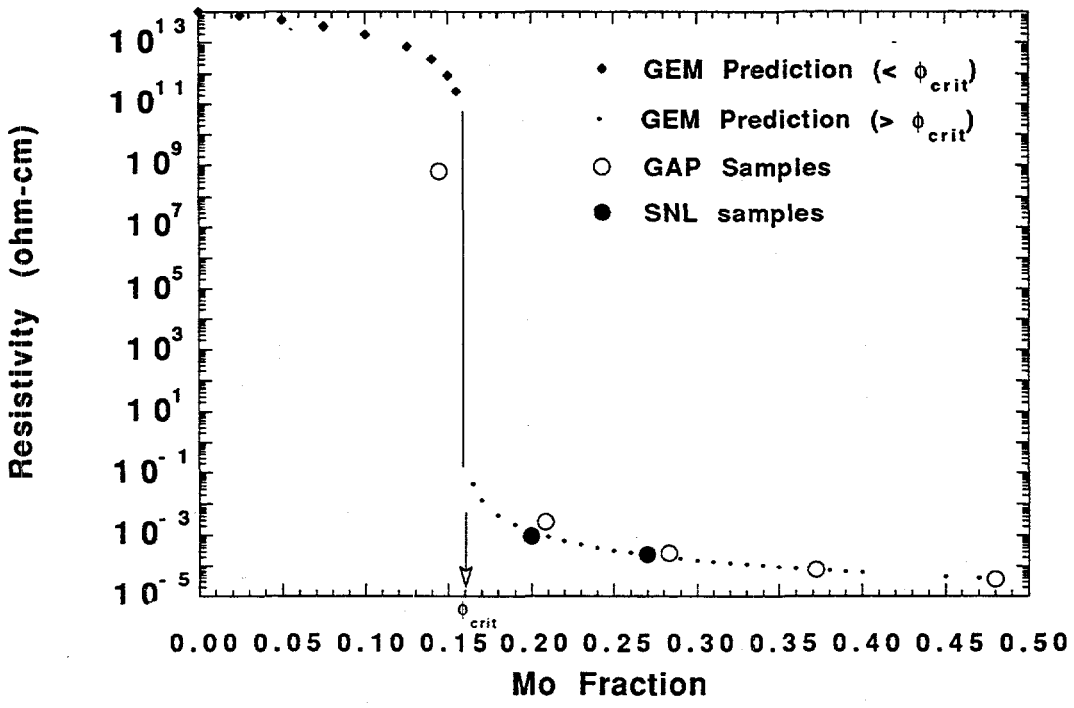

Fig. 26. Electrical resistivities as a function of Mo content (GEM=General Effective Media Equation, GAP=Gary Pressly's samples, SNL=Sandia samples).

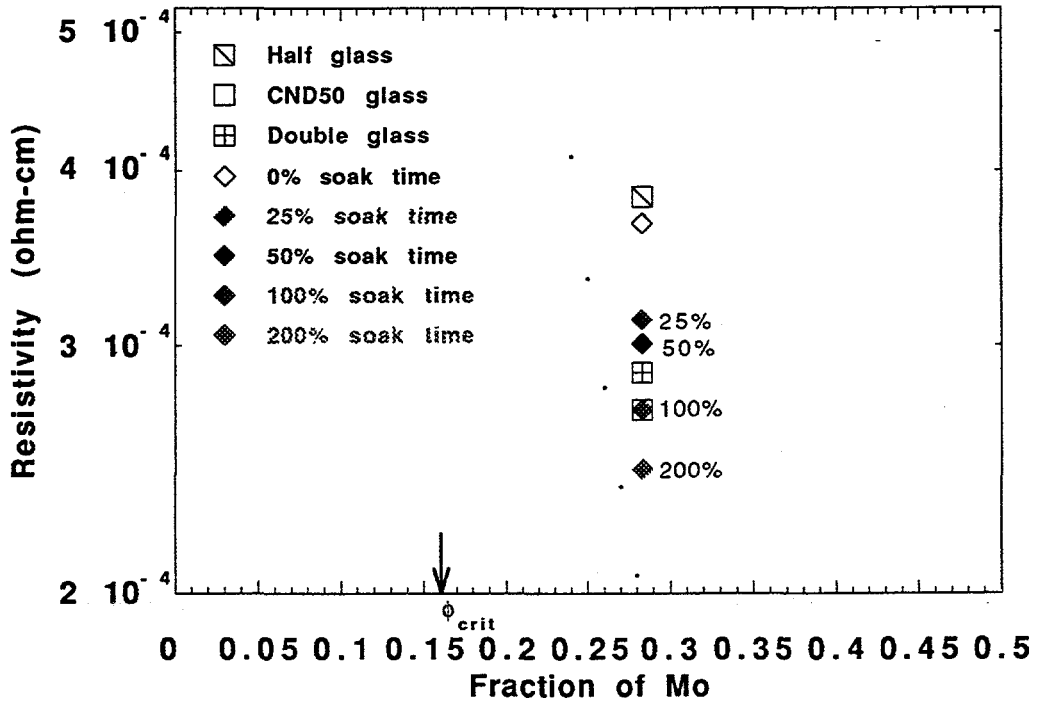

Fig. 27. Expanded vertical scale of electrical resistivity vs. Mo content for 27% Mo samples processed with different sintering times and different glass contents.

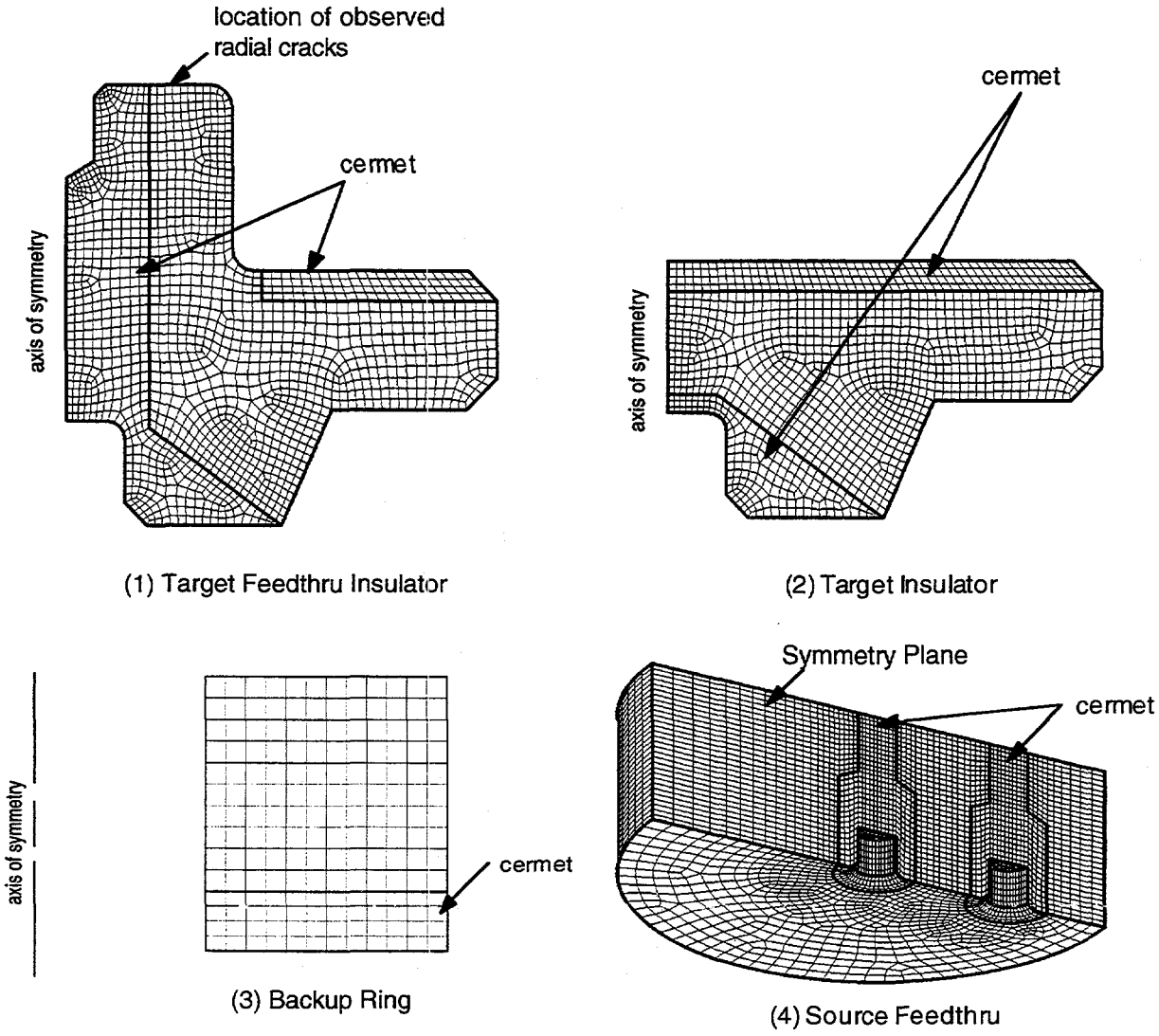

Fig. 28. Finite element meshes of four cermet components: (1) target feedthru insulator, (2) target insulator, (3) back-up ring, and (4) source feedthru.

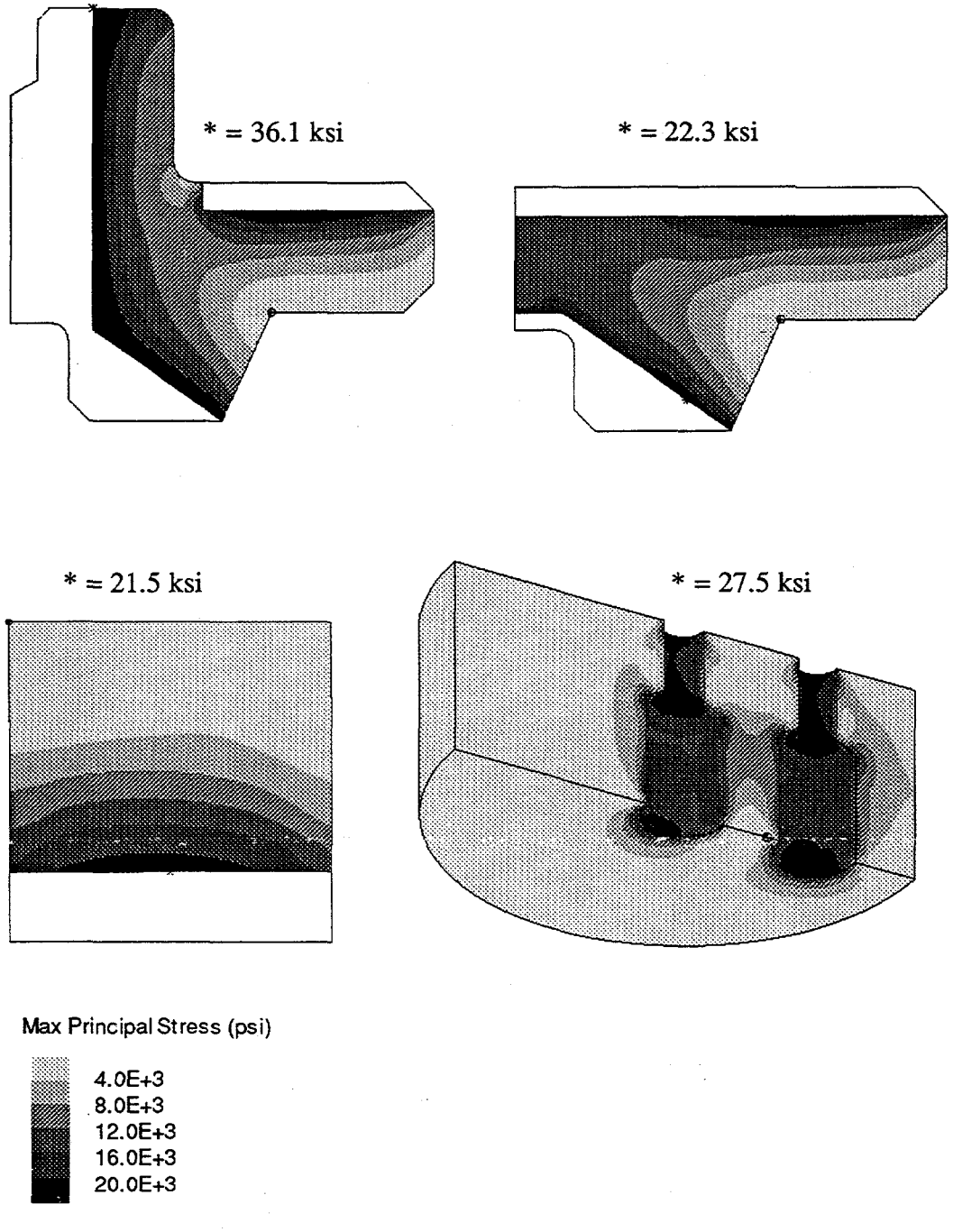

Fig. 29. Maximum principal stress distribution in the various cermet components with CND50 (27 vol% Mo). Maximum stress denoted by (*).

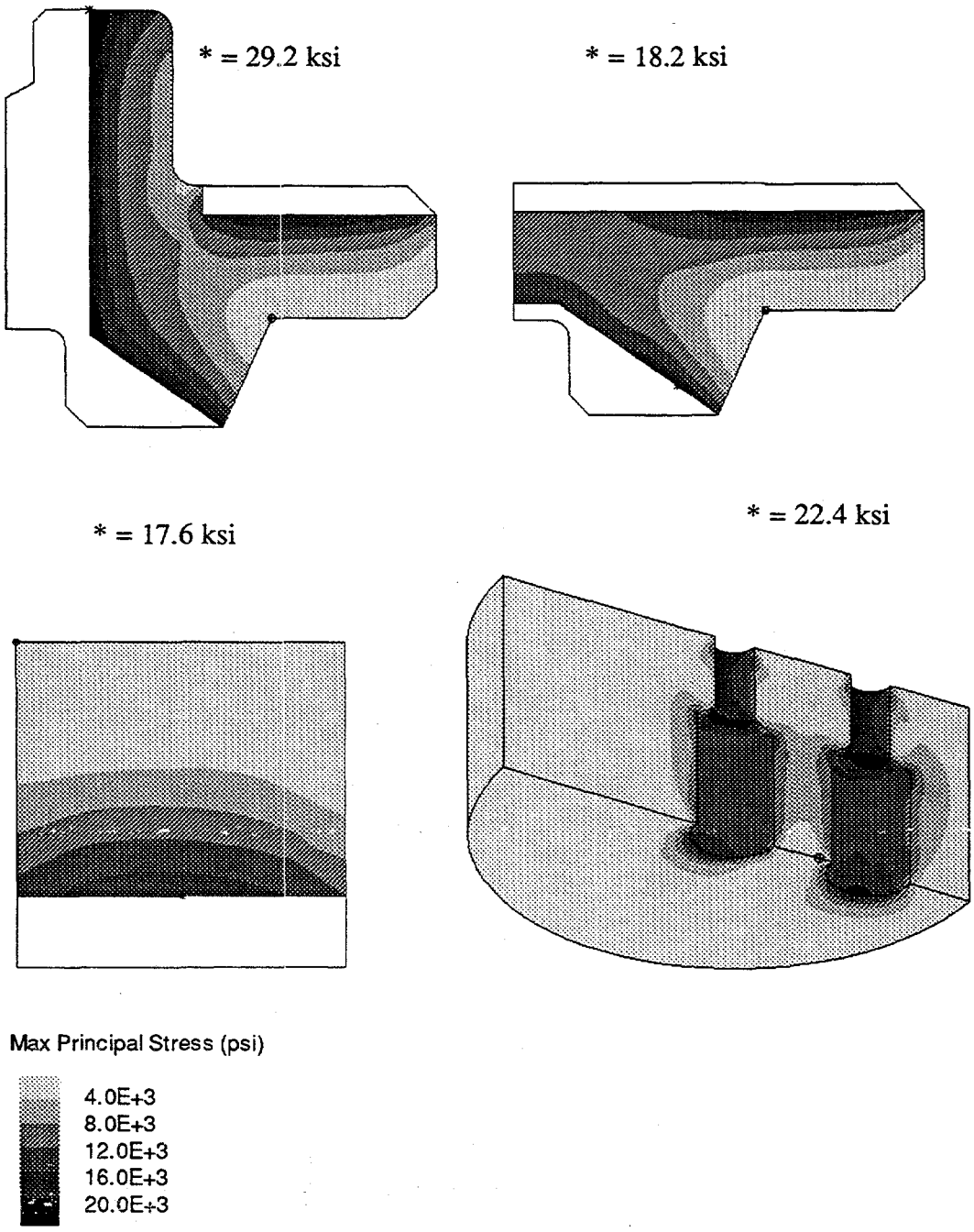

Fig. 30. Maximum principal stress distribution in the various cermet components with low vol% cermet (20 vol% Mo). Maximum stress denoted by a (*).

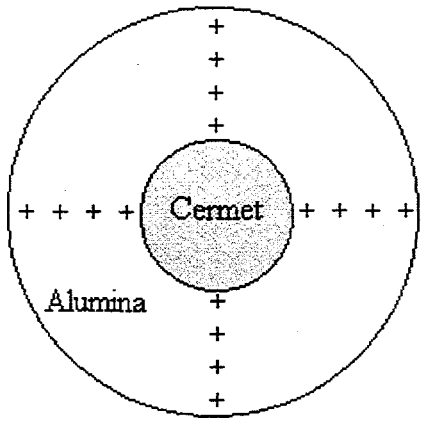

Fig. 31. Schematic of end face of sample with OD of 0.2 inch. Crosses show arrangement of indents.

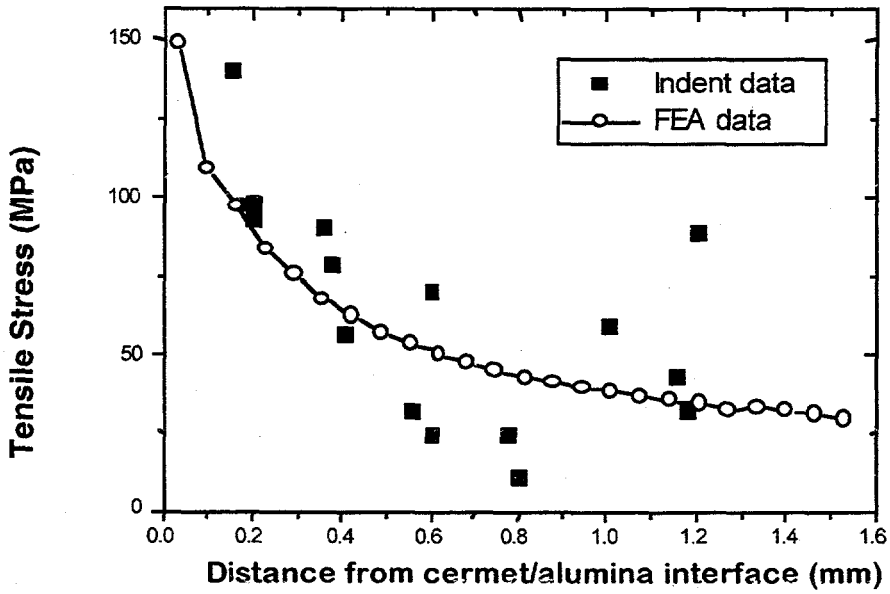

Fig. 32. Hoop stress (avg) in 20D3L2 sample (OD=0.2 inch, L=0.5 inch).

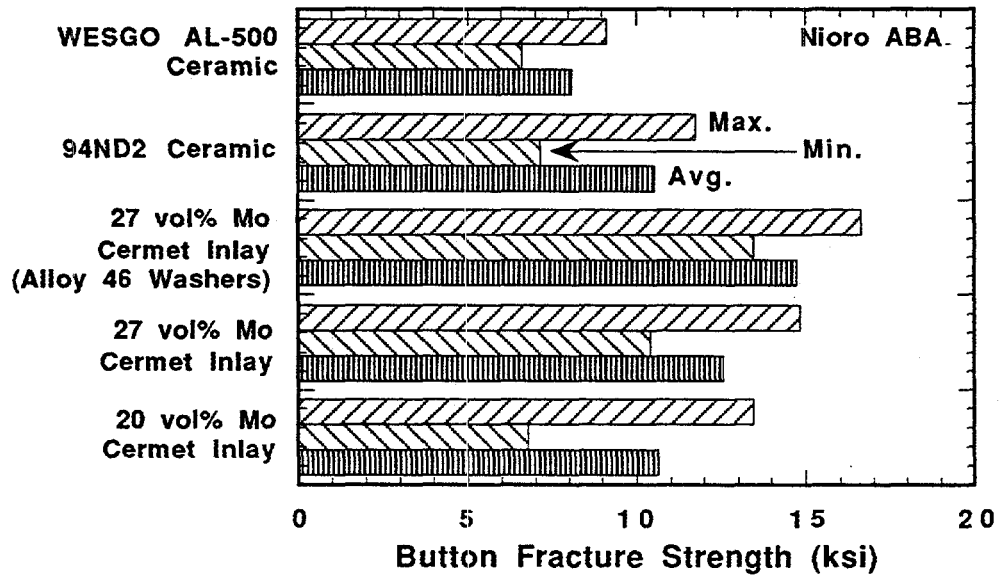

Fig. 33. Horizontal bar chart comparing the tensile button test results for samples brazed with Nioro ABA alloy in dry hydrogen using Process III (1015°C, 1 min.) as described in Ref. 31. For each group of samples, the minimum, maximum and average fracture strength are shown. Three brazed buttons were run for the 94ND2 material; while all other sample conditions had a minimum of five buttons. All of the samples shown exhibited no detectable leak rate, with a minimum leak rate detection of 1 x 10^{-9} atm-cc/s.

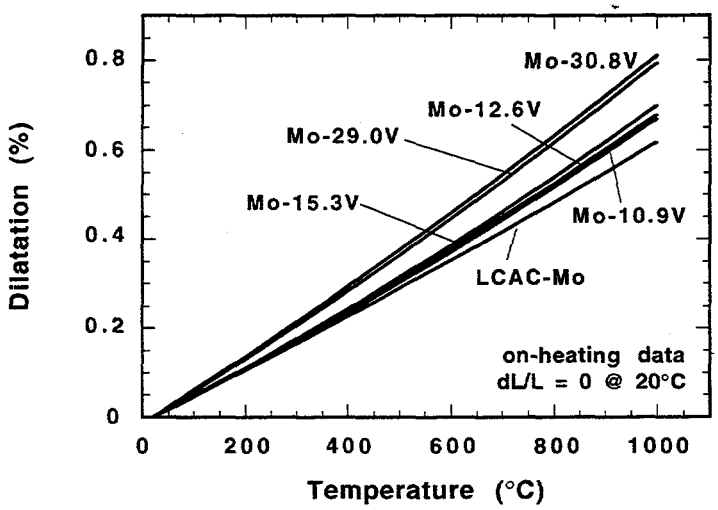

Fig. 34. Dilatation data for LCAC-Mo and the various Mo-V alloys studied. The data shown were collected during the on-heating portion of the run, over the temperature range 20-1000°C. The individual data sets were fit to a polynomial fit and adjusted with a constant to impose dL/L = 0 at 20°C.

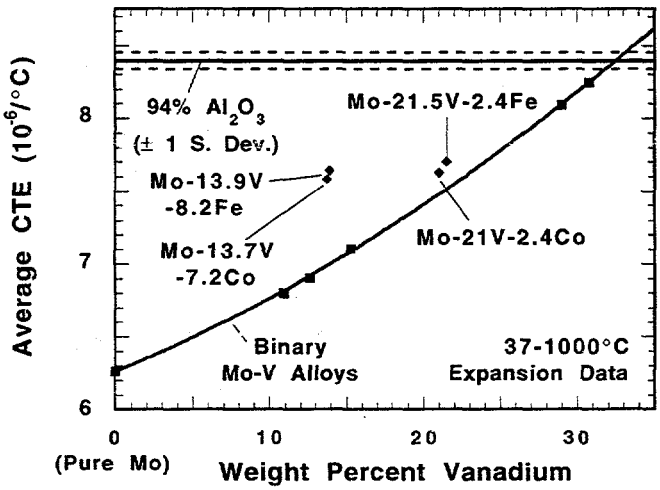

Fig. 35. Effect of Vanadium addition to Mo on the average CTE, for on-heating data. In addition to the binary Mo-V alloys, data are included for 5 different lots of the 94% alumina ceramic (±1 standard deviation shown), and the 4 ternary alloys discussed in this paper.

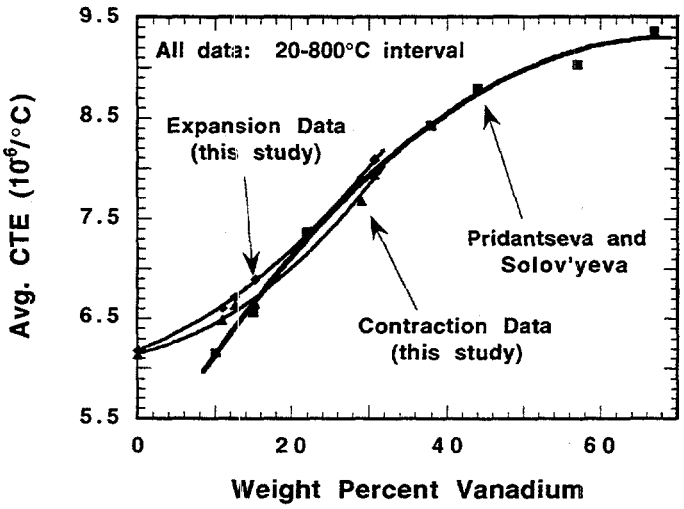

Fig. 36. Comparison of CTE data for Mo-V alloys studied by Pridantseva and Solov'eva (Ref. 34) with the data generated in this study. Note that all of the CTE data shown in this graph are for the temperature interval 20-800°C.

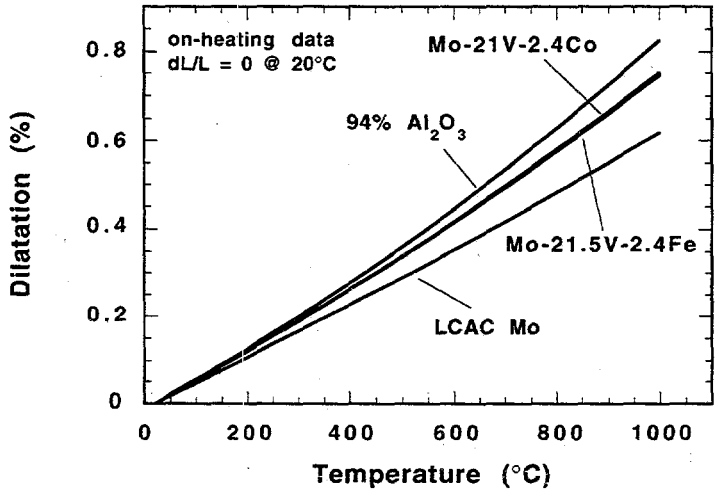

Fig. 37. Comparison of dilatation data for LCAC Mo, Mo-21V-2.4Co, Mo-21.5V-2.4Fe and 94% alumina ceramic materials. On-heating data, dL/L has been set to 0 at 20°C.

DISTRIBUTION:

1 John Kelso
OSRAM SYLVANIA
131 Portsmouth Ave.
Exeter, NH 03801

1 MS 0188 LDRD Office, 4523
1 0333 T. J. Garino, 1846
1 0342 K. Mahin, 1807
1 0367 B. K. Damkroger, 1833
1 0367 E. K. Beauchamp, 1833
2 0367 J. J. Stephens, Jr., 1833
5 0367 S. J. Glass, 1833
2 0367 S. L. Monroe, 1833
2 0443 E. Hoffman, 9117
1 0443 H. Morgan, 9117
1 0443 S. N. Burchett, 9117
1 0516 C. C. Busick, 1564
1 0516 G. L. Laughlin, 1564
1 0516 G. W. Smith, 1564
1 0516 J. P. Brainard, 1564
1 0521 D. L. Wallace, 1567
1 0521 R. A. Damerow, 1502
1 0521 R. A. Pike, 1567
1 0561 D. J. Van Ornum, 1481-2
1 0615 J. H. Gieske, 9752
1 0872 D. R. Boone, 14311
1 0873 D. J. Malbrough, 14402
1 0873 D. R. McCollister, 14403
1 0873 K. Meredith, 14402
1 0873 L. A. Malizia, 14402
1 0873 M. Senkow, 14403
1 0873 N. Demeza, 14403
1 0873 T. B. Mason, 14403
1 0958 G. A. Pressly, 1484
1 0959 D. M. Goy, 1492
1 0959 F. P. Gerstle, Jr., 1492
5 0959 R. H. Moore, 1492
1 0959 S. T. Reed, 1492
1 0961 J. A. Sayre, 1403
1 1159 B. Barrett, 9311
1 1349 D. N. Bencoe, 1833
1 1349 K. Ewsuk, 1841
1 1349 R. Loehman, 1808
1 1434 G. Pike, 1802
1 9403 J. Smugeresky, 8712
1 9405 D. Lindner, 1809
1 AlSiMag J. F. McGinnis
1 9018 Central Technical Files, 8940-2
5 0899 Technical Library, 4916
2 0619 Review & Approval Desk, 12690; For DOE/OSTI